ASSESSMENT OF THE 2018 TURKISH SEISMIC REGULATIONS UNREINFORCED MASONRY CONSTRUCTION SPECIFICATIONS THROUGH A CASE STUDY STRUCTURE

A Thesis Submitted to
the Graduate School of Engineering and Sciences of
İzmir Institute of Technology
in Partial Fulfillment of the Requirements for the Degree of

MASTER OF SCIENCE

in Civil Engineering

by
Egecan TURAN

December 2020

İZMİR

ACKNOWLEDGEMENTS

I would like to thank to my advisor Assoc. Prof. Dr. Cemalettin DÖNMEZ for his motivation and patience in supervising me.

I am thankful to my dear family and friends for their support and believing in me.

ABSTRACT

ASSESSMENT OF THE 2018 TURKISH SEISMIC REGULATIONS UNREINFORCED MASONRY CONSTRUCTION SPECIFICATIONS THROUGH A CASE STUDY STRUCTURE

The new release of the seismic regulation in 2018 resulted in major changes in masonry structures' design approach. It changes from the allowable stress design method to the ultimate strength design method. Also, the effect of vertical earthquake component, which was not considered, is included in the analysis combinations. The seismic risk is started to be defined by parameters determined according to the geographical coordinates of the building that is considered. The presented study is intended to investigate the impact of the listed changes on unreinforced masonry design. A case study building is utilized for this purpose. It is designed to satisfy the TER-2007 requirements and re-evaluated considering the TER-2018 requirements. The results show that the building did not have sufficient capacity, according to the 2018 earthquake regulation. Almost all the walls were beyond their capacities. The same structure has been analyzed by nonlinear static analysis (pushover analysis) as well. According to the nonlinear analysis results, performance assessment was made per the 2018 earthquake regulation and FEMA356. The performance evaluation by nonlinear static analysis using TER-2018 and FEMA356 demands, satisfies the life safety performance level for FEMA356 and TER-2018.

Keywords: Unreinforced Masonry Building; Unreinforced Masonry Structure Design; Nonlinear Static Analysis

ÖZET

ÖRNEK BİR YAPI ÜZERİNDEN 2018 DEPREM YÖNETMELİĞİ DONATISIZ YIĞMA YAPI GEREKLİLİKLERİNİN DEĞERLENDİRİLMESİ

Deprem yönetmeliğinin 2018'deki yeni sürümü yığma yapıların tasarım yaklaşımında değişiklilere neden olmuştu. Tasarım yaklaşımı emniyet gerilmesi yönteminden dayanıma göre tasarım yöntemine evrilmiştir. Ayrıca, dikkate alınmayan düşey deprem bileşeninin etkisi de analiz kombinasyonlarına dahil edilmiştir. Yapıların koordinatlarına göre belirlenen parametreler ile sismik riskler tanımlanmaya başlanmıştır. Sunulan çalışmada, listelenen değişikliklerin, donatısız yığma tasarımı üzerindeki etkisinin araştırılması amaçlanmıştır. Bu amaçla örnek bir yapı değerlendirilmiştir. Bu yapı, TER-2007 donatısız yığma gereksinimlerini karşılayarak tasarlanmış ve TER-2018'e göre tekrar değerlendirilmiştir. Sonuçlar 2007 deprem yönetmeliğine göre tasarlanan binanın 2018 deprem yönetmeliğine göre neredeyse bütün elemanlarının yeterli kapasiteye sahip olmadığını göstermiştir. Aynı yapı, doğrusal olmayan statik analizle de (itme analizi) analiz edilmiştir. Doğrusal olmayan analiz sonuçlarına göre, 2018 deprem yönetmeliği ve FEMA356'ya göre performans değerlendirlmesi yapılmıştır. Bu analizin sonuçları yapının, TER-2018 ve FEMA356 için can güvenliği performans seviyesini karşıladığını ortaya koymuştur.

Anahtar Kelimeler: Donatısız Yığma Bina; Donatısız Yığma Yapı Tasarımı, Doğrusal Olmayan Statik Analiz

TABLE OF CONTENTS

LIST OF FIGURES

Figure **Page**

Figure **Page**

LIST OF TABLES

Table **Page**

Table **Page**

Table **Page**

CHAPTER 1

INTRODUCTION

Masonry structures are one of the readily available important structural systems for humanity from ancient times until today. This type of framing is used in different areas of human needs, such as shelter, health, education, transportation, and entertainment. Until the emergence of the modern construction materials by the beginning of the 20th century, masonry structures dominated the construction for nearly nine millennia. Neolithic settlements in Anatolia started as early as 7100BC in Çatalhöyük. Since the early settlements, construction activity that is relied on the masonry systems. Turkey hosts many examples of such structures from many different civilizations throughout its long human history.

Apart from historical structures, Turkey has a large inventory of masonry structures that are supporting daily life. According to the building census, approximately half of the building stock in Turkey consists of masonry buildings. (%51- 4.001.954 of 7.838.675 according to DIE 2000 (State Institute of Statistics 2000). This ratio is higher in rural areas. Masonry building stock ratio and its numbers per the provinces are presented in Figure 1.1. and 1.2.

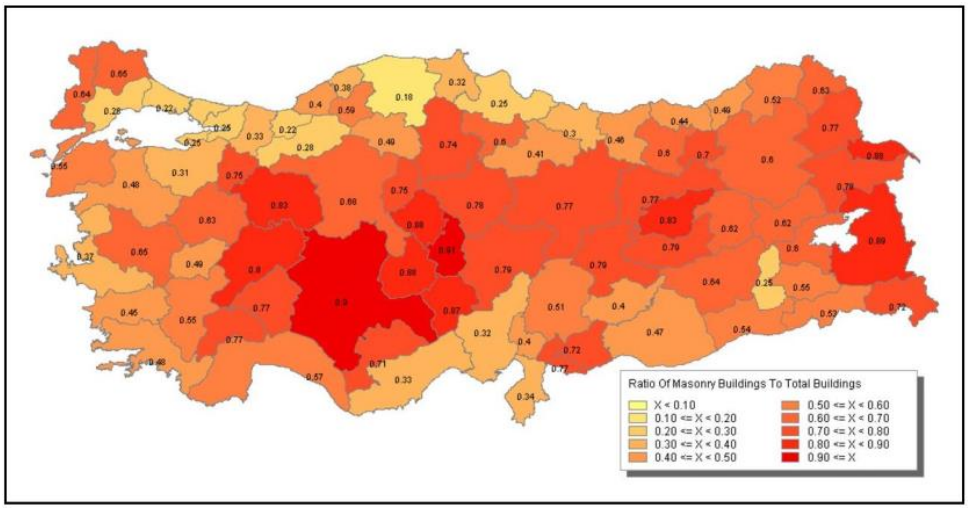

Figure 1.1. Masonry Building Ratios in Cities in Turkey (DİE 2000)

(Source: Dilsiz and Türer 2005)

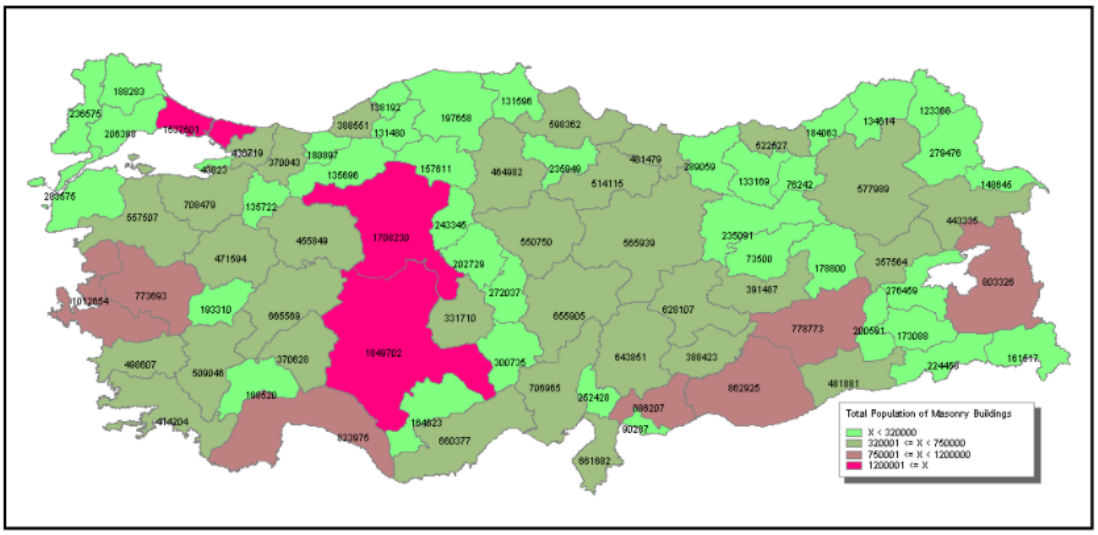

Figure 1.2. Number of People Living in Masonry Buildings in Turkey (DIE ,2000) (Source: Dilsiz and Türer 2005)

Turkey is in a high seismic zone, and almost all of the country could be accepted to carry a certain level of seismic risk. Either historical or modern, the masonry structures' vulnerability makes it necessary to study and investigate these structures' seismic behavior and design.

This thesis investigates the impact of the modifications in previous and current Turkish earthquake regulations on the demand and the selection of the structural system. A secondary purpose is to observe a selected building's earthquake response using the pushover analysis model, which provides more accurate results.

Unreinforced masonry design criteria of 2007 and 2018 Turkish Earthquake Regulations (TER-2007 and TER-2018) are compared. First, the design of a new unreinforced masonry building is performed according to the old design code. Then, the same structure is also designed by using design criteria of the new design code. A pushover-based performance analysis is also performed on the designed building.

The TER-2018 analysis was performed using both defined modeling approaches. These are the equivalent frame and the finite elements models. Structural models were generated using codes of SAP2000 and ETABS, respectively. The pushover model was also done with SAP2000.

The current earthquake regulations formulate the masonry design based on the section capacity formulas. These capacities were estimated based on the observations of failure of the masonry wall under horizontal loads. The failure modes of masonry walls are presented in Section 1.1. and the customary analytical models of the masonry structures are presented in Section 1.2. Literature studies of linear and nonlinear analysis of unreinforced masonry structures using the equivalent frame and the finite element models are given in the related sections.

1.1. Failure Modes of Unreinforced Masonry Walls

Major parameters that affect the in-plane behavior of unreinforced masonry are the wall's aspect ratio: the ratio of height to length of the wall, boundary conditions, and the vertical loads. There are other parameters with secondary importance, such as material characteristics of bricks, mortar, and brick-mortar interface (Magenes and Calvi 1997). FEMA-307 lists test results on unreinforced masonry. It is a good reference to the in-plane behavior of walls, making inferences about damage development, maximum strength and displacement response. The experimental results show that the failure modes of unreinforced masonry could be identified in four general states. These are rocking, sliding, diagonal tension, and toe crushing failures. (FEMA-307 1998) Even the four main different failure mechanism are not enough to describe the complex inelastic behavior of the masonry wall. The inception of any failure mechanism could be triggered another failure mechanism (Yi, Moon, et al. 2006). The overturning moment due to horizontal load could be either decreased or increased the axial load on the wall and convert the flexural failure to shear failure (Magenes, et al. 1995)

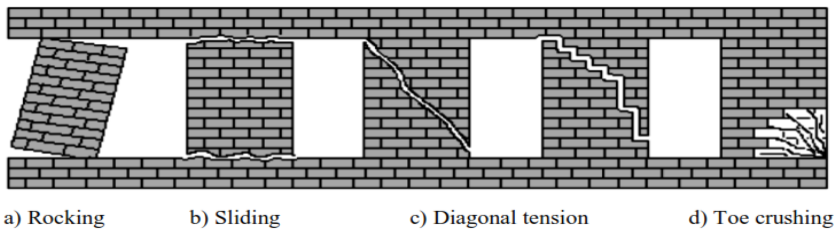

Figure 1.3. Masonry Wall Failure Modes Under In-Plane Loading
(Source: Yi 2004)

1.1.1. Rocking

Rocking failure is a type of failure recognized by the cracks caused by flexure in the lower and upper corners of piers, and it occurs on piers with slender and vertical stress is small. Based on the test on brick walls, (Anthoine et al. 1994) showed that masonry walls could have large displacements without significant loss in strength in case of pure flexural response. It is reported that there is a negligible stress degradation at the same peak displacement in subsequent cycles. Figure 1.4. shows force-displacement response of a fixed-fixed simple pier failing in rocking with an aspect ratio is two and axial compressive pressure of 0.6 MPa. This mode of failure is observed with low vertical compression stress and piers with slender.

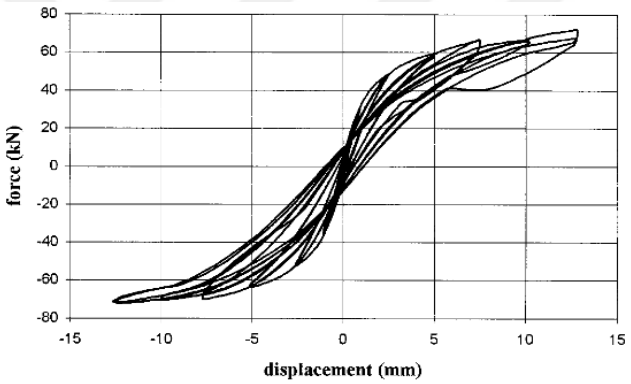

Figure 1.4. Experimental Flexural Response of Brick Masonry Wall
(Source: Magenes, et al. 1997)

1.1.2. Diagonal Tension Failure

Diagonal tension failure occurs on piers that are neither too slender nor too squat. It is distinguished by diagonal cracks opening in the wall about corner to corner. When maximum principle stress in tension exceeds the tension strength of masonry as a composite system, it is observed. Two types cracks occur in this mode of failure. The first is the formation of diagonal cracks and the mortar due to use of strong masonry unit and weak mortar. The other is formation of diagonal cracks moving through the masonry units and mortar due to use of strong mortar. Test results show that diagonal crack through the

mortar beds results relatively large ultimate drifts. Diagonal crack through the masonry units sustains small drifts and cause rapid decrease of strength (FEMA 307). Figure 1.5. is represents behavior a pier fails because of diagonal tension failure, that aspect ratio is 1.35 and compression pressure is 0.6 MPa.

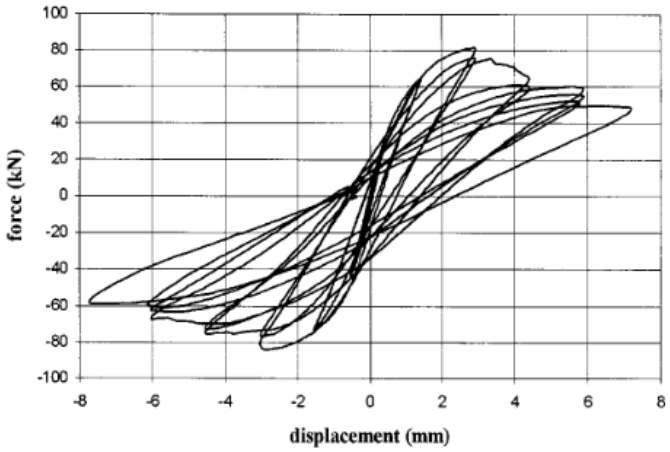

Figure 1.5. Diagonal Tenison Response of Brick Masonry Wall

(Source: Magenes, et al. 1997)

1.1.3. Sliding Shear Failure

Shear sliding or bed-joint sliding failure is described by horizontal cracks occurring on bed joints and head joints. This failure generally observed in squat walls in cases when compressive stress is low. As a general observation, increased slenderness shifts behavior from rocking to sliding shear.

1.1.4. Toe Crushing

This type of failure is related with rocking failure. If axial loads on the wall is high and wall is slender, the compression side of the wall is likely to experience toe crushing. Sudden strength and stiffness decrease with the compression failure of the masonry unit.

1.1.5. Other Possible Failures

1.1.5.1. Spandrel – Unit Cracking

In this type of failure, the spandrels cause sudden cracks in the masonry unit without causing end moments of spandrels convert into shear deformations (FEMA 306).

1.1.5.2. Corner Damage

This type of damage is observed at the roof and wall intersections. In a moderate earthquake, roof and wall intersection could be failed result of in-plane and out of plane demands. (FEMA 306)

1.2. Analytical Model Types for Masonry

Numerous analytical analysis models have been developed to model the behavior of masonry structures adequately. It is not easy to model masonry structures analytically due to complex and nonlinear interaction between components of the walls. Here, the discussion will be limited to equivalent frame model (linear and nonlinear static (pushover) and finite element model (linear and nonlinear) model.

1.1.6. Equivalent Frame Model

The equivalent frame model, which is the most widely used model by practicing engineers to model the masonry structures due to its simplicity and readily available software which are available for frame analysis. It is also possible to perform nonlinear analysis using suitable definitions of nonlinearities in the system. The simplified framing and material definitions permit to perform fast analysis.

The procedure is specifically suitable for the forced base design. In the linear analysis, the elements are modeled as linear elastic, and designed for the forces defined for the defined load combinations. As a composite material, masonry cannot resist tension. Therefore, the weak side of a linear analysis is control of tension developing in the members.

In the nonlinear analysis, the elements could be modelled using concentrated hinges with plastic behavior, and the performance of the structure at the designed displacement demand could be evaluated. The difficulty here arises in the definition of the plastic hinge properties. The brittle character of the masonry makes it very difficult to define plastic hinge definitions from constative material properties.

According to TER-2007, (Aydınoğlu, et al. 2007) linearly analyzed and designed a two-story unreinforced masonry building. The building was designed for the first earthquake zone specified in the code, and effective ground acceleration was taken as 0.4g. The allowable stress method was used in the design, and all brick walls of twenty cm thickness were shown to have sufficient strength under horizontal forces.

The unreinforced masonry building that was designed by (Aydınoğlu, et al 2007) reanalyzed according to TER-2018 code by (Mısır İ.S. et al. 2019). It was observed that all building walls were insufficient in strength under the earthquake demand of 0.4g peak ground acceleration. After re-analysis, all building walls resulted in sufficient strength under an earthquake demand with a peak ground acceleration of 0.091g. The same building walls were increased to twenty-four cm according to TER-2018 design criteria and re-analyzed. As a result of the analysis with the earthquake demand of 0.4g peak ground acceleration, all the walls were failed. Only under earthquake demand of 0.099g peek ground acceleration, the walls were showed sufficient strength. Thus, there was a great difference between an unreinforced masonry building designed with old code and the same building analyzed with new code. Lastly, when an unreinforced masonry building designed with the old code was analyzed with the new code, major differences were observed. This study shows that it seems impossible to design a conventional unreinforced masonry building with the new code for earthquake demand with a peak acceleration above 0.1g.

(Pasticier, et al. 2007) analyzed and validated the walls that were analyzed already by researchers in Catania Project. The reliability of SAP2000 V.10. code was investigated by carrying out static pushover analysis. In the nonlinear model, two rocking hinges were used at the end of the rigid offsets, and one shear hinge was at the middle. In spandrels, only one shear hinge was defined at the middle. In model pier hinges, there were used two different axial load distribution. First assumption was axial loads in piers were calculated under the effect of dead loads only. The second assumption was axial loads were calculated dead loads and increasing lateral load up to the elastic limit of the frame. Results show good validation with other researchers' results and using two different assumption for pier hinge calculation was not affected by the top displacement and ultimate strength. Finally, an unreinforced masonry building was analyzed with this code by using push-over and dynamic nonlinear analysis.

(Kappos et al. 2002) used two and three-dimensional models to compare elastic and plastic analyses of masonry structures and to utilize the equivalent frame modelling technique's accuracy. The nonlinear equivalent frame model was modelled using SAP2000, and to model the nonlinear finite element model, ANSYS was used. The two-dimensional wall was modelled as an equivalent frame and finite element in elastic analysis. Model results were validated with test data eventuated in University of Pavia and Ismes Laboratory. Full horizontal, full horizontal and vertical, full horizontal and half vertical offsets, and diaphragm constraints were used as parameters to assess the equivalent frame model. The full horizontal, full vertical model has resulted in close result to the finite element model. The diaphragm constraint was evaluated as insignificant for planar structures, and it was an important parameter for three-dimensional structure model.

(Penelis 2006) used new modelling method for pushover analysis using an equivalent frame model of unreinforced masonry buildings. With the lump plasticity approach, rotational hinges were evaluated at the end of the components of structures for nonlinear behavior. Nonlinear springs were defined by the moment rotation curve for each component under constant axial load. The rotation was thought as sum of rotations because of flexure and shear. When defining pier hinges in piers, axial loads were determined from linear analysis with the effect of gravity load and prediction of lateral load from base shear capacity. No vertical rigid offsets were used in the model. As a

result, model was validated with test results carried out at University of Pavia and Ismes Laboratory.

1.1.7. Finite Element Model

The finite element approach could be used to analyze complicated structures like buildings, bridges or simple structures like the wall only. In general, it is not preferred in the analysis of complex structures due to the fact that the analysis times are longer and detailed material data compared to equivalent frame models. Structures can be analyzed as linear and nonlinear with this model approach. (Lourenco 1996) summarizes finite element modelling techniques available in literature as detailed micro modelling, simplified micro modelling and macro modelling.

In detailed micro-modeling, masonry unit and mortar are modeled considering continuum element, and the unit-mortar interface is modeled discontinuous element. In simplified micro modelling, masonry units are modelled with continuum elements. The behavior of the mortar joints and unit-mortar interface is modeled as discontinuous elements. In the macro modelling technique, masonry units, mortar, and mortar-unit interfaces are modeled with a continuous element. In this study, the macro model technique was selected for linear model.

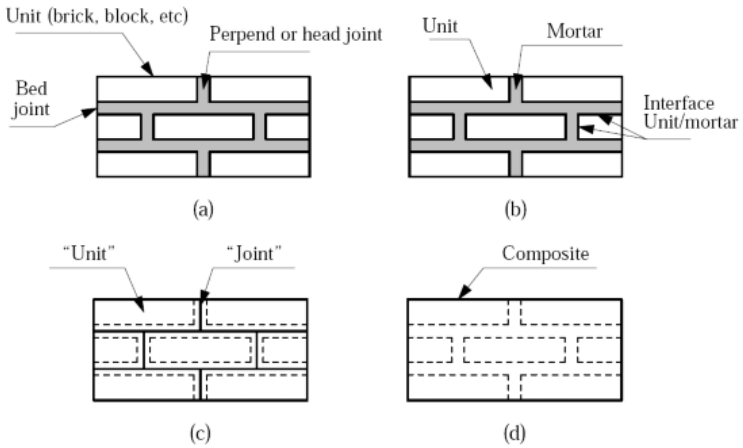

Figure 1.6. Modelling Techniques for Brick Masonry a) Masonry Sample in Typical b) Detailed Micro Modelling c) Simplified Micro Modelling d) Macro Modelling (Source: Lourenco 1996)

(Yi et al. 2006) analyzed a two-floor, unreinforced masonry building using three models: simplified rigid body, three-dimensional nonlinear finite element, and two-dimensional nonlinear pushover models. Analyses were validated with test results of same building. Three-dimensional nonlinear finite element model was modelled on finite element code of ABAQUS 2000. All model method analyzes were quite compatible with test results. It is stated that the rigid body model is suitable for easy estimation, but it is ineffective in determining the local failure modes, the three-dimensional nonlinear finite element method is suitable for in-depth study of important project and not suitable for daily projects, two-dimensional nonlinear model was best alternative for seismic assessment and retrofit projects.

(Aldemir 2010) developed and named Solid65 finite element model. It was used for nonlinear analyzing one hundred forty-four different masonry pier model in ANSYS 11 code. The model was validated by a wall test tested in ETH in Zurich by (Lourenco 2006). Strength formulas for simplified method were created by keeping the length, thickness, aspect ratio, material strength, and axial pressure of piers were variable. Finally, the analysis of a masonry building with the simplified and nonlinear finite element model was performed using these obtained strength formulas. Rigid offsets provided by (Dolce 1989) were used in the piers. The results of the analysis method result in very consistent results between each other.

CHAPTER 2

DESIGN REQUIREMENTS OF UNREINFORCED MASONRY BUILDINGS ACCORDING TO TER-2007 AND TER-2018

The latest Turkish Earthquake Regulation (TER-2018), is published in 2018 and enforced by 2019. It introduced major changes in the analysis and design of masonry structures. The design approach has been shifted from the allowable stress design to ultimate strength design. There are also major revisions in the seismic demand definitions. Three new masonry building types are introduced. These are reinforced masonry, confined masonry, and reinforced panel system masonry buildings. In this chapter, the requirements of unreinforced masonry buildings in TER-2007 and TER-2018 will be summarized and compared.

2.1. The Seismic Demand Calculations for Masonry Structures

The seismic demand in TER-2007 was defined through four seismic zones according to defined effective ground accelerations, and the design spectra were created in relation to these ground accelerations and the soil types. The ground accelerations had fixed values for the zones defined, and there was no variability of the risk for a local area considering the possible seismic sources at its neighboring areas. On the contrary, TER-2018 defines specific seismic risk with a system that is based on the geographic coordinate of the area and the seismic sources in its defined neighborhood. Considering that procedure, TER-2018 is more advanced and it is accepted to be providing better risk analysis. The introduction of local soil effects is modified also to have effects both on the acceleration magnitudes and regions in the design spectra.

The new regulation, TER-2018, also introduced the vertical seismic demand effects into the seismic design.

2.1.1. Calculation of Seismic Base Shear Force by TER-2007

Seismic base shear force, V_t for unreinforced masonry structures is calculated by Eq.2.1. The $S(T_1)$ and $R_a(T_1)$ are accepted to be 2.5 and 2.0 respectively. $S_{ae}(T_1)$ is calculated by Eq.2.2. The effective ground acceleration, A_0, is defined as shown in Table 2.1.

$$V_t = \frac{W\, S_{ae}(T_1)}{R_a(T_1)\, g} \geq 0.10\, A_0\, I\, W \qquad \text{Eq.2.1}$$

$$S_{ae}(T_1) = A_0\, I\, S(T_1)\, g \qquad \text{Eq.2.2}$$

Table 2.1. Effective Ground Acceleration Coefficient (A0)

Seismic Zone	A_0
1	0.40
2	0.30
3	0.20
4	0.10

where $S_{ae}(T_1)$ is linear elastic spectral acceleration corresponding to the first natural vibration period T_1, I is the building importance factor, g is the acceleration of gravity, W is the total weight of the building, and $R_a(T_1)$ is seismic load reduction factor.

2.1.2. Calculation of Seismic Base Shear Force by TER-2018

As mentioned above, elastic design spectrum, $S_{ae}(T)$ in TER-2018 is specific to geographic coordinates. It is determined based on the building natural vibration period, T, and on the short and one second period spectral accelerations, S_{DS} and S_1 respectively. S_{DS} and S_{D1} are provided in a table form for the specific geographic coordinates. Another modification is made to strength reduction factor of unreinforced masonry structures, $R_a(T)$; it becomes system natural period dependent. Considering that the typical period range is less than T_B, the strength reduction factor has a value between 1.5 and 2.5, typically a value close to 2. The values of $S_{ae}(T)$, $R_a(T)$, and V_{tE} are defined to be calculated as follows.

$$S_{ae}(T) = (0.4 + 0.6\,\frac{T}{T_A})\,S_{DS} \qquad (0 \le T \le T_A) \qquad \text{Eq.2.3}$$

$$S_{ae}(T) = S_{DS} \qquad (T_A \le T \le T_B) \qquad \text{Eq.2.4}$$

$$S_{ae}(T) = \frac{S_{D1}}{T} \qquad (T_B \le T \le T_L) \qquad \text{Eq.2.5}$$

$$S_{ae}(T) = \frac{S_{D1}T_L}{T^2} \qquad (T_L \le T) \qquad \text{Eq.2.6}$$

Table 2.2. Earthquake Design Classes

Short Period Design Spectral acceleration coefficient (S_{DS}) at Earthquake Ground Motion level of DD-2	Building Usage Class	
	BKS=1	BKS=2,3
$S_{DS} < 0.33$	DTS=4a	DTS=4
$0.33 \le S_{DS} < 0.50$	DTS=3a	DTS=3
$0.50 \le S_{DS} < 0.75$	DTS=2a	DTS=2
$0.75 \le S_{DS}$	DTS=1a	DTS=1

$$R_a(T) = \frac{R}{I} \qquad T > T_B \qquad \text{Eq.2.7}$$

$$R_a(T) = D + \left(\frac{R}{I} - D\right)\frac{T}{T_B} \qquad T \leq T_B \qquad \text{Eq.2.8}$$

$$S_{aR}(T) = \frac{S_{ae}(T)}{R_a(T)} \qquad \text{Eq.2.9}$$

$$V_{tE} = m_t\, S_{aR}(T) \geq 0.04\, m_t\, I\, S_{DS}\, g \qquad \text{Eq.2.10}$$

where T_A and T_B are horizontal elastic design acceleration spectrum corner period, BKS is building usage class, DTS is earthquake design class, R is bearing system behavior coefficient, D is strength excess coefficient, $S_{aR}(T)$ is reduced design spectral acceleration, V_{tE} is total equivalent earthquake load acting on the entire structure and m_t is total mass of building.

TER-2018 provides an empirical alternative for the period of the structure, T_{pA} instead of T_p. Proposed alternative is limited for the structures with seismic and structural properties as DTS= 1, 1a, 2, 2a & BYS ≥ 6 and DTS=3,3a,4,4a. Here, BYS is defined to be building height class and for a value greater than 6 means a height less than 17.5 meters. Therefore, considering the unreinforced masonry building height limitation, which is restricted with BYS=8 (or less than 7 meters for DTS=1, 1a, 2, 2a), empirical T_{pA} could be used for all unreinforced masonry structures to define the seismic demands. The empirical period calculation is given in Eq. 2.11. The C_t value for masonry buildings is proposed to be 0.07. In chapter 3, both the empirical and analysis results of the case study structure period will be calculated and compared.

$$T_{pA} = C_t\, H_N^{3/4} \qquad \text{Eq.2.11}$$

2.1.3. Calculation of Vertical Seismic Force by TER-2018

The vertical seismic load on a masonry building is defined as below, depending on S_{DS} and G.

$$E_d^{(Z)} = (2/3)\, S_{DS}\, G \qquad \text{Eq.2.12}$$

where G is dead load.

2.2. Load Combinations

The load combinations for TER-2007 and TER-2018 masonry building design are given below in Table 2.3. The difference in load combinations reflect the shift from allowable to ultimate strength design. E_x and E_y represent the earthquake load effect on two perpendicular axes in TER-2007. Conversely, in TER-2018 these loads effect is shown $E_d^{(H)}$ that is a combination of the horizontal and vertical earthquake effects as presented below.

$$E_d^{(H)} = \pm E_d^{(X)} \pm 0.3\, E_d^{(Y)} \qquad \text{Eq.2.13}$$

$$E_d^{(H)} = \pm 0.3\, E_d^{(X)} + E_d^{(Y)} \qquad \text{Eq.2.14}$$

Table 2.3. Load Combinations in TER-2007 & TER-2018

TER-2007 Load Combinations	TER-2018 Load Combinations
G+Q	$G+Q+0.2S+E_d^{(H)}+0.3E_d^{(Z)}$
G+Q±Ex±0.3Ey	
G+Q±0.3Ex±Ey	$0.9G+H+E_d^{(H)}-0.3E_d^{(Z)}$

2.3. The Structure Height Limitations

The number of stories of unreinforced masonry buildings are limited based on the seismic zones in the TER-2007, as it is shown in Table 2.4. Additionally, story heights are restricted to a maximum of 3.0 m. Adobe wall masonry structures has further height limitations.

Table 2.4. Permitted Maximum Number of Stories in TER-2007

Seismic Zone	Maximum number of Stories
1	2
2, 3	3
4	4

In the TER-2018, building height limitations are defined according to building height class and earthquake design classes. Allowable heights for unreinforced masonry buildings could be listed as below in Table 2.5.

Table 2.5. Building Height Ranges According to DTS and BYS

Building Height Class	DTS = 1, 1a, 2, 2a	DTS = 3,3a	DTS = 4,4a
BYS=8	$H_N \leq 7$ m	$H_N \leq 10.5$ m	

As it is explained above, the new version of the Turkish Seismic Code put further height limits on the usage of unreinforced masonry. While there is a certain height limitation in TER-2018, this was limited to the number of floors only in TER-2007.

2.4. Masonry Wall Thickness Definitions

Minimum required thickness values for the unreinforced brick masonry walls in both regulations are presented in Table 2.6. Additionally, TER-2018 dictates thickness to

height limitations, or the wall slenderness ratio. The maximum value of the slenderness ratio for the brick masonry wall, h_{ef}/t_{ef}, is defined to be 12.

Table 2.6. Minimum Thicknesses of Brick Masonry Wall in TER-2007&TER-2018

Seismic Code Version	Ground Floor Thickness (cm)	1st Floor Thickness (cm)
TER-2007	20	20
TER-2018	24	24

Note: The table only presents the brick masonry building properties

2.5. Openings in Load Bearing Walls

Unsupported length of the unreinforced masonry wall did not change with the new version of the seismic code. The maximum unsupported length of any load-bearing wall between axes of walls, which are supporting the wall considered in the perpendicular direction in the plan, should not be greater than 5.5 m in seismic zone 1 in TER-2007 and DTS=1,1a,2,2a in TER-2018. In other zones and seismic design classes, permitted length is restricted to 7.5 m. Figure 2.1. shows the limits of the unsupported wall lengths in TER-2018.

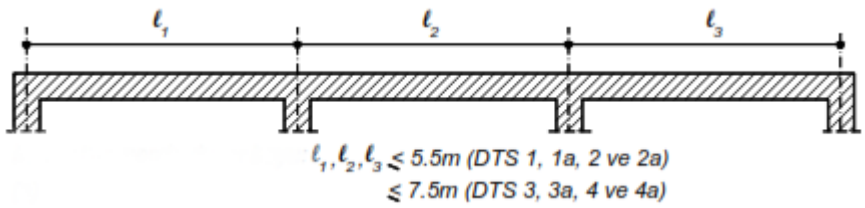

Figure 2.1. Unsupported Wall Length (Source: TER-2018)

No changes are defined for the windows and doors openings as well. In both versions of the seismic code, the openings in plan required to be less than 3.0 m. Openings along the unsupported length limited to 40% of the unsupported length. The length of the wall between the window or door opening that is closest to the building corner and the corner of the building should not be less than 1.5 m in earthquake design classes 1,1a,2,2a, and Seismic Zones 1 and 2. For other seismic zones/classes, it should be at least 1.0 m. Plan

lengths of the wall segments between the windows and door openings, excluding the corners of buildings, should not be less than 1.0 m in Seismic Zone 1,2 and DTS=1,1a,2,2a. Except for these zones and classes, it is taken as 0.8m. Figure 2.2. presents these requirements about opening size and locations for TER-2018.

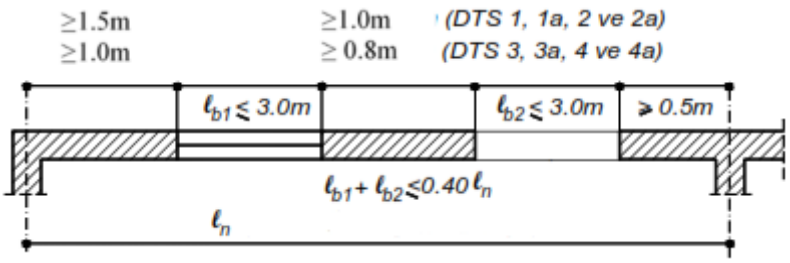

Figure 2.2. Openings and Permitted Lengths for Wall (Source: TER-2018)

2.6. Engineering Properties of Materials and Strength

Due to the shift from allowable stress design to ultimate strength design, the material strength definitions of the 2007 and 2018 regulations are different. While the 2007 regulation considers the allowable stress of materials, the 2018 regulation considers the characteristic strength of materials. The material strength definitions are explained below with an emphasize on the changes.

2.6.1. Compressive Strength for Masonry Wall

Both regulations demand experimental determination of the compressive strength of the wall block samples. In TER-2018, the characteristic compressive strength of the masonry bearing walls is determined by a test that is performed according to TS-EN 1052-1. On the other hand, in TER-2007, allowable compressive stress is equal to quarter of the compressive strength calculated by compressive tests on wall block samples.

In the absence of testing on wall block samples, it is recommended to test the masonry unit and mortar samples in both regulations. In 2007 regulation, the allowable compressive stress of the masonry wall could also be obtained from the values presented in Table 2.7. which designates the stress on mortar class and average free compressive strength of masonry unit given in TS-2510. In TER-2018, wall characteristic compressive strength is determined based on the tests of masonry unit and mortar according to TS EN 772-1 and TS EN 1015-11 respectively. Bearing wall characteristic compressive strength can be taken from Table 2.8 by using masonry compressive strength and mortar compressive strength.

Table 2.7. Allowable Compressive Stresses for Walls Depending on Mortar Class and Free Pressure Strength of Masonry Unit

Average Free Pressure Strength of Masonry Unit (MPa)	**Mortar Class Used in Wall (MPa)**				
	A (15)	**B (11)**	**C (5)**	**D (2)**	**E (0.5)**
25	1.8	1.4	1.2	1.0	0.8
16	1.4	1.2	1.0	0.8	0.7
11	1.0	0.9	0.8	0.7	0.6
7	0.8	0.7	0.7	0.6	0.5
5	0.6	0.5	0.5	0.4	0.4

Table 2.8. Characteristic Compressive Strength of Bearing Masonry Wall (MPa)

Unit- Unit Class	**Mortar Class**	**Mortar compressive strength, fm (MPa*)**	**Masonry unit compressive strength, f_b (MPa)**					
			5	**10**	**15**	**20**	**25**	**30**
Group I	General purpose mortar	M10-M20	3.4-4.2	5.5-6.8	7.3-9.0	8.9-11.0	10.4-12.9	11.9-14.6
		M2.5-M9	2.2-3.3	3.6-5.3	4.8-7.1	5.9-8.7	6.9-10.1	7.8-11.5
		M1-M2	1.7-2.1	2.8-3.4	3.7-4.5	4.5-5.5	5.2-6.4	5.9-7.3
Group II and Stone Wall		M10-M20	2.8-3.4	4.5-5.5	6.0-7.4	7.3-9.0	8.5-10.5	9.7-12.0
		M2.5-M9	1.8-2.7	3.0-4.4	3.9-5.8	4.8-7.1	5.6-8.3	6.4-9.4
		M1-M2	1.4-1.7	2.3-2.8	3.0-3.7	3.7-4.5	4.3-5.3	4.9-6.0
Brick (Group I)	Thin layer mortar **		2.9	5.3	7.5	9.6	11.6	13.5
Brick (Group II)			2.2	3.5	4.7	5.7	6.7	7.6
Concrete (Group I), Autoclaved Cellular Concrete Blocks			3.1	5.7	8.0	10.2	12.3	14.4
Concrete (Group II)			2.6	4.6	6.5	8.3	10.0	11.7

*Mortars are named after the letter M to show the characteristic compressive strength in MPa

**Thin layer mortar is a mortar with inter-unit mortar between 0.5 mm-3.0 mm.

Although the 2018 regulation does not allow the determination of masonry compressive strength without the test, the 2007 regulation allow to use the allowable compressive strength table specified according to the masonry unit and mortar type in the absence of test. Allowable compressive stresses of walls whose free compressive strength is unknown are described as in Table 2.9.

Table 2.9. Allowable compressive strength of walls in which free compressive strength is unknown

Masonry Unit Type and Mortar Used in the Wall	**Allowable Compressive Strength of Wall f_{em} (MPa)**
Hollow Brick with Vertical Holes (Void ratio is less than 35%, with lime-cement mix mortar)	1.0
Hollow Brick with Vertical Holes (Void ratio is between 35 – 45 %, with lime-cement mix mortar)	0.8
Hollow Brick with Vertical Holes (Void ratio is more than 45 %, with lime-cement mix mortar)	0.5
Solid brick or Harman brick (with lime-cement mix mortar)	0.8
Stone wall (with lime mortar supported with cement)	0.3
Autoclaved Cellular Concrete Blocks (with adhesive)	0.6
Solid Concrete Masonry Units (with cement mortar)	0.8

In calculating the compressive strength of masonry walls, it is necessary to regard the slenderness effects of the wall into consideration. The slenderness ratios and equivalent strength reduction coefficients for the regulations are tabulated as given in Table 2.10. and Table 2.11.

Table 2.10. Reduction Coefficients According to Slenderness Ratio in TER-2007

Slenderness Ratio (λ)	6	8	10	12	14	16	18	20	22	24
Reduction Coefficient	1.0	0.95	0.89	0.84	0.78	0.73	0.67	0.62	0.56	0.51

Table 2.11. Reduction Coefficients According to Slenderness Ratio in TER-2018

Slenderness Ratio (h_{ef}/t_{ef})	$\lambda<6$	$6\leq\lambda<10$	$10<\lambda\leq15$
Reduction Coefficients	1.0	0.8	0.7

Both regulations define the effective thickness, t_{ef}, to be equal to the thickness of the load-bearing wall without plaster thickness. The height of the wall is taken as the distance from the top of the floor, if any, to the bottom of the horizontal beam or the top floor. Besides, the 2018 regulation includes the effective height expression in calculating the slenderness. It is defined to be equal to 0.75 of total height according to TS-EN 1996-1-1, Article 11, Description i.

The design compressive capacity depends on wall area, design compressive strength and coefficient related to slenderness in 2018 regulation. The related expression is defined in Eq. 2.15. Opposed to new version in 2007 regulation, the design compressive stress is defined based on the allowable compressive stress and the coefficient of slenderness, as shown in Eq. 2.16 in 2007 regulation.

$$N_{Rd}= \lambda A f_d \qquad \text{(TER-2018)} \qquad \text{Eq.2.15}$$

$$f_{em}' = f_{em}\,\lambda \qquad \text{(TER-2007)} \qquad \text{Eq.2.16}$$

In both approaches, the resisting forces for TER-2018 and allowable stresses for TER-2007 needed to be higher than the internal forces or stresses obtained from analysis for finalizing the design.

2.6.2. Shear Strength for Masonry Wall

New version of seismic regulation also changes the approach to verify the shear demands. The existing allowable stress check is modified to the load-bearing capacity check in the calculation of the shear strength of the walls.

In TER-2007, the shear forces on the walls were calculated in each orthogonal axis of the building separately by considering the shear force and the torsional moments in the story. The shear stress on the walls were calculated by dividing the calculated forces along the axis of the wall by the cross-sectional area and design check was performed by comparing this value with the allowable shear stress of the wall.

The allowable shear stress formula was defined as follows.

$$\tau_{em} = \tau_0 + \mu\sigma \qquad \text{Eq.2.17}$$

where σ is the vertical stress on the wall caused by vertical loads, μ is the friction coefficient that is 0.5 and τ_0 is wall cracking allowable stress.

Wall allowable cracking stress values according to the masonry unit type used in the walls were defined as given in Table 2.12.

Table 2.12. Cracking Allowable Stress of Walls

Type of Masonry Unit and Mortar Used in the Wall	**Allowable Cracking Stress of Wall τ_0 (MPa)**
Hollow Brick with Vertical Holes (Void ratio is less than 35%, with lime-cement mix mortar)	0.25
Hollow Brick with Vertical Holes (Void ratio is more than 35%, with lime-cement mix mortar)	0.12
Solid brick or Harman brick (with lime-cement mix mortar)	0.15
Stone wall (with lime mortar supported with cement)	0.10
Autoclaved Cellular Concrete Blocks (with adhesive)	0.15
Solid Concrete Masonry Units (with cement mortar)	0.20

In TER-2018, characteristic shear strength of the wall, f_{vk}, needed to be determined directly with the testing according to TS-EN 1052-3 or TS-EN 1052-4. Otherwise, initial

shear strength, f_{vk0}, could be taken from Table 2.13. and should be determined by Eq.2.18.

$$f_{vk} = f_{vk0} + 0.4\sigma_d \leq 0.10 f_b \qquad \text{Eq.2.18}$$

where σ_d is the vertical compressive stress calculated under the combined effect of vertical and earthquake loads.

Table 2.13. Initial Shear Strength of Walls, fvk0 (MPa)

Masonry Unit	**General Purpose Mortar***		**Thin Layer Mortar**
Brick	M10-M20	0.30	0.30
	M2.5-M9	0.20	
	M1-M2	0.10	
Concrete	M10-M20	0.20	0.30
Autoclaved Cellular Concrete Blocks	M2.5-M9	0.15	0.30
Natural or Artificial Stone	M1-M2	0.10	No Usable

*Mortars are named after the letter M to show the characteristic compressive strength in MPa

The material strength reduction factor of masonry walls, γ_m, for solid clay bricks is taken as 2.0 when determining the design strengths of the masonry walls. The bearing wall design shear strength, V_{Rd}, is required to be greater than design shear force, V_{Ed}, acting on the wall. V_{Rd} is calculated according to equations 2.19 and 2.20 and is taken as the minimum of the values defined by these equations. In Eq. 2.20, b is the aspect ratio of the wall. It could be calculated by dividing wall height by the length and should be between 1 and 1.5.

$$V_{Rd1} = f_{vd}\, t\, l_c \qquad \text{Eq.2.19}$$

$$V_{Rd2} = l\, t\, \frac{1.5 f_{vd0}}{b} \sqrt{1 + \frac{N_{Ed}}{1.5 l t f_{vd0}}} \qquad \text{Eq.2.20}$$

Equation 2.19 is related to the sliding failure mechanism (Mohr-Coulomb criteria) in horizontal joints of the masonry wall, and Eq. 2.20 is related to the formation of the diagonal tension depending on the tensile strength on the wall. (Tomazevic 2008). The corresponding failure surfaces are illustrated in Fig. 2.3.

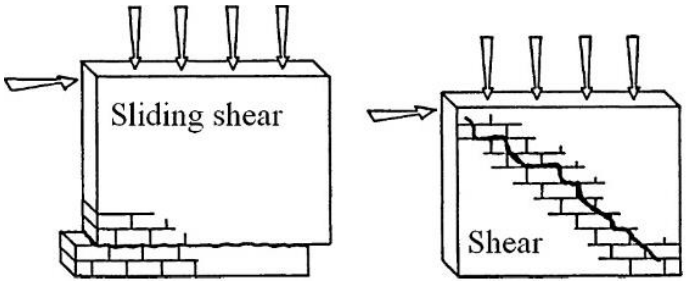

Figure 2.3. (1) Sliding Failure Mechanism (2) Diagonal Tenison Failure Mechanism (Source: Tomazevic 2008)

In equation 2.20, the wall area that is effective for the shear resistance is defined to by the length of compressive zone of the wall, l_c, under consideration considering the lateral and vertical loads. Due to the lateral load and the resulting flexure, depending on the axial load level only a limited portion of the wall could develop compression. Therefore, shear resistance could get smaller.

In TER-2018, there is no explicit definition about the calculation of the compressed zone length of the bearing wall, l_c. Considering that the regulation is based on EN-1996-1-1. and using the definition there the compression zone calculations are performed accepting an elastic wall material and corresponding support reaction through a linear analysis.

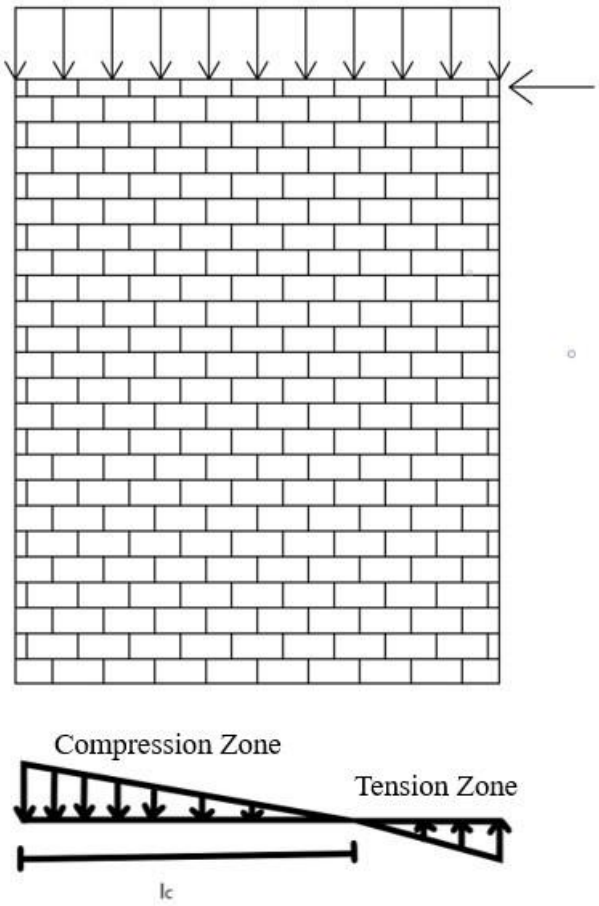

Figure 2.4. Linear Stress Distribution of Wall Under Vertical and Lateral Loadings

Therefore, l_c could be determined assuming a linear strain distribution considering the effect of the moment and axial force on the bearing wall. Assuming the compression to be positive and determining the σ_{max} and σ_{min} (in Eq. 2.21., 2.22.), l_c can be taken as the length of zero to max stress (in eq 2.23.)

$$\sigma_{max} = \frac{N}{A} + \frac{Mc}{I_x} \qquad \text{Eq.2.21}$$

$$\sigma_{min} = \frac{N}{A} - \frac{Mc}{I_x} \qquad \text{Eq.2.22}$$

$$l_c = \frac{\sigma_{max}}{\sigma_{max}+\sigma_{min}} l \qquad \text{Eq.2.23}$$

CHAPTER 3

CASE STUDY UNREINFORCED MASONRY BUILDING

3.1. Introduction

The purpose of this chapter is to demonstrate the extent of the changes in the unreinforced masonry design of the TER-2018 through a case study structure. The structure is selected to satisfy the constructive requirements of both the 2007 and 2018 versions of the Turkish Seismic Regulations. Detailed information about the geometric and material properties of the case study masonry building is given in Table 3.1. The architectural plans and views are presented in Figures 3.1 to 3.3.

The chapter is organized to perform the design and verification of the case study building first with TER-2007, and with TER-2018 later. Then results will be compared, and discussions provided.

3.2. The Example Unreinforced Masonry Building

The selected case study building is a two-story structure with a rectangular plan. The major geometric dimensions and the material properties of the structure are presented in Table 3.1.

Table 3.1. Masonry Building Properties

Masonry Building Properties	
Floor Number	2
Floor Height	3.0 m
Masonry Unit	Solid Clay Brick
Wall Unit Weight	1.9 t/m³
Slab Type	Reinforced Concrete Slab with Horizontal Beams.
1st Floor Wall Thickness	0.4 m
2nd Floor Wall Thickness	0.4 m
RC Slab Thickness	0.12m

The architectural plan of the building is presented in Fig.3.1 and Fig. 3.2. The structure has a 17.90m x 8.90m and could be considered a midsize residential structure in Turkish practice. The elevation of the structure about a different axis is presented in Fig 3.5. As be observed from the plans and elevations, the building is a uniform structure both horizontally and vertically.

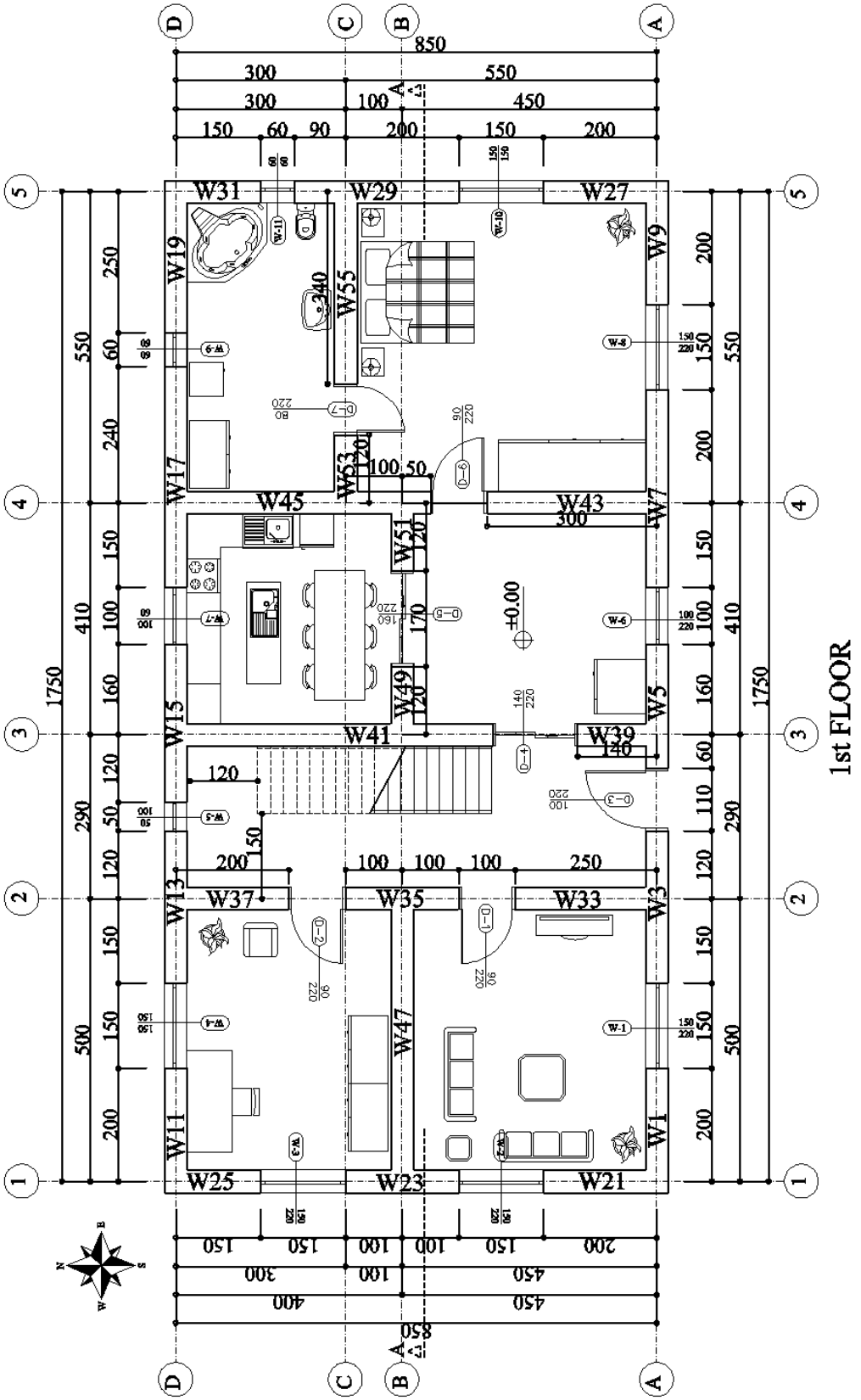

Figure 3.1. 1st Floor Plan (All dimensions are given in cm)

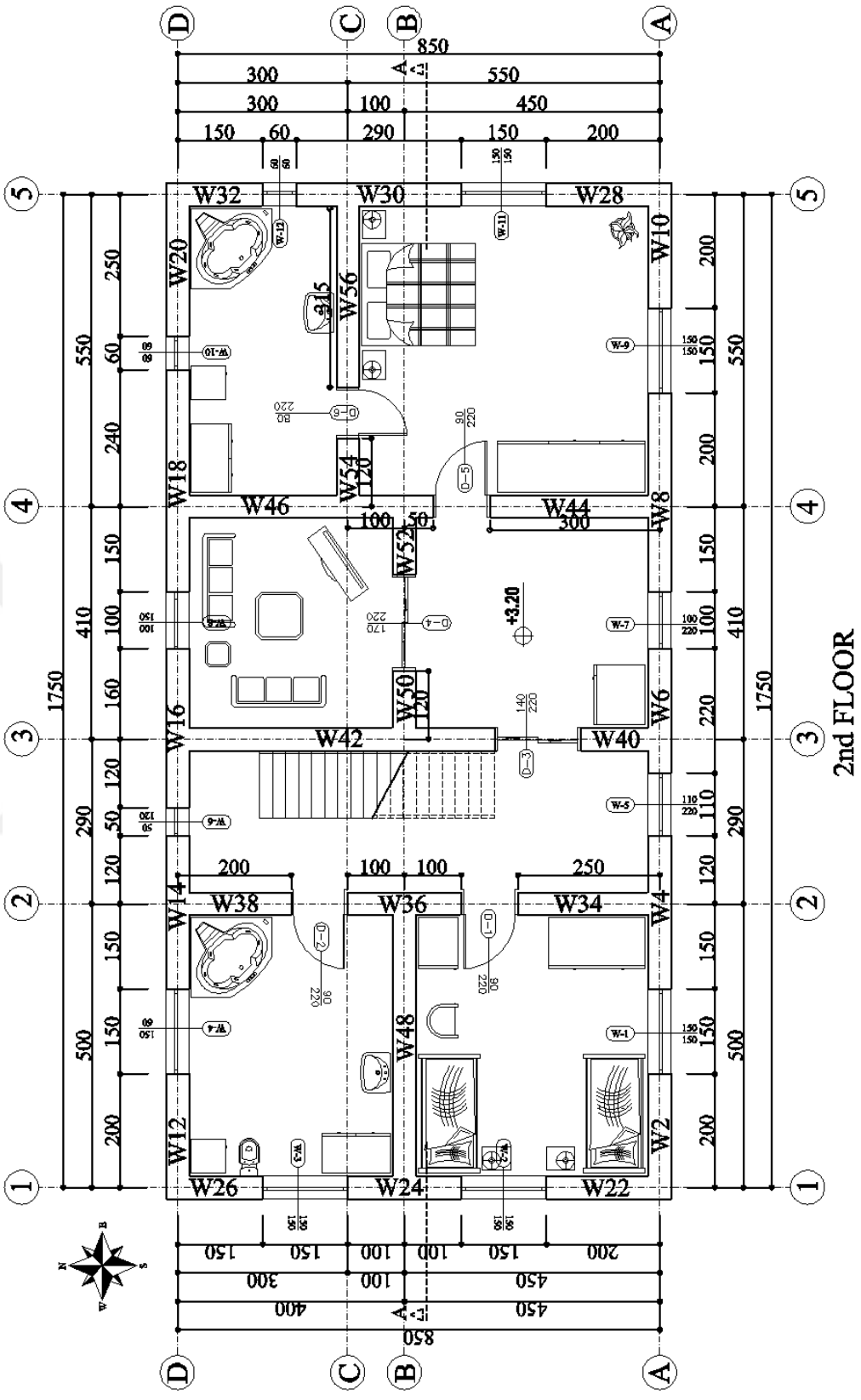

Figure 3.2. 2nd Floor Plan (All dimensions are given in cm)

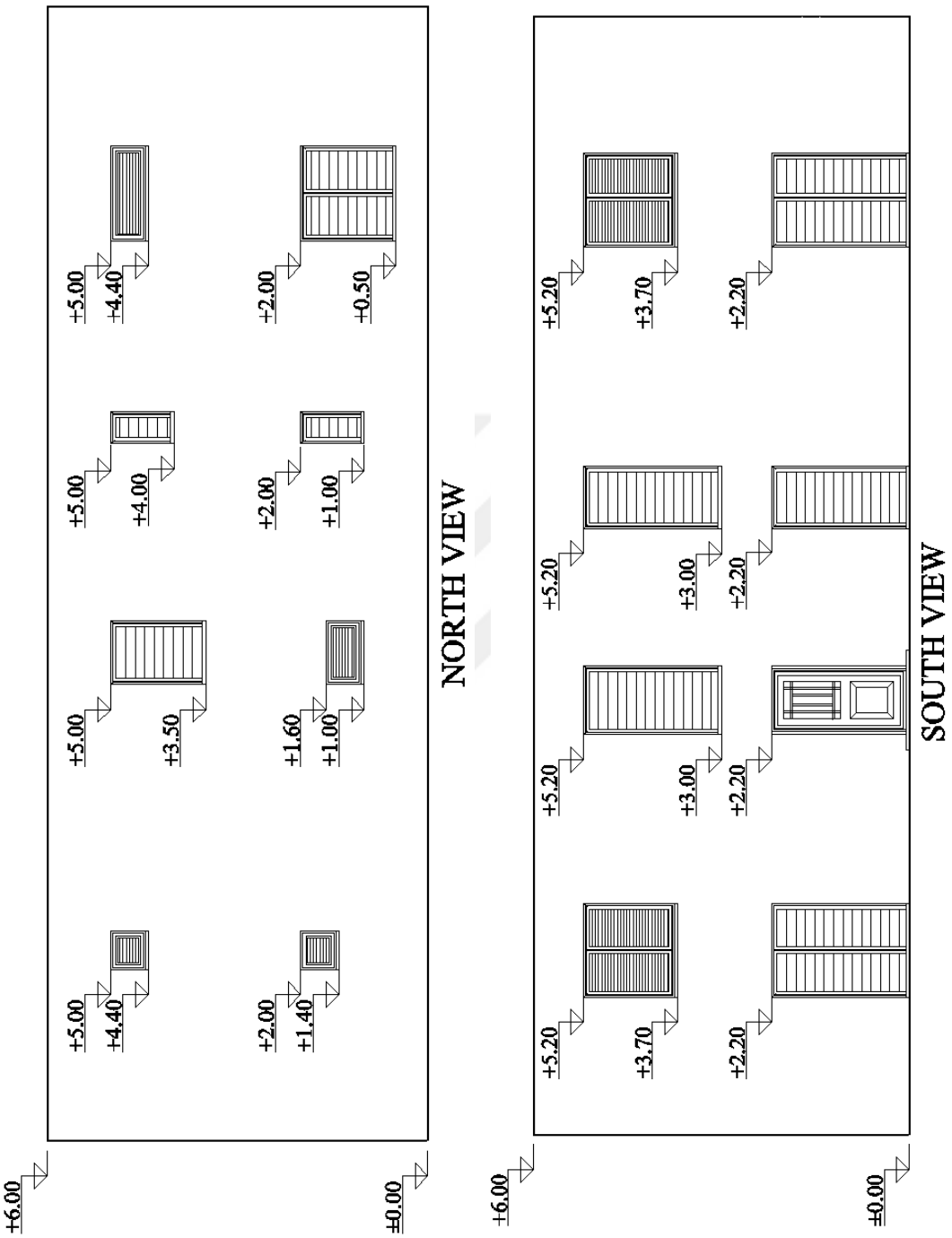

Figure 3.3. North and South Plan View (Elevations are in m.)

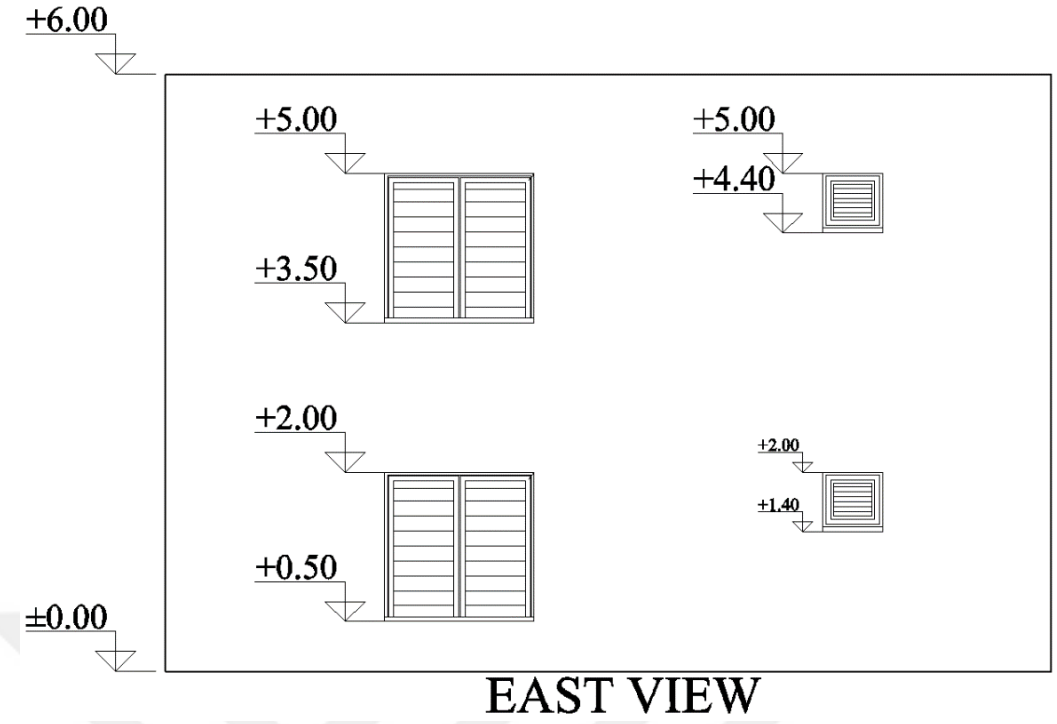

EAST VIEW

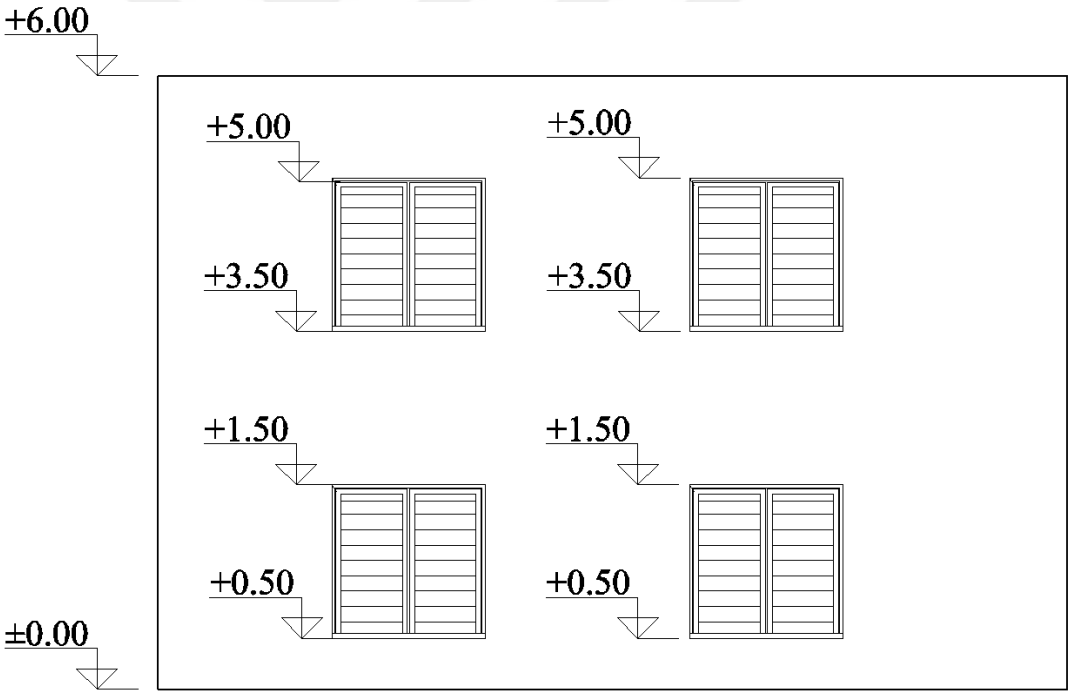

WEST VIEW

Figure 3.4. East and West Plan View (Elevations are in m.)

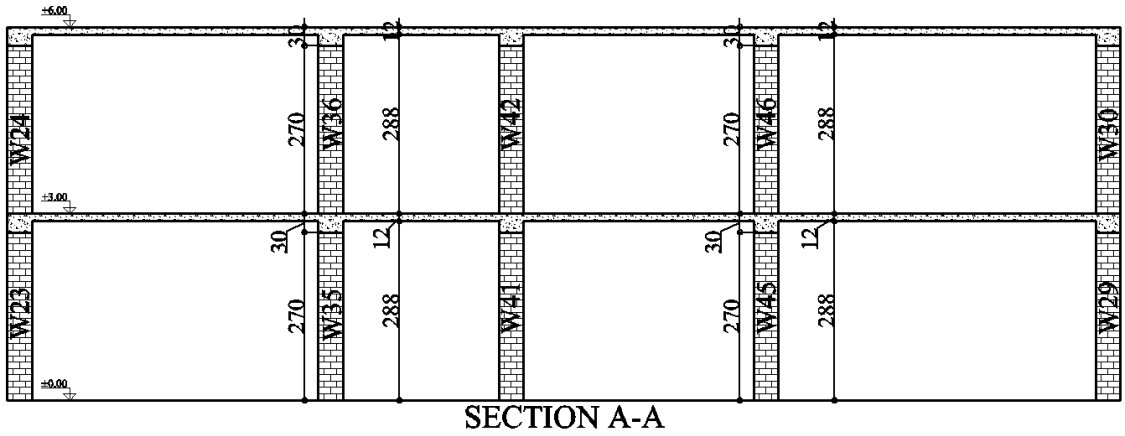

Figure 3.5. Section A-A (All dimensions are in cm)

3.3. Analysis and Design of the Example Building By TER-2007

The structure is proportioned following the constructive requirements of the regulation. The analysis is performed assuming that walls could only resist lateral loads on the axis of their plane. The stiffness of the walls is calculated based on the stiffness definition in the regulation presented here in Eq. 3.1. Here K_{we} is equivalent wall stiffness, and k is the coefficient of geometric properties of the wall. It is taken as 1.0 for rectangular cross-section. A is the horizontal cross-section of wall and h is the height of the wall.

$$K_{we} = k\,A/h \qquad \text{Eq.3.1}$$

The walls' lateral forces are calculated using the stiffness definitions and considering the eccentricity between the stiffness center and the mass center. Such an analysis could be organized with a spreadsheet. Therefore, a spreadsheet is used to perform the analysis. The axial loads on the walls are calculated based on the tributary areas of the walls. The results obtained are verified through the limits in the regulation, which were summarized in Chapter 2.

The spreadsheet is arranged according to the analysis requirements of TER-2007. The calculation of the distribution of forces acting on the walls with the torsional effect is performed using the solution technique of the study of Aydınoğlu et. al. (2007).

The performed preliminary study showed that the ground floor is critical in terms of the structural members. This observation is per the expected higher shear and axial loads at the ground floor. Hence it is selected as the critical floor, and the design is performed for this floor only.

For modeling purposes, the stiffness of each wall in their in-plane axis is determined using Eq. 3.1. As it could be observed, the 2007 regulation consider only the shear stiffness of the walls.

The mechanical properties of the solid brick walls of the case study structure are defined according to Table 2.9. and Table 2.12 of TER-2007. From the tables, the allowable compressive f_{em} and cracking strength τ_0 were taken as 0.8 MPa and 0.15 MPa, respectively. The elastic modulus is defined as $200f_d$ when no test is performed in TER-2007. In this case, the wall compressive strength f_d, is taken twice the allowable compressive strength, and elastic modulus is calculated as 320 MPa.

The case study building is accepted to be located in Çökertme village of Milas district in Muğla. The latitude and longitude values of the location are 37.0074 and 27.7944, respectively. According to TER-2007 definitions, the site is in the Earthquake Zone 1 and, A_o ground acceleration is taken as 0.4.

As mentioned, slabs are designed as reinforced concrete with a thickness of 12 cm. Dead and live loads on slabs are 2.04 kN/m² and 2 kN/m², respectively.

The compressive stresses on the walls are calculated by dividing the axial force to the wall cross-sectional area. The allowable compression strength of the walls is calculated per TER-2007. The nominal capacity is reduced with a factor calculated based on the slenderness ratio of the walls. Based on the performed calculation, the capacities, demands, and the axial capacity check for the walls with the labeling defined in Fig. 3.1 are presented in Tables 3.2. to 3.4.

Table 3.2. Total dead and live loads in building

Total Load of Masonry			
Load Type	G	Q	
1st A-A axis	33.0	0	
1st B-B axis	16.4	0	
1st C-C axis	9.9	0	
1st D-D axis	37.1	0	
1st 1-1 axis	13.8	0	
1st 2-2 axis	14.7	0	
1st 3-3 axis	15.6	0	
1st 4-4 axis	16.4	0	
1st 5-5 axis	16.1	0	
2nd A-A axis	33.0	0	
2nd B-B axis	15.7	0	
2nd C-C axis	9.9	0	
2nd D-D axis	37.4	0	
2nd 1-1 axis	14.7	0	
2nd 2-2 axis	15.1	0	
2nd 3-3 axis	15.6	0	
2nd 4-4 axis	16.4	0	
2nd 5-5 axis	16.1	0	
1st-2nd Slab	161.9	64.97	
TOTAL(tons)	508.7	64.97	
W=G+0.3Q	508.7	19.5	**528.2**
2nd Floor W=	216.7	tons	
1ST Floor W=	311.5	tons	

Table 3.3. Earthquake Loads on Building

Equivalent Earthquake Load Calculation		
S(T)	2.5	
I	1	
$R_a(T)$	2	
A_0	0.4	
A(T)	1	
V_t	264	t
$V_t > 0.1A_0IW$	Satisfied	
$0.1A_0IW$	21.1	t
$\Delta F_N=0.0075NV_t$	4.0	t
F_2	110.7	t
F_1	153.4	t

Table 3.4. Axial Capacity Check of Walls

	N (kN)	A (m²)	λ	f_{duv}=N/A (MPa)	$f_{em}'=f_{em}\lambda$ (MPa)	$f_{em}'\geq f_{duv}$
W1	125.8	0.88	0.99	0.14	0.79	**Satisfied**
W3	102.9	1.08	0.99	0.10	0.79	**Satisfied**
W5	81.5	0.88	0.99	0.09	0.79	**Satisfied**
W7	202.6	1.4	0.99	0.14	0.79	**Satisfied**
W9	129.1	0.88	0.99	0.15	0.79	**Satisfied**
W11	121.4	0.88	0.99	0.14	0.79	**Satisfied**
W13	121.4	1.08	0.99	0.11	0.79	**Satisfied**
W15	85.0	1.12	0.99	0.08	0.79	**Satisfied**
W17	243.1	1.56	0.99	0.16	0.79	**Satisfied**
W19	78.9	1.08	0.99	0.07	0.79	**Satisfied**
W21	87.5	0.88	0.99	0.10	0.79	**Satisfied**
W23	157.7	0.8	0.99	0.20	0.79	**Satisfied**
W25	143.6	0.68	0.99	0.21	0.79	**Satisfied**
W27	129.1	0.88	0.99	0.15	0.79	**Satisfied**
W29	174.7	1.16	0.99	0.15	0.79	**Satisfied**
W31	123.0	0.68	0.99	0.18	0.79	**Satisfied**
W33	186.3	1.08	0.99	0.17	0.79	**Satisfied**
W35	123.5	0.8	0.99	0.15	0.79	**Satisfied**
W37	148.6	0.88	0.99	0.17	0.79	**Satisfied**
W39	129.6	0.64	0.99	0.20	0.79	**Satisfied**
W41	395.7	2.32	0.99	0.17	0.79	**Satisfied**
W43	237.8	1.28	0.99	0.19	0.79	**Satisfied**
W45	231.8	1.88	0.99	0.12	0.79	**Satisfied**
W47	382.7	2.16	0.99	0.18	0.79	**Satisfied**
W49	109.7	0.56	0.99	0.20	0.79	**Satisfied**
W51	113.9	0.56	0.99	0.20	0.79	**Satisfied**
W53	128.2	0.56	0.99	0.23	0.79	**Satisfied**
W55	322.2	1.44	0.99	0.22	0.79	**Satisfied**

where

N = Axial force on walls (kN)

A = Horizontal area of walls (m²)

λ = Strength reduction coefficient in TER-2007

As mentioned above, the shear forces on the walls are calculated by considering the eccentricity and the assumption of wall resistance only in in-plane direction. For this purpose, 1st-floor mass and shear stiffness centers are calculated. The shear force on each wall was found by distributing the floor shear force with the ratio of shear stiffness and considering the effects of the torsional moment. The shear stress is calculated by dividing the calculated shear force to cross-sectional area of the wall. The allowable shear stresses of the walls are calculated as defined in the regulation, also considering the shear friction that develops due to the axial load. The allowable shear stress is calculated by Eq. 2.17.

The calculated demand and capacity of the shear stresses are presented in Tables 3.5. to 3.12. The orientation of the axes mentioned in the tables are along 1 to 5 axes direction for +x and along A to D axes direction for +y per Fig.3.1.

Table 3.5. Walls Capacity Checks Under Loading of Earthquake Load in +x Direction in combination of G+Q+Ex+0.3Ey

	$V_{x,1}$ (t)	A(m²)	τ_x(MPa)	τ_{em}(MPa)	$\tau_{em} \geq \tau_x$
W1	14.8	0.88	0.17	0.22	**Satisfied**
W3	18.2	1.08	0.17	0.20	**Satisfied**
W5	14.8	0.88	0.17	0.20	**Satisfied**
W7	23.6	1.4	0.17	0.22	**Satisfied**
W9	14.8	0.88	0.17	0.22	**Satisfied**
W11	14.1	0.88	0.16	0.22	**Satisfied**
W13	17.3	1.08	0.16	0.21	**Satisfied**
W15	17.9	1.12	0.16	0.19	**Satisfied**
W17	24.9	1.56	0.16	0.23	**Satisfied**
W19	17.3	1.08	0.16	0.19	**Satisfied**
W47	35.4	2.16	0.16	0.24	**Satisfied**
W49	9.2	0.56	0.16	0.25	**Satisfied**
W51	9.2	0.56	0.16	0.25	**Satisfied**
W53	9.1	0.56	0.16	0.26	**Satisfied**
W55	23.5	1.44	0.16	0.26	**Satisfied**

Table 3.6. Walls Capacity Checks Under Loading of Earthquake Load in +x Direction in combination of G+Q+Ex-0.3Ey

	$V_{x,1}$ (t)	A(m^2)	τ_x(MPa)	τ_{em}(MPa)	$\tau_{em} \geq \tau_x$
W1	15.9	0.88	0.18	0.22	**Satisfied**
W3	19.6	1.08	0.18	0.20	**Satisfied**
W5	15.9	0.88	0.18	0.20	**Satisfied**
W7	25.4	1.4	0.18	0.22	**Satisfied**
W9	15.9	0.88	0.18	0.22	**Satisfied**
W11	13.1	0.88	0.15	0.22	**Satisfied**
W13	16.1	1.08	0.15	0.21	**Satisfied**
W15	16.7	1.12	0.15	0.19	**Satisfied**
W17	23.3	1.56	0.15	0.23	**Satisfied**
W19	16.1	1.08	0.15	0.19	**Satisfied**
W47	35.5	2.16	0.16	0.24	**Satisfied**
W49	9.2	0.56	0.16	0.25	**Satisfied**
W51	9.2	0.56	0.16	0.25	**Satisfied**
W53	9.0	0.56	0.16	0.26	**Satisfied**
W55	23.1	1.44	0.16	0.26	**Satisfied**

Table 3.7. Walls Capacity Checks Under Loading of Earthquake Load in -x Direction in combination of G+Q-Ex+0.3Ey

	$V_{x,1}$ (t)	A(m^2)	τ_x(MPa)	τ_{em}(MPa)	$\tau_{em} \geq \tau_x$
W1	-15.9	0.88	0.18	0.22	**Satisfied**
W3	-19.6	1.08	0.18	0.20	**Satisfied**
W5	-15.9	0.88	0.18	0.20	**Satisfied**
W7	-25.4	1.4	0.18	0.22	**Satisfied**
W9	-15.9	0.88	0.18	0.22	**Satisfied**
W11	-13.1	0.88	0.15	0.22	**Satisfied**
W13	-16.1	1.08	0.15	0.21	**Satisfied**
W15	-16.7	1.12	0.15	0.19	**Satisfied**
W17	-23.3	1.56	0.15	0.23	**Satisfied**
W19	-16.1	1.08	0.15	0.19	**Satisfied**
W47	-35.5	2.16	0.16	0.24	**Satisfied**
W49	-9.2	0.56	0.16	0.25	**Satisfied**
W51	-9.2	0.56	0.16	0.25	**Satisfied**
W53	-9.0	0.56	0.16	0.26	**Satisfied**
W55	-23.1	1.44	0.16	0.26	**Satisfied**

Table 3.8. Walls Capacity Checks Under Loading of Earthquake Load in -x Direction in combination of G+Q-Ex-0.3Ey

	$V_{x,1}$ (t)	A(m^2)	τ_x(MPa)	τ_{em}(MPa)	$\tau_{em} \geq \tau_x$
W1	-14.8	0.88	0.17	0.22	**Satisfied**
W3	-18.2	1.08	0.17	0.20	**Satisfied**
W5	-14.8	0.88	0.17	0.20	**Satisfied**
W7	-23.6	1.4	0.17	0.22	**Satisfied**
W9	-14.8	0.88	0.17	0.22	**Satisfied**
W11	-14.1	0.88	0.16	0.22	**Satisfied**
W13	-17.3	1.08	0.16	0.21	**Satisfied**
W15	-17.9	1.12	0.16	0.19	**Satisfied**
W17	-24.9	1.56	0.16	0.23	**Satisfied**
W19	-17.3	1.08	0.16	0.19	**Satisfied**
W47	-35.4	2.16	0.16	0.24	**Satisfied**
W49	-9.2	0.56	0.16	0.25	**Satisfied**
W51	-9.2	0.56	0.16	0.25	**Satisfied**
W53	-9.1	0.56	0.16	0.26	**Satisfied**
W55	-23.5	1.44	0.16	0.26	**Satisfied**

Table 3.9. Walls Capacity Checks Under Loading of Earthquake Load in +y Direction in combination of G+Q+0.3Ex+Ey

	$V_{y,1}$ (t)	A(m^2)	τ_y(MPa)	τ_{em}(MPa)	$\tau_{em} \geq \tau_y$
W21	17.6	0.88	0.20	0.20	**Satisfied**
W23	19.5	0.8	0.24	0.25	**Satisfied**
W25	16.6	0.68	0.24	0.26	**Satisfied**
W27	12.6	0.88	0.14	0.22	**Satisfied**
W29	16.7	1.16	0.14	0.23	**Satisfied**
W31	9.8	0.68	0.14	0.24	**Satisfied**
W33	23.1	1.08	0.21	0.24	**Satisfied**
W35	17.1	0.8	0.21	0.23	**Satisfied**
W37	18.8	0.88	0.21	0.23	**Satisfied**
W39	12.6	0.64	0.20	0.25	**Satisfied**
W41	45.5	2.32	0.20	0.24	**Satisfied**
W43	21.9	1.28	0.17	0.24	**Satisfied**
W45	32.2	1.88	0.17	0.21	**Satisfied**

Table 3.10. Walls Capacity Checks Under Loading of Earthquake Load in +y Direction in combination of G+Q-0.3Ex+Ey

	$V_{y,1}$ (t)	A(m^2)	τ_y(MPa)	τ_{em}(MPa)	$\tau_{em} \geq \tau_y$
W21	17.5	0.88	0.20	0.20	**Satisfied**
W23	19.9	0.8	0.25	0.25	**Satisfied**
W25	17.3	0.68	0.25	0.26	**Satisfied**
W27	11.7	0.88	0.13	0.22	**Satisfied**
W29	15.5	1.16	0.13	0.23	**Satisfied**
W31	9.1	0.68	0.13	0.24	**Satisfied**
W33	23.9	1.08	0.22	0.24	**Satisfied**
W35	17.7	0.8	0.22	0.23	**Satisfied**
W37	19.5	0.88	0.22	0.23	**Satisfied**
W39	12.7	0.64	0.20	0.25	**Satisfied**
W41	46.2	2.32	0.20	0.24	**Satisfied**
W43	21.5	1.28	0.17	0.24	**Satisfied**
W45	31.6	1.88	0.17	0.21	**Satisfied**

Table 3.11. Walls Capacity Checks Under Loading of Earthquake Load in -y Direction in combination of G+Q+0.3Ex-Ey

	$V_{y,1}$ (t)	A(m^2)	τ_y(MPa)	τ_{em}(MPa)	$\tau_{em} \geq \tau_y$
W21	-17.6	0.88	0.20	0.20	**Satisfied**
W23	-19.5	0.8	0.24	0.25	**Satisfied**
W25	-16.6	0.68	0.24	0.26	**Satisfied**
W27	-12.6	0.88	0.14	0.22	**Satisfied**
W29	-16.7	1.16	0.14	0.23	**Satisfied**
W31	-9.8	0.68	0.14	0.24	**Satisfied**
W33	-23.1	1.08	0.21	0.24	**Satisfied**
W35	-17.1	0.8	0.21	0.23	**Satisfied**
W37	-18.8	0.88	0.21	0.23	**Satisfied**
W39	-12.6	0.64	0.20	0.25	**Satisfied**
W41	-45.5	2.32	0.20	0.24	**Satisfied**
W43	-21.9	1.28	0.17	0.24	**Satisfied**
W45	-32.2	1.88	0.17	0.21	**Satisfied**

Table 3.12. Walls Capacity Checks Under Loading of Earthquake Load in -y Direction in combination of G+Q-0.3Ex-Ey

	$V_{y,1}$ (t)	A(m^2)	τ_y(MPa)	τ_{em}(MPa)	$\tau_{em} \geq \tau_y$
W21	-17.5	0.88	0.20	0.20	**Satisfied**
W23	-19.9	0.8	0.25	0.25	**Satisfied**
W25	-17.3	0.68	0.25	0.26	**Satisfied**
W27	-11.7	0.88	0.13	0.22	**Satisfied**
W29	-15.5	1.16	0.13	0.23	**Satisfied**
W31	-9.1	0.68	0.13	0.24	**Satisfied**
W33	-23.9	1.08	0.22	0.24	**Satisfied**
W35	-17.7	0.8	0.22	0.23	**Satisfied**
W37	-19.5	0.88	0.22	0.23	**Satisfied**
W39	-12.7	0.64	0.20	0.25	**Satisfied**
W41	-46.2	2.32	0.20	0.24	**Satisfied**
W43	-21.5	1.28	0.17	0.24	**Satisfied**
W45	-31.6	1.88	0.17	0.21	**Satisfied**

3.4. Analysis and Design of the Example Building by TER-2018

The case study building is also analyzed and designed according to TER-2018 to observe its effect on the design results. As described in Chapter 2, the design methodology is changed from allowable stress design to ultimate strength design with the new version of the regulation. The seismic risk definitions are also modified with TER-2018. Rather than having earthquake zones, the seismic risk is defined based on geographical coordinates.

The spectral parameters of building location are obtained through the webpage provided by the Ministry of Interior, Disaster and Emergency Management Presidency (AFAD). The values are interpolated from the provided spectral parameters of the selected grid locations of the earthquake hazard map to the building's exact position. The case study building coordinates are 37.0074° latitude, 27.7944° longitude; the obtained spectral parameters are presented in the Table 3.13. Design spectral parameters are calculated from obtained spectral parameters for ZC ground class using Eq.3.2. and Eq.3.3.

Table 3.13. Spectral Parameters of Building Site According to Earthquake Hazard Map

Site Parameters	Values
S_S	1.102
S_1	0.272
PGA	0.463

where

S_s = Short period map spectral acceleration coefficient [dimensionless]

S_1 = Map spectral acceleration for 1.0. second period [dimensionless]

PGA = Peak ground acceleration [g]

$$S_{DS} = S_S F_S \quad \text{Eq.3.2}$$

$$S_{D1} = S_1 F_1 \quad \text{Eq.3.3}$$

where

S_{DS} = Short period design spectral acceleration coefficient [dimensionless]

S_{D1} = Design spectral acceleration for 1.0. second period [dimensionless]

F_s = Local ground effect coefficient for the short period zone and 1.2 for ZC ground class [dimensionless]

F_1 = Local ground effect coefficient for the 1.0. second period and 1.5 for ZC ground class [dimensionless]

TER-2018 demands the analysis of unreinforced masonry either by using the equivalent frame or the finite element model.

As described in Chapter 1, the equivalent frame model is formed by identifying each wall element's mechanical and structural properties to represent the matching frame element that passes through the centroid axis of the wall element. The finite element model is formed using the shell elements whose properties represent the mechanical and structural properties of the corresponding walls. Both these analyses are performed for linear, elastic structure.

The analysis of case study structure is provided for both analysis methods. The equivalent frame analysis is performed using SAP2000 structural analysis software, but the finite element model is performed using ETABS structural analysis software. The analysis program is changed due to the convenience of the ETABS software in converting the selected shell element results into equivalent frame element internal forces. Otherwise, each software has similar solvers and definitions if not the same.

3.4.1. The Equivalent Frame Model

Wall stiffnesses are calculated and defined for each element in the model according to the definition in TER-2018 using Eq. 3.4. The regulation dictates to calculate each wall stiffness as half of its gross value as a cracked section property as shown in Eq. 3.5.

$$k_{duv} = \frac{1}{\frac{H^3}{12E_{duv}I} + \frac{H}{1.2G_{duv}A}} \qquad \text{Eq.3.4}$$

$$k'_{duv} = 0.5k_{duv} \qquad \text{Eq.3.5}$$

When calculating the frame stiffnesses, each wall stiffness is calculated considering the bending and shear deformations together according to Eq.3.6. The modeling effort is simplified by considering the total stiffness of each wall as if they are flexure members only.

$$k'_{duv} = 0.5 \frac{1}{\frac{H^3}{12E_{duv}I} + \frac{H}{1.2G_{duv}A}} = 0.5 \frac{1}{\frac{H^3}{12E_{duv}I'}} \qquad \text{Eq.3.6}$$

The TER-2018 regulation does not allow to use of the strength values directly from its tables to determine material parameters. It is enforced to perform tests to determine the masonry unit and mortar compressive strengths. After obtaining these values, the masonry wall compressive strength value could be selected by using Table 2.8.

The material properties for the case study building are obtained by using the test result of solid clay brick of (Cöğürcü M. et al. 2007). The compressive strength tests on solid clay brick were made according to TS EN 772-1. The solid clay brick was used in the experiment was per the TS-EN 771-1 standard. The test results indicated a compressive strength of the brick as 23.17 MPa. In design calculations, this value was rounded to 23.0 MPa. The compressive strength of the mortar was accepted to be 8 MPa. Using the defined values for a general-purpose mortar, the compressive strength of the masonry wall, f_k was determined to be 9 MPa per Table 2.8. As it is defined in TER-2018, the elastic modulus could be determined by experiments according to TS EN 1052-1. In the absence of this experiment, the masonry wall elastic modulus could be taken equal to $750f_k$. Thus, the elastic modulus was chosen as 6750 MPa. Initial shear strength f_{vko} was selected 0.20 MPa, according to Table 2.13. again, for general-purpose mortar.

The free height of the wall is defined to be taken from the top of the slab to the bottom of the bond beam per TER-2018. Therefore, upper parts of the walls that includes the bond beam and thickness of the slab are defined as full rigid regions in the frame model. The slabs are designed as 12 cm thick reinforced concrete elements and defined as rigid diagrams. Masonry material unit weight is assigned to be 1.9 t/m² and reinforced concrete unit weight is 2.5 t/m².

The portion of walls that are bridging the window or door openings and working like spandrel beams, are modified with the factors calculated by proportioning the openings along their lengths. The slab dead and live loads are defined to be 2.04 kN/m² and 2.0 kN/m² respectively.

In order to calculate the seismic load, the total weight of the case study building is determined. Seismic loads are calculated according to TER-2018, as mentioned in Chapter 2. Regulation allows the use of an empirical formula for determining the natural vibration period of the building to calculate the seismic loads. The first natural vibration periods are found to be 0.27 and 0.07 seconds from empirical formulation and structural model analysis, respectively. Considering the case study structure analysis result, this difference might be caused by the empirical C_t coefficient value. The result obtained from the analysis was used because the empirical formula was calculated with very limited parameters and too rough.

Information about the building and seismic load calculation results are shown in Table 3.14 and Table 3.15. respectively.

Table 3.14. Site Seismic and Building Information for Frame Model

Site and Building Model Information	
Site Latitude	37.0074°
Site Longitude	27.7944°
Total Dead Load, G (tons)	488.88
Total Live Load, Q (tons)	60.67
Total Mass (G+0.3Q) (tons)	507.08
Number of Floor, N	2
1st Floor Height (m)	3
2nd Floor Height (m)	3
R	2.5
I	1
D	1.5
PGA (g)	0.463
S_{DS} (for DD2)	1.322
S_{D1} (for DD2)	0.408
1st Mode Natural Vibration Period $T_p^{(x)}$ (sec)	0.07
1st Floor Mass (m)	257.14
2nd Floor Mass (m)	249.94

Table 3.15. Equivalent Earthquake Load Calculation for Frame Model

Equivalent Earthquake Load Calculation (DD2)		
$T_A=0.2\ S_{D1}\ /\ S_{DS}$	0.062	sec
$T_B=S_{D1}/S_{DS}$	0.309	sec
S_{ae}	1.322	-
$Ra(T_p^{(x)})=D+(R^{(x)}/I-D)*(T_p^{(x)}/T_B)$	1.72	-
$S_{aR}(T_p^{(x)}) = S_{ae}\ /\ Ra(T_p^{(x)})$	0.77	g
$V_{tE}^{(x)}=m_t\ S_{aR}\ (T_p^{(x)}) \geq 0.04m_tIS_{DS}g$	389.67	tons
$\Delta F_{NE}^{(x)}=0.0075NV_{tE}^{(x)}$	5.85	tons
Earthquake Load acting on 1st Floor $F_{1E}^{(x)}$	194.6	tons
Earthquake Load acting on 2nd Floor $F_{2E}^{(x)}$	195.0	tons

Design of unreinforced masonry building according to the new regulation is performed using a spreadsheet. The spreadsheet is organized to compare the axial force and in-plane shear force obtained from the analysis of each wall with the axial and in-plane shear capacities of the wall sections calculated according to TER-2018. A three-dimensional view of the model is presented in Fig.3.6.

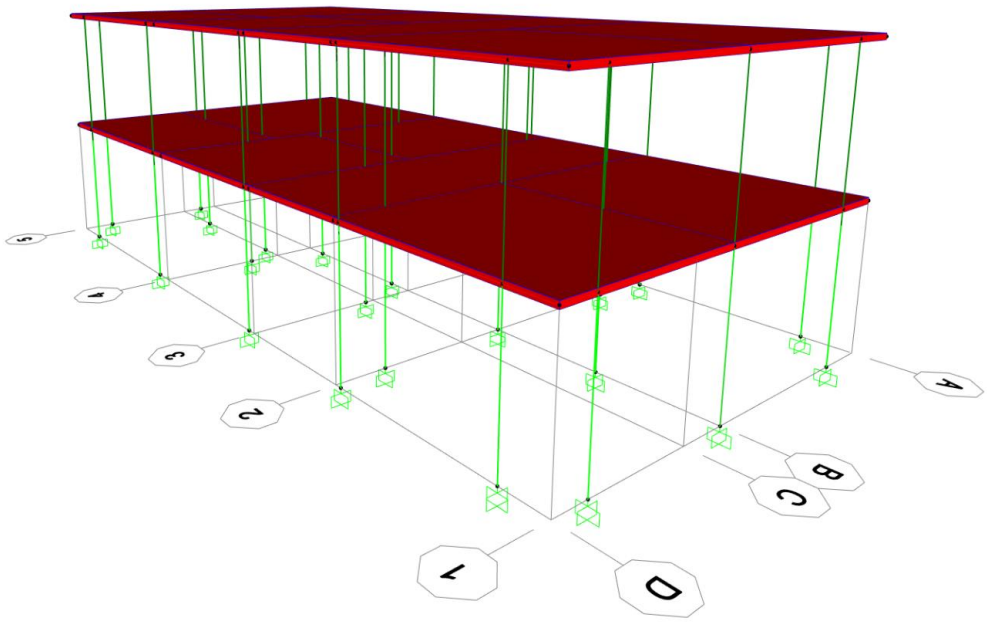

Figure 3.6. 3D Frame View in SAP2000 of Equivalent Frame Model

In order to observe the effect of changes in the regulations, the walls are selected to be 40cm thick same as the case study building designed according to TER-2007. It is known from the preliminary checks that 40 cm wall thickness is not sufficient for all the design requirements; therefore, it could reflect the effect of changes in the new version of the seismic regulation. Finals checks reveal that most of the walls are inadequate both in axial compressive and shear strength. Examples of design results of Wall-1 and Wall-21 are presented in Table 3.16. and Table 3.17.

Table 3.16. Frame Model Wall-1 Design Check

CALCULATION ACCORDING TO ULTIMATE BEARING CAPACITY								Wall	21																			
Combination	M_{ed}	N_{ed}	V_{ed}	t_{ef}	l	lx	λ	A	σ_{max}	σ_{min}	$\sigma_{min}>0$	lc_1	lc_2	Sel.lc	b	σd=Ned/A	f_{vk}	f_{vd}	$f_{vk}\leq 0.10 f_b$	$N_{rd}=\lambda A f_d$	Nrd≥Ned	V_{Rd1}	V_{Rd2}	Min V_{rd}	$DV_{ed}=1.5V_{ed}$	$V_{rd} \geq D\ V_{ed}$	Failure Criteria
-	KN-mm	KN	KN	mm	mm	mm^4	-	mm^2	Mpa	Mpa	-	mm	mm	mm	-	Mpa	Mpa	Mpa	-	KN	-	KN	KN	KN	KN	-	-
G+Q+Edx+0.3Edy+0.3Edz	54583	-81	37	400	2200	3,55E+11	1	880000	0,08	-0,26	Partly comp.	2200	502	502	1,23	-0,09	0,16	0,08	Satisfy	3960	Not Satisfy	16	67	16	56	Not Satisfy	AxialTensionFailure
G+Q+Edx-0.3Edy+0.3Edz	79783	-76	59	400	2200	3,55E+11	1	880000	0,16	-0,33	Partly comp.	2200	716	716	1,23	-0,09	0,17	0,08	Satisfy	3960	Not Satisfy	24	70	24	89	Not Satisfy	AxialTensionFailure
G+Q+0.3Edx+Edy+0.3Edz	65546	151	47	400	2200	3,55E+11	1	880000	0,37	-0,03	Partly comp.	2200	2028	2028	1,23	0,17	0,27	0,13	Satisfy	3960	Satisfy	109	157	109	70	Satisfy	Fully Satisfy
G+Q-Edx-0.3Edy+0.3Edz	55688	433	38	400	2200	3,55E+11	1	880000	0,67	0,32	Full comp.	2200	2200	2200	1,23	0,49	0,40	0,20	Satisfy	3960	Satisfy	175	223	175	58	Satisfy	Fully Satisfy
G+Q-Edx+0.3Edy+0.3Edz	78678	428	58	400	2200	3,55E+11	1	880000	0,73	0,24	Full comp.	2200	2200	2200	1,23	0,49	0,39	0,20	Satisfy	3960	Satisfy	174	222	174	87	Satisfy	Fully Satisfy
G+Q-0.3Edx-Edy+0.3Edz	220882	261	158	400	2200	3,55E+11	1	880000	0,98	-0,39	Partly comp.	2200	1576	1576	1,23	0,30	0,32	0,16	Satisfy	3960	Satisfy	100	186	100	237	Not Satisfy	Sliding Failure
G+Q+0.3Edx-Edy+0.3Edz	228110	108	164	400	2200	3,55E+11	1	880000	0,83	-0,58	Partly comp.	2200	1291	1291	1,23	0,12	0,25	0,12	Satisfy	3960	Satisfy	64	145	64	246	Not Satisfy	Sliding Failure
G+Q-0.3Edx+Edy+0.3Edz	227005	244	163	400	2200	3,55E+11	1	880000	0,98	-0,43	Partly comp.	2200	1534	1534	1,23	0,28	0,31	0,16	Satisfy	3960	Satisfy	95	182	95	245	Not Satisfy	Sliding Failure
0.9G+Edx+0.3Edy-0.3Edz	54915	-174	38	400	2200	3,55E+11	1	880000	-0,03	-0,37	Partly comp.	2200	0	0	1,23	-0,20	0,12	0,06	Satisfy	3960	Not Satisfy	-	-	-	56	-	AxialTensionFailure
0.9G-Edx-0.3Edy-0.3Edz	55356	340	38	400	2200	3,55E+11	1	880000	0,56	0,21	Full comp.	2200	2200	2200	1,23	0,39	0,35	0,18	Satisfy	3960	Satisfy	156	203	156	57	Satisfy	Fully Satisfy
0.9G+Edx-0.3Edy-0.3Edz	79451	-169	59	400	2200	3,55E+11	1	880000	0,05	-0,44	Partly comp.	2200	240	240	1,23	-0,19	0,12	0,06	Satisfy	3960	Not Satisfy	-	-	-	88	-	AxialTensionFailure
0.9G-Edx+0.3Edy-0.3Edz	79010	335	58	400	2200	3,55E+11	1	880000	0,63	0,14	Full comp.	2200	2200	2200	1,23	0,38	0,35	0,18	Satisfy	3960	Satisfy	155	202	155	88	Satisfy	Fully Satisfy
0.9G+0.3Edx+Edy-0.3Edz	220109	-2	157	400	2200	3,55E+11	1	880000	0,68	-0,68	Partly comp.	2200	1097	1097	1,23	0,00	0,20	0,10	Satisfy	3960	Not Satisfy	-	-	-	236	-	AxialTensionFailure
0.9G-0.3Edx-Edy-0.3Edz	220550	168	158	400	2200	3,55E+11	1	880000	0,87	-0,49	Partly comp.	2200	1406	1406	1,23	0,19	0,28	0,14	Satisfy	3960	Satisfy	78	162	78	236	Not Satisfy	Sliding Failure
0.9G+0.3Edx-Edy-0.3Edz	227779	15	164	400	2200	3,55E+11	1	880000	0,72	-0,69	Partly comp.	2200	1126	1126	1,23	0,02	0,21	0,10	Satisfy	3960	Satisfy	47	113	47	246	Not Satisfy	Sliding Failure
0.9G-0.3Edx+Edy-0.3Edz	227337	151	163	400	2200	3,55E+11	1	880000	0,88	-0,53	Partly comp.	2200	1368	1368	1,23	0,17	0,27	0,13	Satisfy	3960	Satisfy	73	157	73	245	Not Satisfy	Sliding Failure

Table 3.17. Frame Model Wall-21 Design Check

CALCULATION ACCORDING TO ULTIMATE BEARING CAPACITY								Wall	1																			
Combination	M_{ed}	N_{ed}	V_{ed}	t_{ef}	l	lx	λ	A	σ_{max}	σ_{min}	$\sigma_{min}>0$	lc_1	lc_2	Sel.lc	b	σd=Ned/A	f_{vk}	f_{vd}	$f_{vk}\leq 0.10 f_b$	$N_{rd}=\lambda A f_d$	Nrd≥Ned	V_{Rd1}	V_{Rd2}	Min V_{rd}	$DV_{ed}=1.5V_{ed}$	$V_{rd} \geq D\ V_{ed}$	Failure Criteria
-	KN-mm	KN	KN	mm	mm	mm^4	-	mm^2	Mpa	Mpa	-	mm	mm	mm	-	Mpa	Mpa	Mpa	-	KN	-	KN	KN	KN	KN	-	-
G+Q+Edx+0.3Edy+0.3Edz	223434	106	161	400	2200	3,55E+11	1	880000	0,81	-0,57	Partly comp.	2200	1292	1292	1,23	0,12	0,25	0,12	Satisfy	3960	Satisfy	64	145	64	241	Not Satisfy	Sliding Failure
G+Q+Edx-0.3Edy+0.3Edz	220304	241	160	400	2200	3,55E+11	1	880000	0,96	-0,41	Partly comp.	2200	1542	1542	1,23	0,27	0,31	0,15	Satisfy	3960	Satisfy	96	181	96	241	Not Satisfy	Sliding Failure
G+Q+0.3Edx+Edy+0.3Edz	20798	112	14	400	2200	3,55E+11	1	880000	0,19	0,06	Full comp.	2200	2200	2200	1,23	0,13	0,25	0,13	Satisfy	3960	Satisfy	110	146	110	21	Satisfy	Fully Satisfy
G+Q-Edx-0.3Edy+0.3Edz	225049	255	162	400	2200	3,55E+11	1	880000	0,99	-0,41	Partly comp.	2200	1557	1557	1,23	0,29	0,32	0,16	Satisfy	3960	Satisfy	98	184	98	243	Not Satisfy	Sliding Failure
G+Q-Edx+0.3Edy+0.3Edz	221919	120	162	400	2200	3,55E+11	1	880000	0,82	-0,55	Partly comp.	2200	1318	1318	1,23	0,14	0,25	0,13	Satisfy	3960	Satisfy	67	149	67	243	Not Satisfy	Sliding Failure
G+Q-0.3Edx-Edy+0.3Edz	72826	408	50	400	2200	3,55E+11	1	880000	0,69	0,24	Full comp.	2200	2200	2200	1,23	0,46	0,39	0,19	Satisfy	3960	Satisfy	170	217	170	75	Satisfy	Fully Satisfy
G+Q+0.3Edx-Edy+0.3Edz	60780	404	47	400	2200	3,55E+11	1	880000	0,65	0,27	Full comp.	2200	2200	2200	1,23	0,46	0,38	0,19	Satisfy	3960	Satisfy	169	217	169	71	Satisfy	Fully Satisfy
G+Q-0.3Edx+Edy+0.3Edz	62395	-43	49	400	2200	3,55E+11	1	880000	0,15	-0,24	Partly comp.	2200	825	825	1,23	-0,05	0,18	0,09	Satisfy	3960	Not Satisfy	-	-	-	73	-	AxialTensionFailure
0.9G+Edx+0.3Edy-0.3Edz	223976	9	161	400	2200	3,55E+11	1	880000	0,70	-0,68	Partly comp.	2200	1116	1116	1,23	0,01	0,20	0,10	Satisfy	3960	Satisfy	46	111	46	242	Not Satisfy	Sliding Failure
0.9G-Edx-0.3Edy-0.3Edz	224506	157	162	400	2200	3,55E+11	1	880000	0,87	-0,52	Partly comp.	2200	1383	1383	1,23	0,18	0,27	0,14	Satisfy	3960	Satisfy	75	159	75	243	Not Satisfy	Sliding Failure
0.9G+Edx-0.3Edy-0.3Edz	220847	144	161	400	2200	3,55E+11	1	880000	0,85	-0,52	Partly comp.	2200	1363	1363	1,23	0,16	0,27	0,13	Satisfy	3960	Satisfy	72	156	72	241	Not Satisfy	Sliding Failure
0.9G-Edx+0.3Edy-0.3Edz	221377	22	161	400	2200	3,55E+11	1	880000	0,71	-0,66	Partly comp.	2200	1141	1141	1,23	0,03	0,21	0,11	Satisfy	3960	Satisfy	48	116	48	242	Not Satisfy	Sliding Failure
0.9G+0.3Edx+Edy-0.3Edz	71754	-144	49	400	2200	3,55E+11	1	880000	0,06	-0,39	Partly comp.	2200	291	291	1,23	-0,16	0,13	0,07	Satisfy	3960	Not Satisfy	-	-	-	73	-	AxialTensionFailure
0.9G-0.3Edx-Edy-0.3Edz	72284	310	49	400	2200	3,55E+11	1	880000	0,58	0,13	Full comp.	2200	2200	2200	1,23	0,35	0,34	0,17	Satisfy	3960	Satisfy	150	197	150	74	Satisfy	Fully Satisfy
0.9G+0.3Edx-Edy-0.3Edz	61322	306	48	400	2200	3,55E+11	1	880000	0,54	0,16	Full comp.	2200	2200	2200	1,23	0,35	0,34	0,17	Satisfy	3960	Satisfy	149	196	149	71	Satisfy	Fully Satisfy
0.9G-0.3Edx+Edy-0.3Edz	61852	-140	48	400	2200	3,55E+11	1	880000	0,03	-0,35	Partly comp.	2200	188	188	1,23	-0,16	0,14	0,07	Satisfy	3960	Not Satisfy	-	-	-	72	-	AxialTensionFailure

3.4.2. The Finite Element Model

The structure is modeled by shell elements to build the finite element model. According to TER-2018 requirements, the effective stiffness of the elements is taken to be half of the gross stiffness values. Similar to the equivalent frame model, 40 cm thick walls are defined. The masonry and concrete unit weight did not change. Slabs are again modeled with 12 cm thick shell elements, and a rigid diagram is defined. The distributed dead and live loads are taken to be 2.04 kN/m² and 2.0 kN/m², respectively as well.

Seismic loads are calculated using the same design spectrum and the calculated period. Since the calculated periods are the same, the seismic loads are the same as the equivalent frame. The values are as given in Table 3.11. A 3-D view of the finite element model is presented in Figure 3.7.

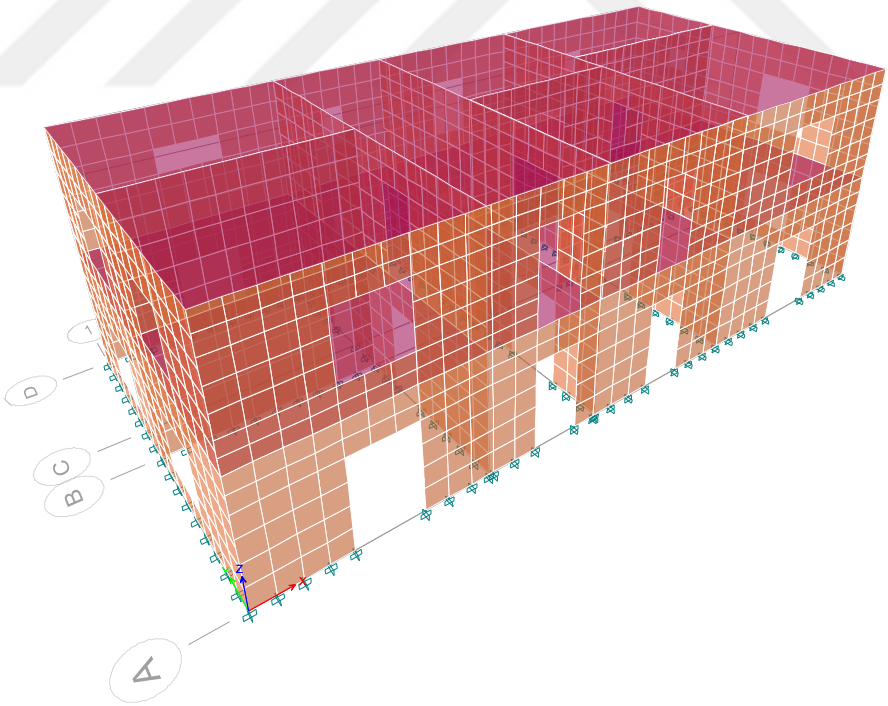

Figure 3.7. Finite Element Model of Case Study Building 3D View in ETABS

The design checks are performed using the same spreadsheet that was prepared for the frame model. The shell element results of the walls are converted to internal forces using the ETABS integration scheme for the shell elements. The forces are defined at the centroid of the individually defined wall panels. Results show that the walls do not satisfy the design requirements similar to frame model results. Both the compressive and shear strength are insufficient. The design results of Wall-1 and Wall-21 are presented in Table 3.18 and Table 3.19 as examples.

Table 3.18. Finite Element Model Wall-1 Design Check

CALCULATION ACCORDING TO ULTIMATE BEARING CAPACITY							Wall	21																				
Combination	M_{ed}	N_{ed}	V_{ed}	t_{ef}	l	lx	λ	A	σ_{max}	σ_{min}	$\sigma_{min}>0$	lc_1	lc_2	Sel.lc	b	σd=Ned/A	f_{vk}	f_{vd}	$f_{vk}\leq 0.10 f_b$	$N_{rd}=\lambda A f_d$	Nrd≥Ned	V_{Rd1}	V_{Rd2}	Min V_{rd}	$DV_{ed}=1.5V_{ed}$	$V_{rd} \geq D\ V_{ed}$	Failure Criteria
-	KN-mm	KN	KN	mm	mm	mm^4	-	mm^2	Mpa	Mpa	-	mm	mm	mm	-	Mpa	Mpa	Mpa	-	KN	-	KN	KN	KN	KN	-	-
G+Q+Edx+0.3Edy+0.3Edz	70076	-41	6	400	2200	3,55E+11	1	880000	0,17	-0,26	Partly comp.	2200	867	867	1,23	-0,05	0,18	0,09	Satisfy	3960	Not Satisfy	-	-	-	9	-	AxialTensionFailure
G+Q+Edx-0.3Edy+0.3Edz	29219	-11	80	400	2200	3,55E+11	1	880000	0,08	-0,10	Partly comp.	2200	944	944	1,23	-0,01	0,19	0,10	Satisfy	3960	Not Satisfy	-	-	-	119	-	AxialTensionFailure
G+Q+0.3Edx+Edy+0.3Edz	163514	68	126	400	2200	3,55E+11	1	880000	0,58	-0,43	Partly comp.	2200	1268	1268	1,23	0,08	0,23	0,12	Satisfy	3960	Satisfy	59	132	59	189	Not Satisfy	Sliding Failure
G+Q-Edx-0.3Edy+0.3Edz	93238	397	23	400	2200	3,55E+11	1	880000	0,74	0,16	Full comp.	2200	2200	2200	1,23	0,45	0,38	0,19	Satisfy	3960	Satisfy	167	215	167	34	Satisfy	Fully Satisfy
G+Q-Edx+0.3Edy+0.3Edz	6057	367	63	400	2200	3,55E+11	1	880000	0,44	0,40	Full comp.	2200	2200	2200	1,23	0,42	0,37	0,18	Satisfy	3960	Satisfy	161	209	161	95	Satisfy	Fully Satisfy
G+Q-0.3Edx-Edy+0.3Edz	186676	288	143	400	2200	3,55E+11	1	880000	0,91	-0,25	Partly comp.	2200	1722	1722	1,23	0,33	0,33	0,17	Satisfy	3960	Satisfy	114	192	114	214	Not Satisfy	Sliding Failure
G+Q+0.3Edx-Edy+0.3Edz	167471	166	160	400	2200	3,55E+11	1	880000	0,71	-0,33	Partly comp.	2200	1499	1499	1,23	0,19	0,28	0,14	Satisfy	3960	Satisfy	83	162	83	240	Not Satisfy	Sliding Failure
G+Q-0.3Edx+Edy+0.3Edz	144309	190	143	400	2200	3,55E+11	1	880000	0,66	-0,23	Partly comp.	2200	1632	1632	1,23	0,22	0,29	0,14	Satisfy	3960	Satisfy	94	168	94	215	Not Satisfy	Sliding Failure
0.9G+Edx+0.3Edy-0.3Edz	76424	-136	11	400	2200	3,55E+11	1	880000	0,08	-0,39	Partly comp.	2200	383	383	1,23	-0,15	0,14	0,07	Satisfy	3960	Not Satisfy	-	-	-	16	-	AxialTensionFailure
0.9G-Edx-0.3Edy-0.3Edz	86890	301	18	400	2200	3,55E+11	1	880000	0,61	0,07	Full comp.	2200	2200	2200	1,23	0,34	0,34	0,17	Satisfy	3960	Satisfy	148	195	148	27	Satisfy	Fully Satisfy
0.9G+Edx-0.3Edy-0.3Edz	22871	-107	75	400	2200	3,55E+11	1	880000	-0,05	-0,19	Partly comp.	2200	0	0	1,23	-0,12	0,15	0,08	Satisfy	3960	Not Satisfy	-	-	-	112	-	AxialTensionFailure
0.9G-Edx+0.3Edy-0.3Edz	12406	272	68	400	2200	3,55E+11	1	880000	0,35	0,27	Full comp.	2200	2200	2200	1,23	0,31	0,32	0,16	Satisfy	3960	Satisfy	142	188	142	102	Satisfy	Fully Satisfy
0.9G+0.3Edx+Edy-0.3Edz	169863	-27	131	400	2200	3,55E+11	1	880000	0,50	-0,56	Partly comp.	2200	1035	1035	1,23	-0,03	0,19	0,09	Satisfy	3960	Not Satisfy	-	-	-	196	-	AxialTensionFailure
0.9G-0.3Edx-Edy-0.3Edz	180328	193	138	400	2200	3,55E+11	1	880000	0,78	-0,34	Partly comp.	2200	1531	1531	1,23	0,22	0,29	0,14	Satisfy	3960	Satisfy	88	169	88	207	Not Satisfy	Sliding Failure
0.9G+0.3Edx-Edy-0.3Edz	161122	70	155	400	2200	3,55E+11	1	880000	0,58	-0,42	Partly comp.	2200	1276	1276	1,23	0,08	0,23	0,12	Satisfy	3960	Satisfy	59	133	59	233	Not Satisfy	Sliding Failure
0.9G-0.3Edx+Edy-0.3Edz	150657	95	148	400	2200	3,55E+11	1	880000	0,58	-0,36	Partly comp.	2200	1355	1355	1,23	0,11	0,24	0,12	Satisfy	3960	Satisfy	66	141	66	222	Not Satisfy	Sliding Failure

Table 3.19. Finite Element Model Wall-21 Design Check

CALCULATION ACCORDING TO ULTIMATE BEARING CAPACITY							Wall	1																				
Combination	M_{ed}	N_{ed}	V_{ed}	t_{ef}	l	lx	λ	A	σ_{max}	σ_{min}	$\sigma_{min}>0$	lc_1	lc_2	Sel.lc	b	σd=Ned/A	f_{vk}	f_{vd}	$f_{vk}\leq 0.10 f_b$	$N_{rd}=\lambda A f_d$	Nrd≥Ned	V_{Rd1}	V_{Rd2}	Min V_{rd}	$DV_{ed}=1.5V_{ed}$	$V_{rd} \geq D\ V_{ed}$	Failure Criteria
-	KN-mm	KN	KN	mm	mm	mm^4	-	mm^2	Mpa	Mpa	-	mm	mm	mm	-	Mpa	Mpa	Mpa	-	KN	-	KN	KN	KN	KN	-	-
G+Q+Edx+0.3Edy+0.3Edz	181767	130	125	400	2200	3,55E+11	1	880000	0,71	-0,42	Partly comp.	2200	1390	1390	1,23	0,15	0,26	0,13	Satisfy	3960	Satisfy	72	152	72	188	Not Satisfy	Sliding Failure
G+Q+Edx-0.3Edy+0.3Edz	159308	284	148	400	2200	3,55E+11	1	880000	0,82	-0,17	Partly comp.	2200	1818	1818	1,23	0,32	0,33	0,16	Satisfy	3960	Satisfy	120	191	120	221	Not Satisfy	Sliding Failure
G+Q+0.3Edx+Edy+0.3Edz	85715	-62	0	400	2200	3,55E+11	1	880000	0,20	-0,34	Partly comp.	2200	810	810	1,23	-0,07	0,17	0,09	Satisfy	3960	Not Satisfy	-	-	-	0	-	AxialTensionFailure
G+Q-Edx-0.3Edy+0.3Edz	189990	245	136	400	2200	3,55E+11	1	880000	0,87	-0,31	Partly comp.	2200	1619	1619	1,23	0,28	0,31	0,16	Satisfy	3960	Satisfy	101	182	101	205	Not Satisfy	Sliding Failure
G+Q-Edx+0.3Edy+0.3Edz	167531	92	159	400	2200	3,55E+11	1	880000	0,62	-0,42	Partly comp.	2200	1321	1321	1,23	0,10	0,24	0,12	Satisfy	3960	Satisfy	64	140	64	238	Not Satisfy	Sliding Failure
G+Q-0.3Edx-Edy+0.3Edz	93938	437	11	400	2200	3,55E+11	1	880000	0,79	0,21	Full comp.	2200	2200	2200	1,23	0,50	0,40	0,20	Satisfy	3960	Satisfy	175	223	175	17	Satisfy	Fully Satisfy
G+Q+0.3Edx-Edy+0.3Edz	10851	449	74	400	2200	3,55E+11	1	880000	0,54	0,48	Full comp.	2200	2200	2200	1,23	0,51	0,40	0,20	Satisfy	3960	Satisfy	178	226	178	111	Satisfy	Fully Satisfy
G+Q-0.3Edx+Edy+0.3Edz	19074	-73	85	400	2200	3,55E+11	1	880000	-0,02	-0,14	Partly comp.	2200	0	0	1,23	-0,08	0,17	0,08	Satisfy	3960	Not Satisfy	-	-	-	128	-	AxialTensionFailure
0.9G+Edx+0.3Edy-0.3Edz	184115	30	129	400	2200	3,55E+11	1	880000	0,60	-0,54	Partly comp.	2200	1166	1166	1,23	0,03	0,21	0,11	Satisfy	3960	Satisfy	50	119	50	193	Not Satisfy	Sliding Failure
0.9G-Edx-0.3Edy-0.3Edz	187642	144	133	400	2200	3,55E+11	1	880000	0,75	-0,42	Partly comp.	2200	1410	1410	1,23	0,16	0,27	0,13	Satisfy	3960	Satisfy	75	156	75	200	Not Satisfy	Sliding Failure
0.9G+Edx-0.3Edy-0.3Edz	161656	183	151	400	2200	3,55E+11	1	880000	0,71	-0,29	Partly comp.	2200	1557	1557	1,23	0,21	0,28	0,14	Satisfy	3960	Satisfy	88	166	88	226	Not Satisfy	Sliding Failure
0.9G-Edx+0.3Edy-0.3Edz	165182	-9	155	400	2200	3,55E+11	1	880000	0,50	-0,52	Partly comp.	2200	1079	1079	1,23	-0,01	0,20	0,10	Satisfy	3960	Not Satisfy	-	-	-	233	-	AxialTensionFailure
0.9G+0.3Edx+Edy-0.3Edz	88063	-162	3	400	2200	3,55E+11	1	880000	0,09	-0,46	Partly comp.	2200	358	358	1,23	-0,18	0,13	0,06	Satisfy	3960	Not Satisfy	-	-	-	5	-	AxialTensionFailure
0.9G-0.3Edx-Edy-0.3Edz	91590	336	8	400	2200	3,55E+11	1	880000	0,67	0,10	Full comp.	2200	2200	2200	1,23	0,38	0,35	0,18	Satisfy	3960	Satisfy	155	203	155	12	Satisfy	Fully Satisfy
0.9G+0.3Edx-Edy-0.3Edz	13199	348	77	400	2200	3,55E+11	1	880000	0,44	0,35	Full comp.	2200	2200	2200	1,23	0,40	0,36	0,18	Satisfy	3960	Satisfy	158	205	158	116	Satisfy	Fully Satisfy
0.9G-0.3Edx+Edy-0.3Edz	16726	-174	82	400	2200	3,55E+11	1	880000	-0,15	-0,25	Partly comp.	2200	0	0	1,23	-0,20	0,12	0,06	Satisfy	3960	Not Satisfy	-	-	-	123	-	AxialTensionFailure

3.4.3. Comparison of Two Modeling Results

Periods, shear capacities and demand results of selected critical walls of 11 and 21 are given in Table 3.20, 3.21 and 3.22. in order to assess the differences of modeling results. The models are modeled with different approaches in terms of total stiffness according to TER-2018. Period results in both orthogonal directions were found to be almost the same. It had been proved that; these two modeling types give results close to each other.

Table 3.20. 1st and 2nd Modal Period of Two Modelings

	1st Period (sec)	2nd Period (sec)
Frame Model	0.068	0.065
Finite Element Model	0.071	0.065

Table 3.21. Wall 1 Shear Capacities and Demand Forces Comparison

	Frame Model	Finite Element Model	Frame Model	Finite Element Model
	Min V_{rd} (kN)	Min V_{rd} (kN)	DV_{ed} (kN)	DV_{ed} (kN)
G+Q+Edx+0.3Edy+0.3Edz	64	72	241	188
G+Q+Edx-0.3Edy+0.3Edz	96	120	241	221
G+Q+0.3Edx+Edy+0.3Edz	110	-	21	0
G+Q-Edx-0.3Edy+0.3Edz	98	101	243	205
G+Q-Edx+0.3Edy+0.3Edz	67	64	243	238
G+Q-0.3Edx-Edy+0.3Edz	170	175	75	17
G+Q+0.3Edx-Edy+0.3Edz	169	178	71	111
G+Q-0.3Edx+Edy+0.3Edz	-	-	73	128
0.9G+Edx+0.3Edy-0.3Edz	46	50	242	193
0.9G-Edx-0.3Edy-0.3Edz	75	75	243	200
0.9G+Edx-0.3Edy-0.3Edz	72	88	241	226
0.9G-Edx+0.3Edy-0.3Edz	48	-	242	233
0.9G+0.3Edx+Edy-0.3Edz	-	-	73	5
0.9G-0.3Edx-Edy-0.3Edz	150	155	74	12
0.9G+0.3Edx-Edy-0.3Edz	149	158	71	116
0.9G-0.3Edx+Edy-0.3Edz	-	-	72	123

Table 3.22. Wall 21 Shear Capacities and Demand Forces Comparison

	Frame Model	Finite Element Model	Frame Model	Finite Element Model
	Min V_{rd} (kN)	Min V_{rd} (kN)	DV_{ed} (kN)	DV_{ed} (kN)
G+Q+Edx+0.3Edy+0.3Edz	-	-	56	9
G+Q+Edx-0.3Edy+0.3Edz	-	-	89	119
G+Q+0.3Edx+Edy+0.3Edz	109	59	70	189
G+Q-Edx-0.3Edy+0.3Edz	175	167	58	34
G+Q-Edx+0.3Edy+0.3Edz	174	161	87	95
G+Q-0.3Edx-Edy+0.3Edz	100	114	237	214
G+Q+0.3Edx-Edy+0.3Edz	64	83	246	240
G+Q-0.3Edx+Edy+0.3Edz	95	94	245	215
0.9G+Edx+0.3Edy-0.3Edz	-	-	56	16
0.9G-Edx-0.3Edy-0.3Edz	156	148	57	27
0.9G+Edx-0.3Edy-0.3Edz	-	-	88	112
0.9G-Edx+0.3Edy-0.3Edz	155	142	88	102
0.9G+0.3Edx+Edy-0.3Edz	-	-	236	196
0.9G-0.3Edx-Edy-0.3Edz	78	88	236	207
0.9G+0.3Edx-Edy-0.3Edz	47	59	246	233
0.9G-0.3Edx+Edy-0.3Edz	73	66	245	222

3.4.4. Appropriate Seismic Level for the Equivalent Frame Model that Satisfies TER-2018

The results presented in the previous sections show that the structure that satisfies the TER-2007 is insufficient for the TER-2018. In order to see the seismic level that is satisfied by the case study structure per TER-2018, the matching seismic level is sought. The appropriate peak ground acceleration value is sought by gradually decreasing the peak ground acceleration values and repeating the analysis. Finally, the seismic values of the site of 36.856338° latitude 40.056115° longitude with ZC ground class of site, Ceylanpınar district of Şanlıurfa province, is defined to have the sought seismic level. This region is one of the low seismicity regions in Turkey. The seismic parameters of this site and the building-related information is presented in Table 3.23. The elastic design spectrums of two selected sites are shown in Figure 3.8. Earthquake demand and drift ratio checks are presented in Table 3.24. and Table 3.25. respectively.

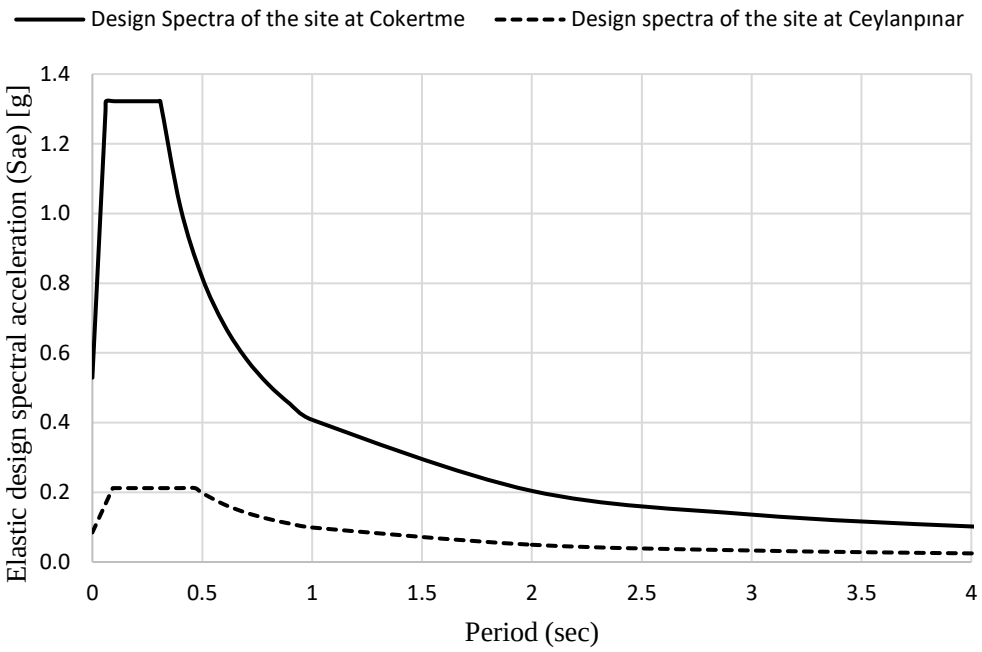

Figure 3.8. The Elastic Design Spectrums for Selected Sites

The equivalent frame model that was developed in Section 3.4.1 is used for this analysis. The results are checked whether the walls have the sufficient strength. The drift check demanded by TER-2018 is also performed. It is shown that the drift ratio calculated by using effective stiffness of walls and multiplied with R/I is less than 0.007. Drift control for wall number W8 which seems to be most critical in all combinations in frame-2 model is presented in Table 3.25 as a demonstration. The drift levels are small due to the low earthquake load and the design requirements were fully met. Design results of wall-1 and wall-21 in frame are also presented in Table 3.26. and Table 3.27.

Table 3.23. Site Seismic and Building Model Information for Frame Model-2

Site and Building Model Information	
Site Latitude	36.8563°
Site Longitude	40.0561°
Total Dead Load, G (tons)	488.88
Total Live Load, Q (tons)	60.67
Total Mass (G+0.3Q) (tons)	507.08
Number of Floor, N	2
1st Floor Height (m)	3
2nd Floor Height (m)	3
R	2.5
I	1
D	1.5
PGA (g)	0.075
S_{DS} (for DD2)	0.212
S_{D1} (for DD2)	0.099
1st Mode Natural Vibration Period $T_p^{(x)}$ (sec)	0.068
1st Floor Mass (m)	257.14
2nd Floor Mass (m)	249.94

Table 3.24. Equivalent Seismic Load Calculation for Frame Model-2

Seismic Load Calculation (DD2)		
$T_A=0.2xS_{D1}/S_{DS}$	0.093	sec
$TB=S_{D1}/S_{DS}$	0.467	sec
S_{ae}	0.177	-
$Ra(T_p^{(x)})=D+(R^{(x)}/I-D)*(T_p^{(x)}/T_B)$	1.65	-
$S_{aR}(T_p^{(x)}) = S_{ae} / R_a(T_p^{(x)})$	0.11	g
$V_{tE}^{(x)}=m_tS_{aR}(T_p^{(x)})\geq 0.04m_tIS_{DS}g$	54.67	tons
$\Delta F_{NE}^{(x)}=0.0075NV_{tE}^{(x)}$	0.82	tons
Earthquake Load acting on 1st Floor $F_{1E}^{(x)}$	27.3	tons
Earthquake Load acting on 2nd Floor $F_{2E}^{(x)}$	27.4	tons

Table 3.25. Drift Ratio Check of Frame Model-2

Combinations	**Drift Ratio x R/I**	**Drift Ratio x R/I < 0.007**
$G+Q+Ed_x+0.3Ed_y+0.3Ed_z$	0.00006	Satisfied
$G+Q+Ed_{x-}0.3Ed_y+0.3Ed_z$	0.000057	Satisfied
$G+Q-Ed_{x-}0.3Ed_y+0.3Ed_z$	0.00006	Satisfied
$G+Q-Ed_{x+}0.3Ed_y+0.3Ed_z$	0.000057	Satisfied
$G+Q+0.3Ed_{x+}Ed_y+0.3Ed_z$	0.00006	Satisfied
$G+Q+0.3Ed_{x-}Ed_y+0.3Ed_z$	0.000065	Satisfied
$G+Q-0.3Ed_{x-}Ed_y+0.3Ed_z$	0.000066	Satisfied
$G+Q-0.3Ed_{x+}Ed_y+0.3Ed_z$	0.000066	Satisfied
$0.9G+Edx+0.3Edy-0.3Ed_z$	0.00006	Satisfied
$0.9G-Edx-0.3Edy-0.3Ed_z$	0.00006	Satisfied
$0.9G+Edx-0.3Edy-0.3Ed_z$	0.000057	Satisfied
$0.9G-Edx+0.3Edy-0.3Ed_z$	0.000057	Satisfied
$0.9G+0.3Edx+Edy-0.3Ed_z$	0.000067	Satisfied
$0.9G-0.3Edx-Edy-0.3Ed_z$	0.000067	Satisfied
$0.9G+0.3Edx-Edy-0.3Ed_z$	0.000065	Satisfied
$0.9G-0.3Edx+Edy-0.3Ed_z$	0.000066	Satisfied

Table 3.26. Frame Model-2 Wall-1 Design Check

CALCULATION ACCORDING TO ULTIMATE BEARING CAPACITY								Wall	1																			
Combination	M_{ed}	N_{ed}	V_{ed}	t_{ef}	l	lx	λ	A	σ_{max}	σ_{min}	$\sigma_{min}>0$	lc_1	lc_2	Sel.lc	b	σd=Ned/A	f_{vk}	f_{vd}	$f_{vk}\leq 0.10 f_b$	$N_{rd}=\lambda A f_d$	Nrd≥Ned	V_{Rd1}	V_{Rd2}	Min V_{rd}	$DV_{ed}=1.5V_{ed}$	$V_{rd}\geq D\,V_{ed}$	Failure Criteria
-	KN-mm	KN	KN	mm	mm	mm^4	-	mm^2	Mpa	Mpa	-	mm	mm	mm	-	Mpa	Mpa	Mpa	-	KN	-	KN	KN	KN	KN	-	-
G+Q+Edx+0.3Edy+0.3Edz	30677	170	22	400	2200	3,55E+11	1	880000	0,29	0,10	Full comp.	2200	2200	2200	1,23	0,19	0,28	0,14	Satisfy	3960	Satisfy	122	163	122	33	Satisfy	Fully Satisfy
G+Q+Edx-0.3Edy+0.3Edz	30238	189	22	400	2200	3,55E+11	1	880000	0,31	0,12	Full comp.	2200	2200	2200	1,23	0,21	0,29	0,14	Satisfy	3960	Satisfy	126	168	126	33	Satisfy	Fully Satisfy
G+Q+0.3Edx+Edy+0.3Edz	2226	171	1	400	2200	3,55E+11	1	880000	0,20	0,19	Full comp.	2200	2200	2200	1,23	0,19	0,28	0,14	Satisfy	3960	Satisfy	122	163	122	2	Satisfy	Fully Satisfy
G+Q-Edx-0.3Edy+0.3Edz	32292	191	23	400	2200	3,55E+11	1	880000	0,32	0,12	Full comp.	2200	2200	2200	1,23	0,22	0,29	0,14	Satisfy	3960	Satisfy	126	168	126	35	Satisfy	Fully Satisfy
G+Q-Edx+0.3Edy+0.3Edz	31853	172	23	400	2200	3,55E+11	1	880000	0,29	0,10	Full comp.	2200	2200	2200	1,23	0,20	0,28	0,14	Satisfy	3960	Satisfy	122	163	122	35	Satisfy	Fully Satisfy
G+Q-0.3Edx-Edy+0.3Edz	10919	212	8	400	2200	3,55E+11	1	880000	0,28	0,21	Full comp.	2200	2200	2200	1,23	0,24	0,30	0,15	Satisfy	3960	Satisfy	130	174	130	12	Satisfy	Fully Satisfy
G+Q+0.3Edx-Edy+0.3Edz	7840	212	6	400	2200	3,55E+11	1	880000	0,27	0,22	Full comp.	2200	2200	2200	1,23	0,24	0,30	0,15	Satisfy	3960	Satisfy	130	174	130	9	Satisfy	Fully Satisfy
G+Q-0.3Edx+Edy+0.3Edz	9455	149	8	400	2200	3,55E+11	1	880000	0,20	0,14	Full comp.	2200	2200	2200	1,23	0,17	0,27	0,13	Satisfy	3960	Satisfy	118	157	118	11	Satisfy	Fully Satisfy
0.9G+Edx+0.3Edy-0.3Edz	31220	73	22	400	2200	3,55E+11	1	880000	0,18	-0,01	Partly comp.	2200	2040	2040	1,23	0,08	0,23	0,12	Satisfy	3960	Satisfy	95	134	95	34	Satisfy	Fully Satisfy
0.9G-Edx-0.3Edy-0.3Edz	31750	94	23	400	2200	3,55E+11	1	880000	0,20	0,01	Full comp.	2200	2200	2200	1,23	0,11	0,24	0,12	Satisfy	3960	Satisfy	107	141	107	34	Satisfy	Fully Satisfy
0.9G+Edx-0.3Edy-0.3Edz	30781	92	22	400	2200	3,55E+11	1	880000	0,20	0,01	Full comp.	2200	2200	2200	1,23	0,10	0,24	0,12	Satisfy	3960	Satisfy	106	140	106	34	Satisfy	Fully Satisfy
0.9G-Edx+0.3Edy-0.3Edz	31310	75	23	400	2200	3,55E+11	1	880000	0,18	-0,01	Partly comp.	2200	2061	2061	1,23	0,08	0,23	0,12	Satisfy	3960	Satisfy	96	135	96	34	Satisfy	Fully Satisfy
0.9G+0.3Edx+Edy-0.3Edz	9847	51	7	400	2200	3,55E+11	1	880000	0,09	0,03	Full comp.	2200	2200	2200	1,23	0,06	0,22	0,11	Satisfy	3960	Satisfy	98	127	98	10	Satisfy	Fully Satisfy
0.9G-0.3Edx-Edy-0.3Edz	10377	115	7	400	2200	3,55E+11	1	880000	0,16	0,10	Full comp.	2200	2200	2200	1,23	0,13	0,25	0,13	Satisfy	3960	Satisfy	111	147	111	11	Satisfy	Fully Satisfy
0.9G+0.3Edx-Edy-0.3Edz	8383	114	6	400	2200	3,55E+11	1	880000	0,16	0,10	Full comp.	2200	2200	2200	1,23	0,13	0,25	0,13	Satisfy	3960	Satisfy	111	147	111	10	Satisfy	Fully Satisfy
0.9G-0.3Edx+Edy-0.3Edz	8912	52	7	400	2200	3,55E+11	1	880000	0,09	0,03	Full comp.	2200	2200	2200	1,23	0,06	0,22	0,11	Satisfy	3960	Satisfy	98	127	98	10	Satisfy	Fully Satisfy

Table 3.27. Frame Model-2 Wall-21 Design Check

CALCULATION ACCORDING TO ULTIMATE BEARING CAPACITY								Wall	21																			
Combination	M_{ed}	N_{ed}	V_{ed}	t_{ef}	l	lx	λ	A	σ_{max}	σ_{min}	$\sigma_{min}>0$	lc_1	lc_2	Sel.lc	b	σd=Ned/A	f_{vk}	f_{vd}	$f_{vk}\leq 0.10 f_b$	$N_{rd}=\lambda A f_d$	Nrd≥Ned	V_{Rd1}	V_{Rd2}	Min V_{rd}	$DV_{ed}=1.5V_{ed}$	$V_{rd}\geq D\,V_{ed}$	Failure Criteria
-	KN-mm	KN	KN	mm	mm	mm^4	-	mm^2	Mpa	Mpa	-	mm	mm	mm	-	Mpa	Mpa	Mpa	-	KN	-	KN	KN	KN	KN	-	-
G+Q+Edx+0.3Edy+0.3Edz	7188	140	5	400	2200	3,55E+11	1	880000	0,18	0,14	Full comp.	2200	2200	2200	1,23	0,16	0,26	0,13	Satisfy	3960	Satisfy	116	154	116	7	Satisfy	Fully Satisfy
G+Q+Edx-0.3Edy+0.3Edz	11678	141	9	400	2200	3,55E+11	1	880000	0,20	0,12	Full comp.	2200	2200	2200	1,23	0,16	0,26	0,13	Satisfy	3960	Satisfy	116	155	116	13	Satisfy	Fully Satisfy
G+Q+0.3Edx+Edy+0.3Edz	8728	173	6	400	2200	3,55E+11	1	880000	0,22	0,17	Full comp.	2200	2200	2200	1,23	0,20	0,28	0,14	Satisfy	3960	Satisfy	123	163	123	9	Satisfy	Fully Satisfy
G+Q-Edx-0.3Edy+0.3Edz	8293	212	6	400	2200	3,55E+11	1	880000	0,27	0,22	Full comp.	2200	2200	2200	1,23	0,24	0,30	0,15	Satisfy	3960	Satisfy	130	174	130	9	Satisfy	Fully Satisfy
G+Q-Edx+0.3Edy+0.3Edz	10573	212	8	400	2200	3,55E+11	1	880000	0,27	0,21	Full comp.	2200	2200	2200	1,23	0,24	0,30	0,15	Satisfy	3960	Satisfy	130	174	130	11	Satisfy	Fully Satisfy
G+Q-0.3Edx-Edy+0.3Edz	31488	188	23	400	2200	3,55E+11	1	880000	0,31	0,12	Full comp.	2200	2200	2200	1,23	0,21	0,29	0,14	Satisfy	3960	Satisfy	126	167	126	34	Satisfy	Fully Satisfy
G+Q+0.3Edx-Edy+0.3Edz	32503	167	24	400	2200	3,55E+11	1	880000	0,29	0,09	Full comp.	2200	2200	2200	1,23	0,19	0,28	0,14	Satisfy	3960	Satisfy	121	162	121	35	Satisfy	Fully Satisfy
G+Q-0.3Edx+Edy+0.3Edz	31398	186	22	400	2200	3,55E+11	1	880000	0,31	0,11	Full comp.	2200	2200	2200	1,23	0,21	0,28	0,14	Satisfy	3960	Satisfy	125	167	125	34	Satisfy	Fully Satisfy
0.9G+Edx+0.3Edy-0.3Edz	7520	47	5	400	2200	3,55E+11	1	880000	0,08	0,03	Full comp.	2200	2200	2200	1,23	0,05	0,22	0,11	Satisfy	3960	Satisfy	97	125	97	8	Satisfy	Fully Satisfy
0.9G-Edx-0.3Edy-0.3Edz	7961	119	6	400	2200	3,55E+11	1	880000	0,16	0,11	Full comp.	2200	2200	2200	1,23	0,14	0,25	0,13	Satisfy	3960	Satisfy	112	148	112	8	Satisfy	Fully Satisfy
0.9G+Edx-0.3Edy-0.3Edz	11346	47	8	400	2200	3,55E+11	1	880000	0,09	0,02	Full comp.	2200	2200	2200	1,23	0,05	0,22	0,11	Satisfy	3960	Satisfy	97	125	97	13	Satisfy	Fully Satisfy
0.9G-Edx+0.3Edy-0.3Edz	10904	118	8	400	2200	3,55E+11	1	880000	0,17	0,10	Full comp.	2200	2200	2200	1,23	0,13	0,25	0,13	Satisfy	3960	Satisfy	112	148	112	12	Satisfy	Fully Satisfy
0.9G+0.3Edx+Edy-0.3Edz	30715	71	22	400	2200	3,55E+11	1	880000	0,18	-0,01	Partly comp.	2200	2032	2032	1,23	0,08	0,23	0,12	Satisfy	3960	Satisfy	94	133	94	33	Satisfy	Fully Satisfy
0.9G-0.3Edx-Edy-0.3Edz	31156	95	22	400	2200	3,55E+11	1	880000	0,20	0,01	Full comp.	2200	2200	2200	1,23	0,11	0,24	0,12	Satisfy	3960	Satisfy	107	141	107	33	Satisfy	Fully Satisfy
0.9G+0.3Edx-Edy-0.3Edz	32171	73	23	400	2200	3,55E+11	1	880000	0,18	-0,02	Partly comp.	2200	2019	2019	1,23	0,08	0,23	0,12	Satisfy	3960	Satisfy	94	134	94	35	Satisfy	Fully Satisfy
0.9G-0.3Edx+Edy-0.3Edz	31730	92	23	400	2200	3,55E+11	1	880000	0,20	0,01	Full comp.	2200	2200	2200	1,23	0,11	0,24	0,12	Satisfy	3960	Satisfy	106	140	106	34	Satisfy	Fully Satisfy

3.4.5. Comparison of the Analysis Model Results

The study shows that the two-story case study building sufficient for TER-2007 is not enough for the TER-2018. Therefore, a closer investigation of the global and local demands could be useful to follow the differences of the regulations.

The ratio of the earthquake demands to the building mass in both regulations is shown in Table 3.28. The ground acceleration value of 0.4g used in TER-2007 was increased to the value of 0.463g in the TER-2018 for location in Çökertme. Based on the modified design spectra, the base shear vs. building weight increased from 50% to 77%.

According to the analysis result of TER-2018, shear capacities could not be calculated due to axial insufficiency due to tensile stress. Therefore, to more accurately compare the demand and capacity variations of the walls, the maximum demands and minimum shear capacities in the critical combinations at the 0.075g peak acceleration for location in Ceylanpınar, whose design had been completed, are given in Table 3.29.

Table 3.28. Ratios of Base Shear to Total Mass According to Regulations at the selected location in Çökertme

Regulation	Base Shear/ Total Mass
TER-2007	0.50
TER-2018	0.77

The seismic force calculation, according to TER-2007 and TER-2018 regulations, the earthquake demand has increased by 27 percent by mass in the new regulation. The shear forces were also, increased by 50 percent with the excess strength coefficient according to demand calculation in TER-2018.

The total shear force demands on the walls are increased 38 percent in the x-direction based on the analysis values of the 2007 regulation according to the analysis result of seismic demand, that location is in Ceylanpınar. Besides, the 34 percent increase in total seismic demand is observed in y-direction walls. In element-based comparison,

there was a decrease in seismic demands with values ranging from 2 to 58 percent generally in short walls in both directions.

On the other hand, the 37 and 38 percent reductions were observed in total shear capacities, respectively in x and y directions. The decrease was observed in element-based shear capacity comparisons, with percentages varying between 23 to 65 percent in both directions.

Table 3.29. Analyzed and Calculated Demand and Resisting Forces According to TER-2007 and TER-2018 at 0.075g peak ground acceleration seismic demand in the location of Ceylanpınar at critical combinations

					DEMANDS			CAPACITIES		
					TER-2007	TER-2018		TER-2007	TER-2018 (Frame Model-2)	
				Wall	V (t)	DV_{ed} (t)	%Diff.	V_r(t)	min V_{rd}(t)	%Diff.
Combinations	TER-2007: G+Q+Ex-0.3Ey	TER-2018: G+Q+Edx-0.3Edy+0.3Edz	Walls in x-direction	W1	3.4	3.3	-2	19.6	12.6	-36
				W3	4.1	4.9	19	21.4	16.6	-23
				W5	3.4	2.8	-17	17.3	13.1	-24
				W7	5.4	6.4	20	31.2	20.7	-34
				W9	3.4	3.4	1	19.7	13.0	-34
				W11	2.7	3.4	28	19.3	12.1	-37
				W13	3.3	6.0	84	22.4	15.5	-31
				W15	3.4	6.1	80	21.1	16.2	-23
				W17	4.7	9.7	105	35.7	21.5	-40
				W19	3.3	5.2	59	20.2	15	-26
				W47	7.3	13.1	78	51.7	30.2	-42
				W49	1.9	1.3	-32	13.9	9.7	-30
				W51	1.9	0.8	-58	14.1	9.4	-34
				W53	1.9	1.1	-41	14.9	9.2	-38
				W55	4.8	7.7	62	37.8	13.1	-65
TOTAL					**54.7**	**75.2**	**38**	**360.5**	**227.9**	**-37**
Combinations	TER-2007: G+Q-0.3Ex+Ey	TER-2018: G+Q-0.3Edx+Edy+0.3Edz	Walls in y-direction	W21	4.6	3.4	-27	17.6	12.6	-29
				W23	4.2	3.6	-15	20.0	13	-35
				W25	3.6	2.1	-41	17.4	9.8	-44
				W27	2.3	4.1	75	19.7	12.4	-37
				W29	3.1	7.8	152	26.2	16.3	-38
				W31	1.8	2.5	38	16.4	9.3	-43
				W33	4.8	5.4	12	25.6	16.8	-34
				W35	3.6	2.8	-22	18.2	12.4	-32
				W37	3.9	3.7	-6	20.7	11.7	-43
				W39	2.6	1.5	-42	16.1	11.0	-32
				W41	9.3	15.5	66	54.8	30.0	-45
				W43	4.3	7.7	78	31.2	20.6	-34
				W45	6.4	13.2	107	39.9	24.4	-39
TOTAL					**54.7**	**73.3**	**34**	**324.0**	**200.3**	**-38**

3.5. Discussion and Result

The case study building was designed according to TER-2007. The design is based on an earthquake demand with peak ground acceleration of 0.4g and results show that walls with 40 cm thickness walls were sufficient for earthquake demand. In contrast, same building with 40 cm thick walls was not sufficient according to TER-2018. The same building had sufficient strength only if the peak ground acceleration drops from 0.463g to 0.075g.

Analysis and design results according to allowable stress and ultimate strength methods were compared. The demands and capacities of the walls in x and y directions are calculated according to critical combinations of seismic actions in different directions.

As a result, the earthquake demand is increased 38 and 34 percent in total in TER-2018, respectively x and y directions. The capacities are also decreased 37 and 38 percent in total in TER-2018, respectively x and y directions. When the demands on the walls are examined on element basis, it has been observed that the demands on the short walls have generally decreased due to the change in the stiffness calculation in the short walls.

CHAPTER 4

NONLINEAR STATIC ANALYSIS OF THE CASE STUDY BUILDING

Significant difference between the analysis results of the case study building designed according to 2007 and 2018 Turkish Earthquake Regulations, and the examined behavior of unreinforced masonry structures during earthquakes is observed. Therefore, it will be informative to perform a nonlinear analysis that have an alternative view to the behavior of the case study building. Hence, the same structure analyzed in the previous chapters is subjected to pushover analysis for this purpose.

The previous and existing Turkish regulations do not define any nonlinear procedure for unreinforced masonry structures. Therefore, the procedure used by Pasticier et.al. (2007) and Dolce (1989) is adopted.

4.1. Nonlinear Modelling of Case Study Building

The nonlinear behavior of the unreinforced masonry structure is attempted to be modeled by introducing the force-displacement response of individual members through a frame model with lumped nonlinearity through plastic hinges. Two type of hinges are defined at members to represent the flexure and shear failure modes independently.

Extensive studies are done by the Italian researchers for modeling the nonlinear behavior of unreinforced masonry structures in Catania Project (2000). In this project, two masonry buildings in Catania were selected and their mechanical properties were determined by in-situ and laboratory tests. Numerical models of these buildings were analyzed using different and advanced analysis software by different universities and research groups in Italy. A no tensile strength microelement model with crushing and shear failures was used by Basilica research group. In the Genoa research group, a finite element model that had layer failures was used. The University of Pavia research group used the code SAM (Simplified Analysis of Masonry Building). This study had become

an important reference for the failure criteria that (Pasticier et. al. 2007) also used in their work.

SAM code is based on the equivalent frame model and had been validated by many experimental studies. (Pasticier et. al. 2007) is underlying that there is difference between the SAM code and SAP2000 analysis software. It is stated that SAP2000 code does not update variable axial stress and H_0 values of the individual elements' strength under varying forces during the pushover analysis. Since the H_0 value did not vary greatly, (Pasticier et. al. 2007) applied the pushover analysis in two procedures to reveal the difference in updating axial stress only. The first method was performed by employing the pushover analysis with strengths calculated under gravitational loads only. In the second method, model was analyzed under both gravity load and lateral load under increasing magnitudes up to the elastic limit of the frame. As a result, there is no significant differences between the results of these two procedures.

The modelling started through partitioning the existing walls into piers and spandrels according to their position and geometry. The masonry walls are modelled by two flexural hinges at the end of the effective height of piers and one shear hinge at the mid-height of effective height of the wall. Also, one shear hinge is defined at the middle of each spandrels. (Pasticier et. al. 2007) provide limits on the ultimate displacement and rotation values of shear and flexural hinges. In piers, ultimate rotation of flexural hinges is restricted to 0.8% and ultimate displacement of shear hinges is restricted to 0.4% lateral deflection of the deformable height. Shear hinge in spandrels, there is no deformation limit but 25% of the strength of is defined as residual strength after reaching the limit deflection. In moment hinges, ultimate moment M_u is defined as presented in Eq.4.1. according to test result of (Magenes et. al. 1977). In shear hinges, two strength criteria are considered.

In shear hinges, first one is shear failure with diagonal cracking as given Eq. 4.2. which was originally proposed by Turnsek et.al. (1971) and later developed by Turnsek et.al. (1980). Another criterion is related with shear failure with sliding defined in Eq.4.3. In spandrels, only shear failure criterion that is in the mid height of deformable part is used as given in Eq. 4.4.

$$Mu = \frac{\sigma_0 D^2 t}{2}\left(1-\frac{\sigma_0}{k f_d}\right) \quad \text{Eq.4.1}$$

$$V_u^f = \frac{1.5 f_{v0d} D t}{\xi}\sqrt{1+\frac{\sigma_0}{1.5 f_{v0d}}} \quad \text{Eq.4.2.}$$

$$V_u^s = \frac{\frac{3}{2} f_{v0d} + \mu\frac{\sigma_0}{\gamma_m}}{1+\frac{3H_0}{D\sigma_0} f_{v0d}} Dt \quad \text{Eq.4.3.}$$

$$V_u = h t f_{v0d} \quad \text{Eq.4.4}$$

where,

σ_0: mean vertical stress that is determined by analysis result of combination G+0.3Q,

D: pier plan length,

t: pier or spandrel thickness,

k: the coefficient of vertical stress distribution at the compressed toe and it is taken as 0.85 as rectangular stress block,

f_d: design compressive strength

f_{v0d}: design shear strength with no axial stress,

ξ: geometrical ratio parameter that is equal to pier height over pier length,

H_0: effective pier height that is height from zero bending moment to the applied force and it was taken as half of the pier height,

γ_m: safety factor taken as 2.0

h: spandrel effective length.

The individual wall element boundaries are defined by adopting the Dolce (1989) approach. Here, the portions of the panels at the intersection of the walls are transformed to rigid end zones following a procedure that follow the geometrical boundaries between walls. A representative example of the procedure to determine the effective pier heights is presented in Figure 4.1. For spandrels, effective lengths are equal to corresponding opening lengths. The frame model is constructed by first defining each element end zones and then connecting the corner walls with rigid spandrels.

A representative example of how to use defined procedure in one of wall axis of the case study structure is presented in Figure 4.2. The corresponding wire frame model with the end length offsets in SAP2000 is also presented in Figure 4.3. The whole case study building wire frame model is 3D is presented in Figure 4.4.

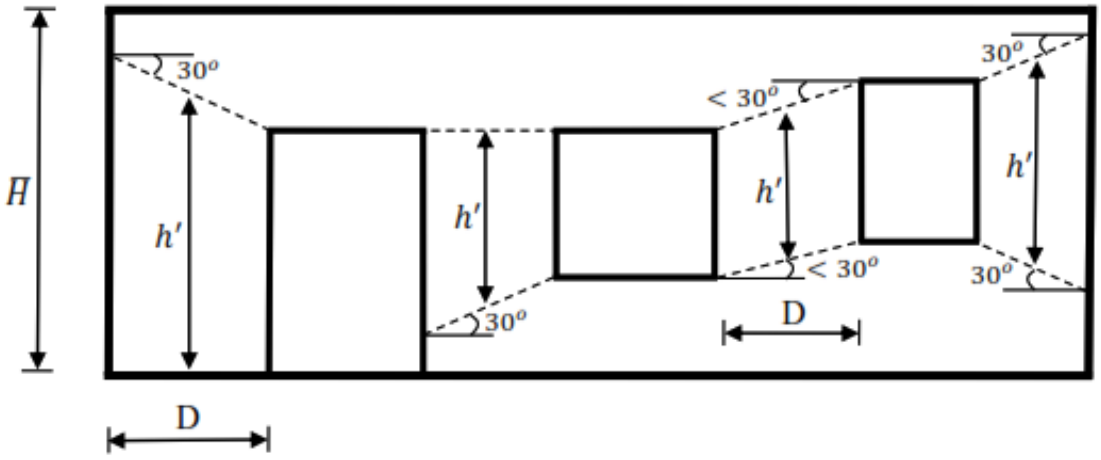

Figure 4.1. Determination of Effective Height (Source: Dolce 1989)

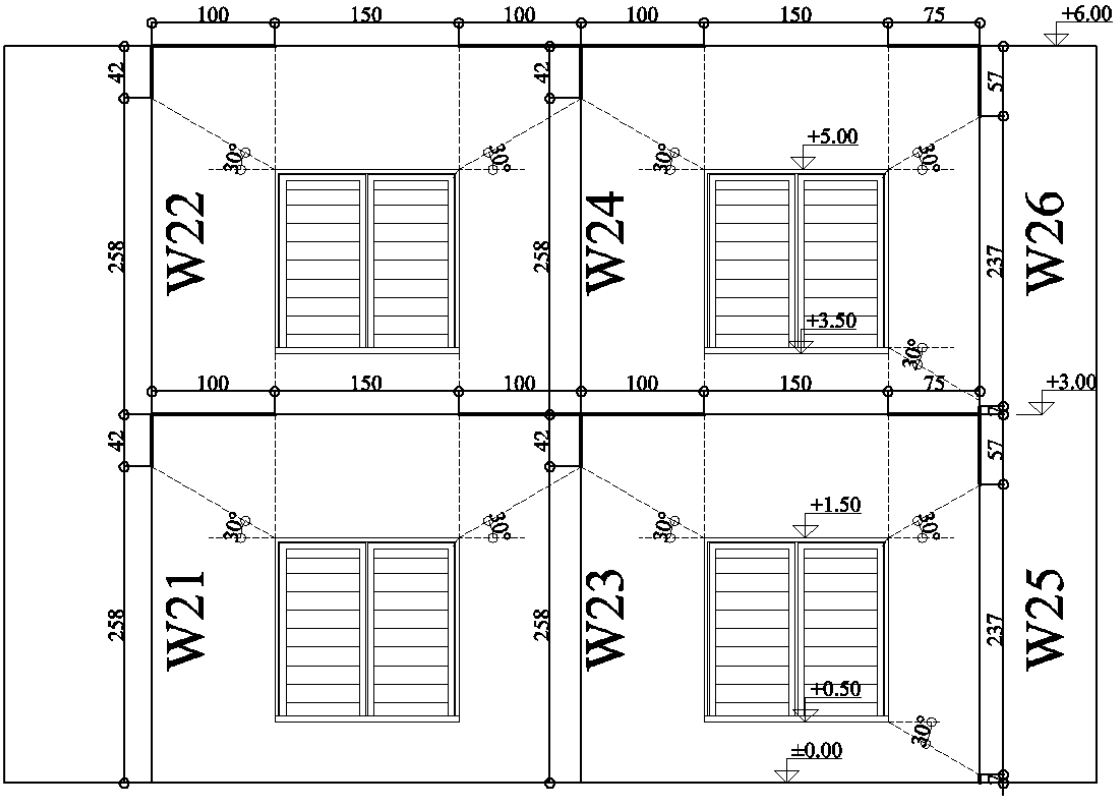

Figure 4.2. 1-1 Axis End Length Offsets Determination

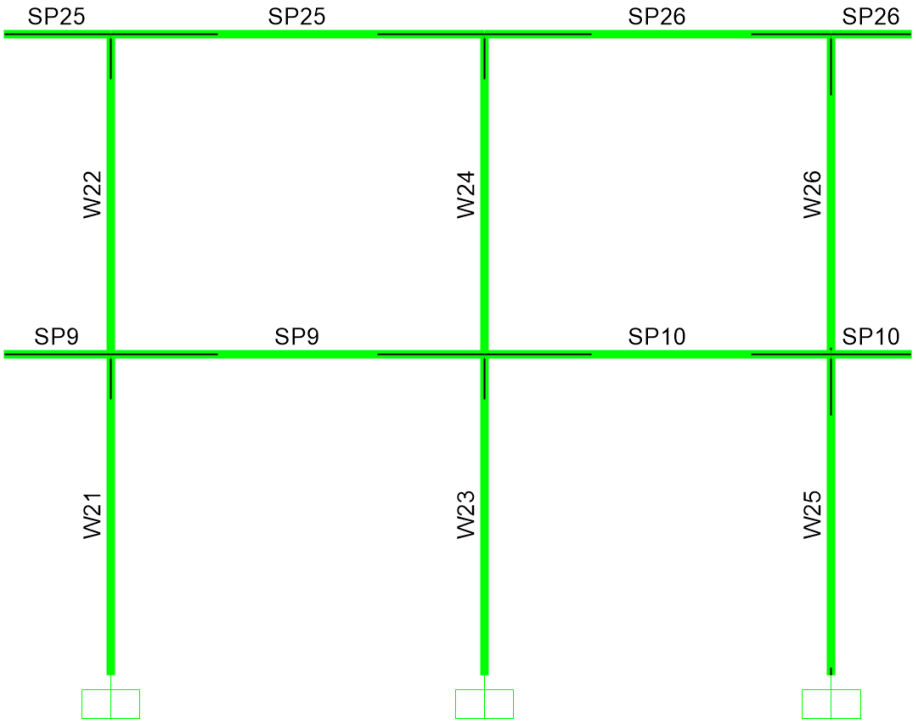

Figure 4.3. End Length Offsets of Frame of 1-1 Axis in SAP-2000

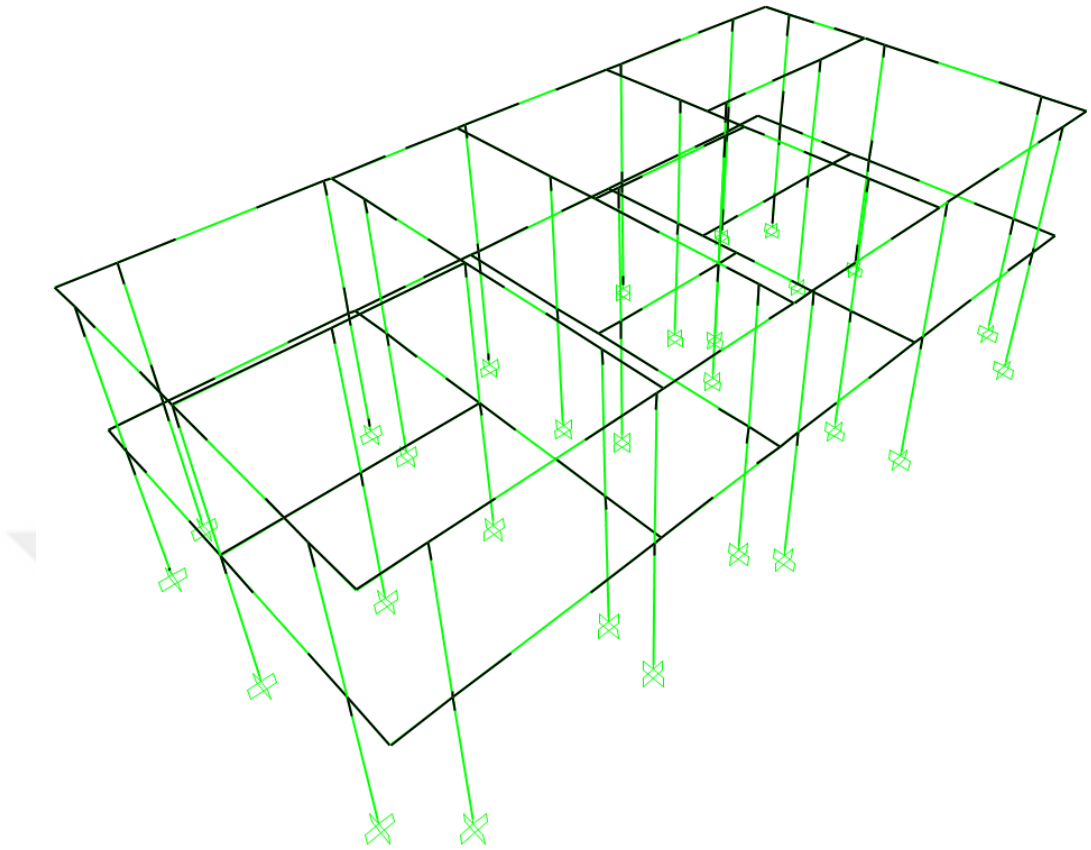

Figure 4.4. Effective Heights and Lengths in Nonlinear Model in SAP2000

The material properties in nonlinear model are same as the material properties that are used in linear model. In order to start the analysis with the cracked elements as defined in TER-2018, the stiffness of individual elements is reduced by fifty percent of the gross values that are calculated according to effective heights and lengths. Thus, the major difference of the model will be the plastic deformations at the hinges of each element. Static pushover analysis is performed using the numerical model. Pushover analysis was applied with displacement control and two joints were selected at the roof level in order to monitor displacement that was reaching up to 30 mm.

4.2. Analysis Results of Case Study Building

Modal and nonlinear static (pushover) analyses for x and y directions are performed. In modal analysis, the first natural vibration period T_1 is calculated 0.079 seconds for y-direction and the second period T_2 is obtained as 0.073 seconds for x-direction. These results showed that the stiffness, which is directly proportional to the wall areas, is lower along y-direction. Further information about the results of modal analysis is given in Table 4.1 below.

Table 4.1. Modal Properties of Building

Mode Number	Direction	Period (sec)	Modal Participation Factor (Γ)	Mode Shapes
1	y-direction	0.079	20.24	(0.0312, 0.0590)
2	x-direction	0.073	22.51	(0.0280, 0.0531)

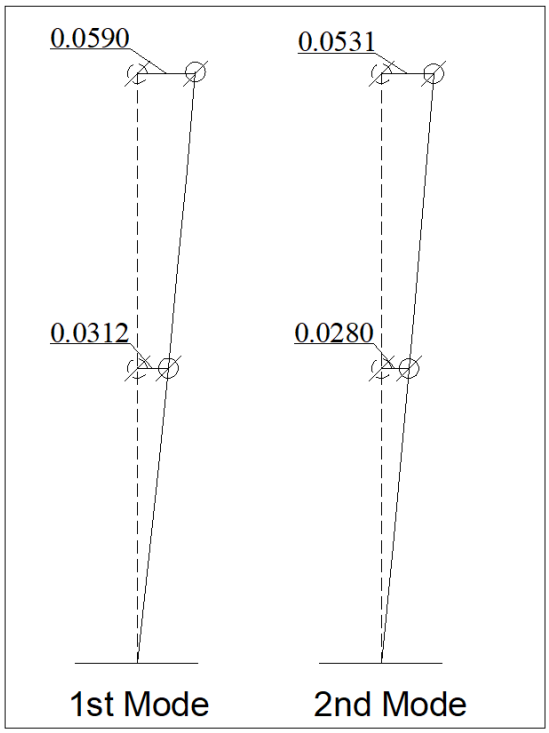

Figure 4.5. Modal Vector of 1st and 2nd Modes

Pushover analysis resulted the maximum base shear force along the Y-direction as 2191 kN at about 10 mm displacement. The maximum base shear force along the X-direction is determined as 2326 kN at 10.5 mm displacement. Pushover curves for the Y and X-directions are presented in Figure 4.6. and Figure 4.7.

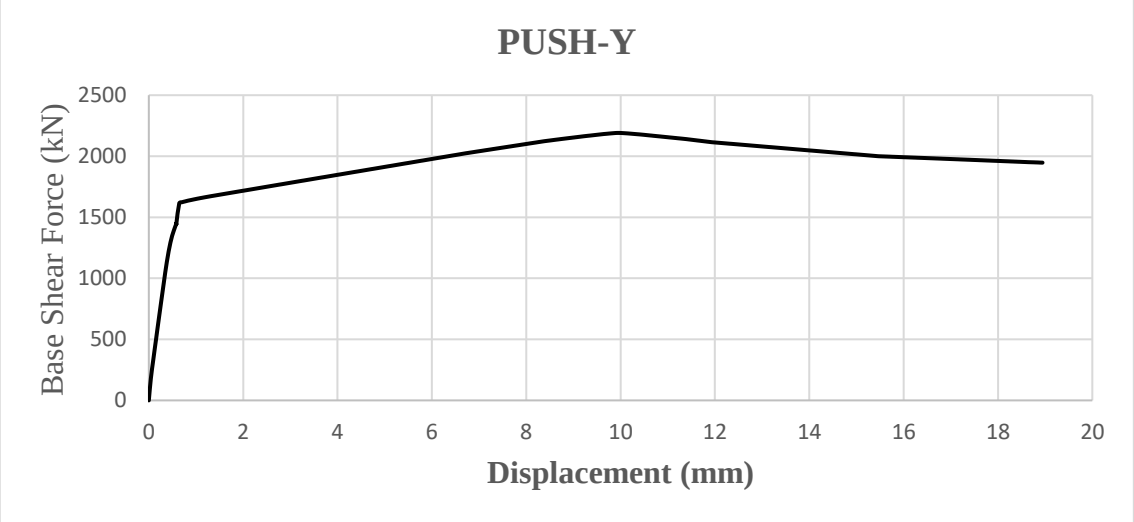

Figure 4.6. Pushover Curve for Push-Y

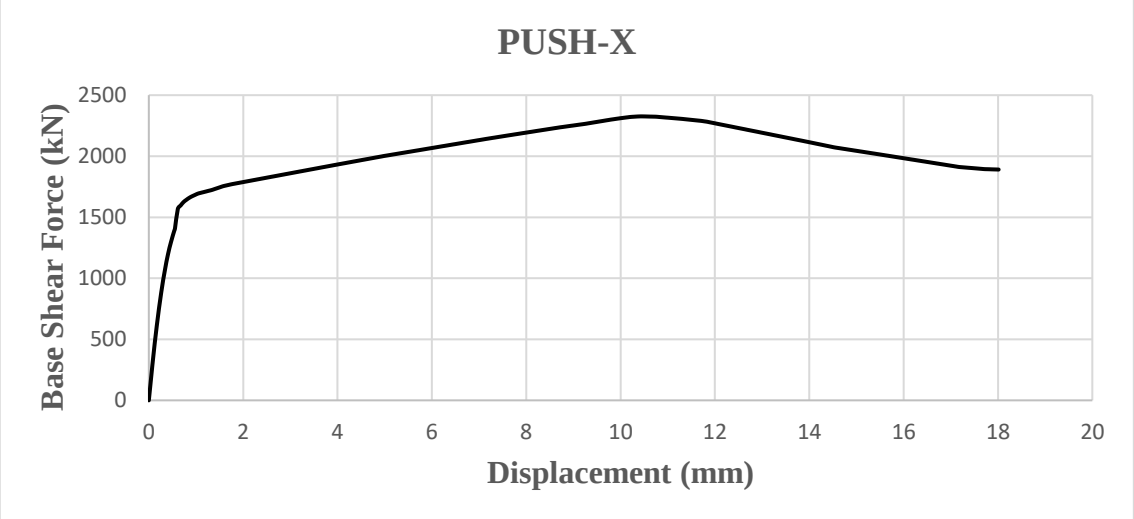

Figure 4.7. Pushover Curve for Push-X

In order to define displacement demands for the case study structure, both TER-2018 and FEMA-356 procedures are used. These procedures are basically defined by similar equations. However, the way the process is presented is different.

4.3. Calculation of Demand According to TER-2018

First the design spectrum for earthquake ground motion level DD-2 and soil type ZC obtained and the roof displacement demand calculated according to procedure defined in TER-2018. In order to find earthquake demand of building, capacity curves of the building in two orthogonal directions should be converted to acceleration displacement response spectrum (ADRS) format. (Figure 4.8 and 4.9.) Design spectra conversion is performed with the assumption that acceleration and displacement are related through pseudo-acceleration relation. Using period values corresponding to the spectral acceleration values in design spectrum, spectral displacements are easily calculated by using the acceleration design spectrum defined through Eq.4.5to 4.9. in TER-2018.

$$S_{ae}(T) = (0.4 + 0.6\,\frac{T}{T_A})\,S_{DS} \qquad (0 \le T \le T_A) \qquad \text{Eq.4.5}$$

$$S_{ae}(T) = S_{DS} \qquad (T_A \le T \le T_B) \qquad \text{Eq.4.6}$$

$$S_{ae}(T) = \frac{S_{DS}}{T} \qquad (T_B \le T \le T_L) \qquad \text{Eq.4.7}$$

$$S_{ae}(T) = \frac{S_{D1}}{T} T_L \qquad (T_L \le T) \qquad \text{Eq.4.8}$$

$$S_{de}(T) = \frac{T^2}{4\pi^2}\, g\, S_{ae}(T) \qquad \text{Eq.4.9}$$

where,

$S_{ae}(T)$ = Horizontal elastic design spectral acceleration [g]

S_{de} = Linear elastic spectral displacement [mm]

S_{DS} = Short period design spectral acceleration coefficient

T = Natural vibration period [s]

T_A = Horizontal elastic design acceleration spectrum corner period [s]

T_B = Horizontal elastic design acceleration spectrum corner period [s]

T_L = Transition period to constant displacement zone in horizontal elastic design spectrum [s]

Capacity curve conversion was determined according to Eq.4.10. to 4.13., as defined in TER-2018.

$$m_{ix1}^{(X,1)} = m_i \, \Phi_{ix1}^{(1)} \, \Gamma_1^{(X,1)} \quad \text{Eq.4.10}$$

$$m_{tx1}^{(X,1)} = m_{1x1}^{(X,1)} + m_{2x1}^{(X,1)} \quad \text{Eq.4.11}$$

$$\alpha_1^{(X,k)} = \frac{V_{tx1}^{(X,k)}}{m_{tx1}^{(X,1)}} \quad \text{Eq.4.12}$$

$$d_1^{(X,k)} = \frac{u_{Nx1}^{(X,k)}}{\Phi_{Nx1}^{(1)} \, \Gamma_1^{(X,1)}} \quad \text{Eq.4.13}$$

where,

m_i = i^{th} floor mass [t]

$\Phi_{ix1}^{(1)}$ = The amplitude of the fixed mode shape determined in the first push step on the i^{th} floor and not changed during the push calculation in x-direction.

$\Gamma_1^{(X,1)}$ = Modal contribution multiplier for X earthquake direction determined in the first push step and calculated according to the fixed mode shape that has never been changed during the push calculation.

$m_{ix1}^{(X,1)}$ = i^{th} floor effective modal mass determined in the first push step in the direction of x-axis for x earthquake direction and calculated according to the fix mode shape that has never been changed during the push calculation. [t]

$m_{tx1}^{(X,1)}$ = Effective modal mass for base shear force determined in the first push step in the direction of x axis for X earthquake direction and calculated according to the fix mode shape that has never been changed during the push calculation. [t]

$\alpha_1^{(X,k)}$ = Modal pseudo acceleration of the first mode modal single degree of freedom system in the kth push step for the X earthquake direction. [m/s^2]

$V_{tx1}^{(X,k)}$ = Base shear force calculated in the kth push step for the X earthquake direction in the direction of x-axis. [kN]

$d_1^{(X,k)}$ = Modal displacement of the first mode modal single degree of freedom system in the kth push step for the x earthquake direction. [mm]

$u_{Nx1}^{(X,k)}$ = Displacement calculated in the direction of x-axis on the Nth floor (at the top of the building) at the kth push step for the x earthquake direction. [mm]

Mode shapes and modal participation factors according to modal analysis result of building is given in table 4.1.

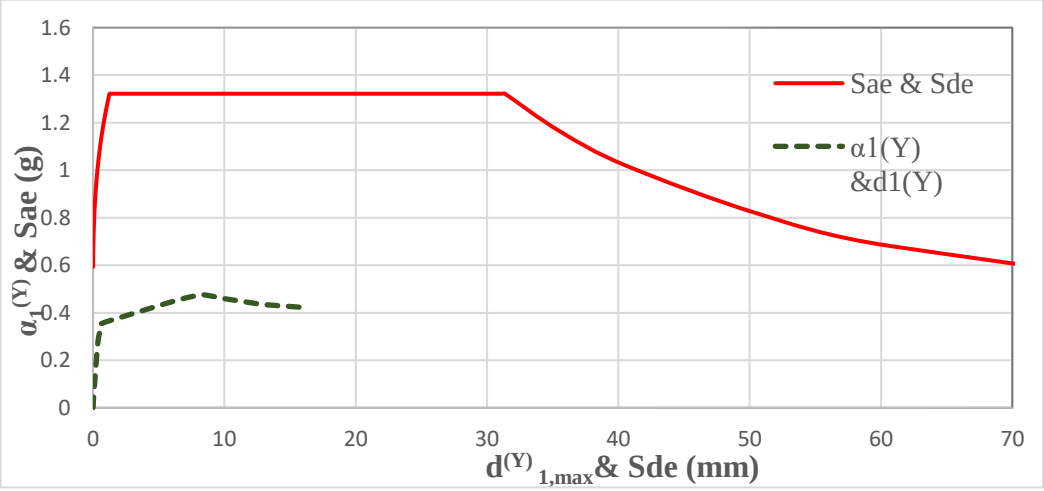

Figure 4.8. ADRS Representation of Capacity Demand for Push-Y

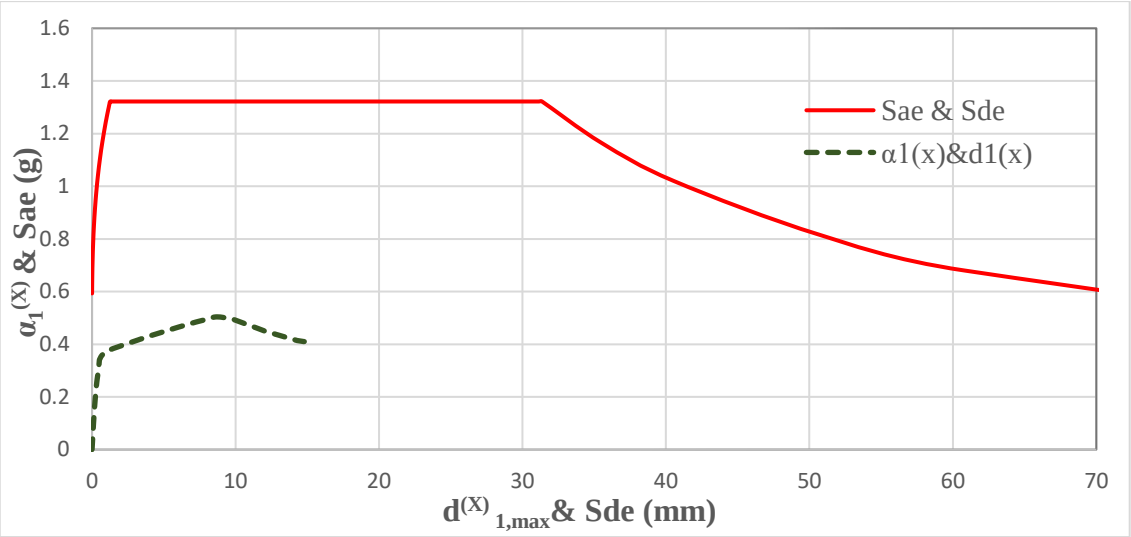

Figure 4.9. ADRS Representation of Capacity Demand for Push-X

Roof displacement demands of building are determined with an iteration procedure defined in TER-2018. Firstly, $S_{de}(T_1)$ is calculated according to $S_{ae}(T_1)$ and ω values with using Eq.4.14. Then, α_{y1}^{0} that is the pseudo yield acceleration, is located by assuming the initial tangent drawn tangent to the initial almost linear portion of the pushover curve. Then a secondary line that will provide similar areas below and above the pushover curves and these lines is drawn. Next, using Eq.4.15. and Eq.4.16., yield strength reduction coefficient R_y and spectral displacement ratio C_R were calculated.

Finally, the maximum displacement of the modal single degree of freedom system, $S_{di}(T_1)$ is determined according to Eq.4.17. The procedure continues until the expected maximum displacement of the modal single degree of freedom system, $d_{1,max}^{(X)}$ and calculated $S_{di}(T_1)$ values are in the close proximity.

$$S_{de}(T_1) = \frac{S_{ae}(T_1)}{(\omega_1)^2} \qquad \text{Eq.4.14}$$

$$R_y = \frac{S_{ae}(T_1)}{\alpha_{y1}^{0}} \qquad \text{Eq.4.15.}$$

$$C_R = \frac{1+(R_y-1)\frac{T_B}{T_1}}{R_y} \qquad \text{for } (T_1 \leq T_B) \qquad \text{Eq.4.16.}$$

$$S_{di}(T_1) = C_R S_{de}(T_1) \quad \text{Eq.4.17}$$

The application of the procedure defined above, resulted in the roof displacement demands of 7.8 mm (0.11% drift ratio) and 7.2 mm (0.11% drift ratio) along Y and X-directions respectively. The calculated displacement demands are represented on pushover curves in Fig. 4.10 and Fig.4.11.

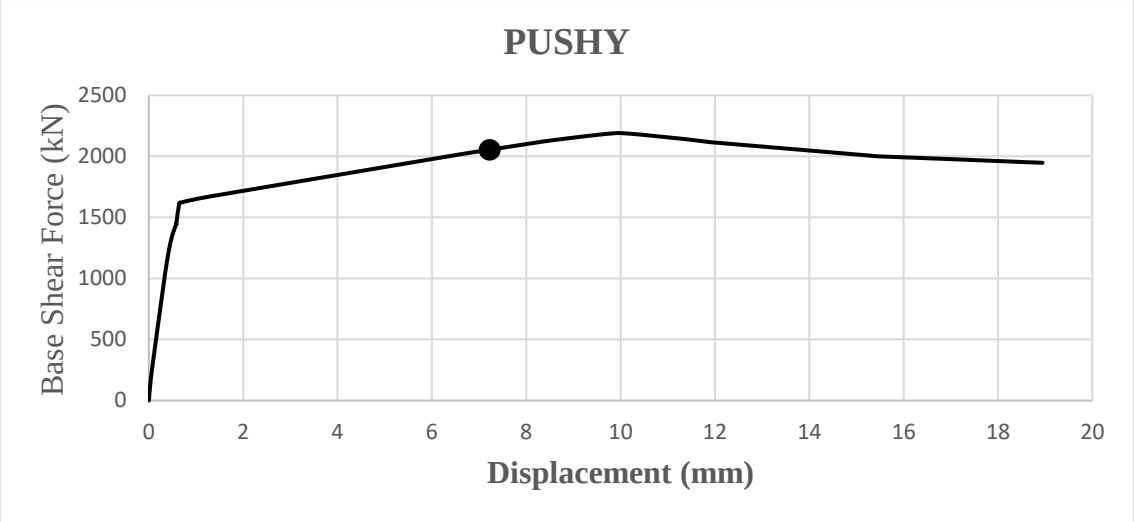

Figure 4.10. Calculated Displacement Demand Point Along Y-direction by TER-2018

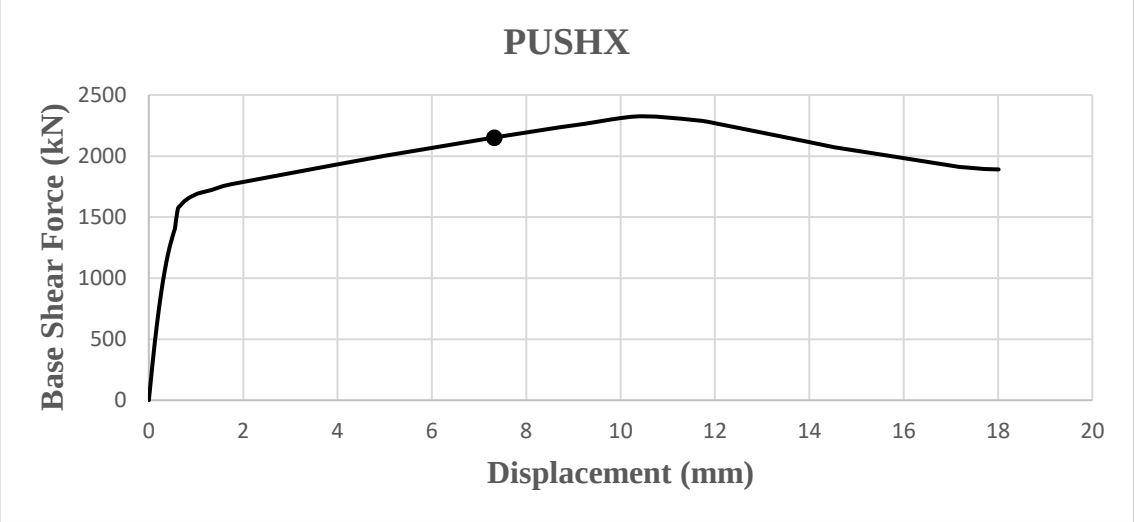

Figure 4.11. Calculated Displacement Demand Point Along X-direction by TER-2018

4.4. Calculation of Demand According to FEMA356

Unlike TER-2018, FEMA356 formulates a procedure to calculate the displacement demand by constructing a bilinear force displacement relation from the calculated pushover curves and through using a series of coefficients. Bilinear force-displacement curve is completed by arranging the horizontal line drawn from the first assumed target displacement value and the lines drawn from origin of the pushover curve so that there are equal areas above and below the curve. After the point where lower and upper areas of the lines are equalized, the process continues until the previous assumed target displacement value is equalized with the displacement value found with the target displacement formula. In figure 4.12., an example of creation of the bilinear of the curve from the pushover curve is presented. In figures 4.13. and 4.15. created bilinear force-displacement relations along two orthogonal directions according to procedure that is shown in Fig.4.12. are represented.

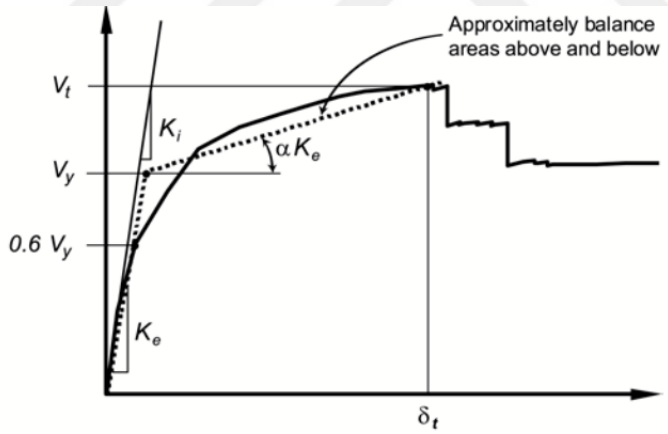

Figure 4.12. Creation of the Bilinear Curve from the Pushover Curve according to FEMA356 (Source: FEMA356)

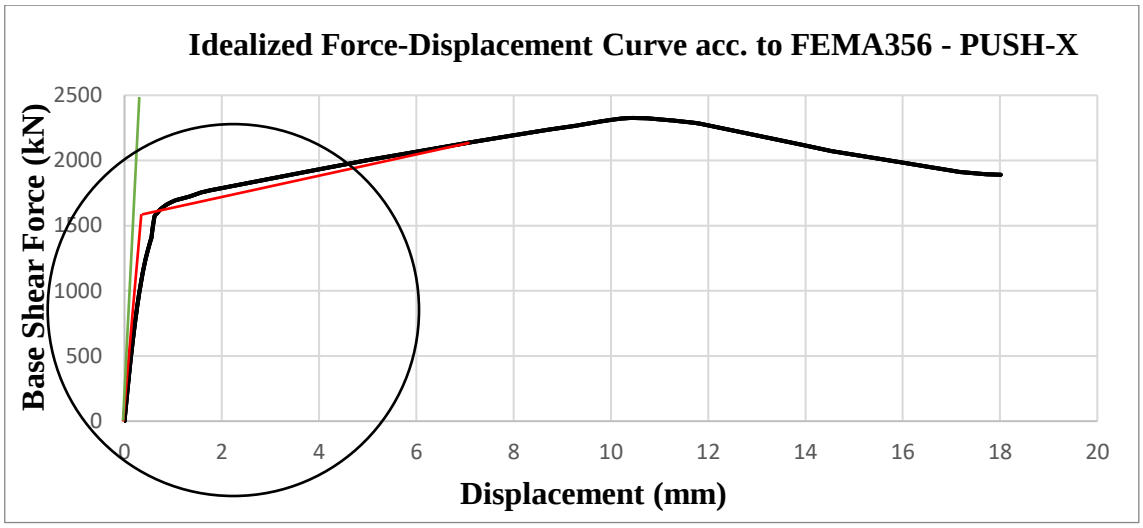

Figure 4.13. Bilinearized Pushover Curve in X-direction

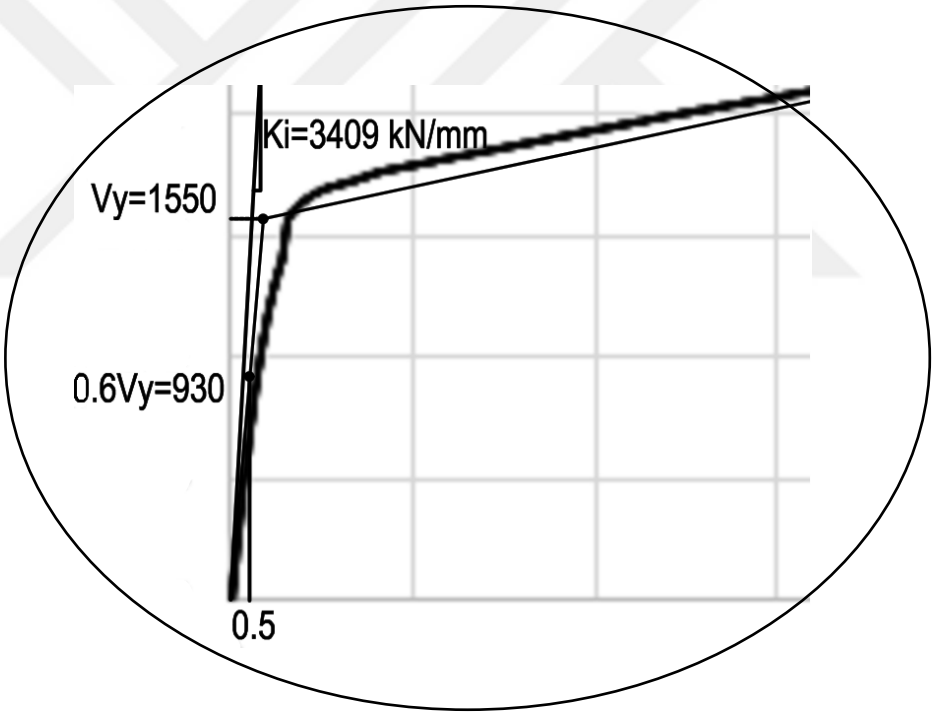

Figure 4.14. Details of Bilinearized Pushover Curve in X-direction

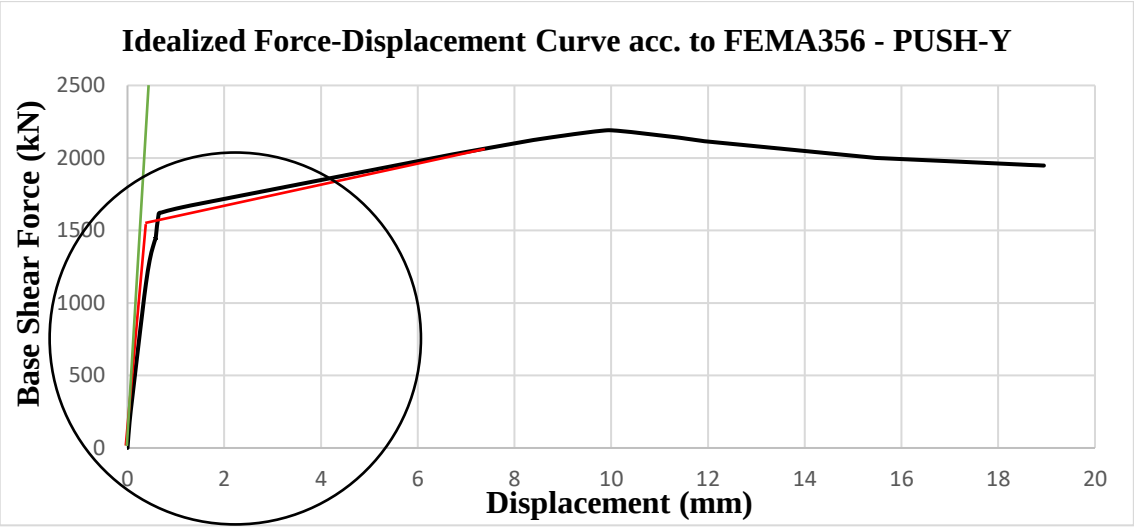

Figure 4.15. Bilinearized Pushover Curve in Y-direction

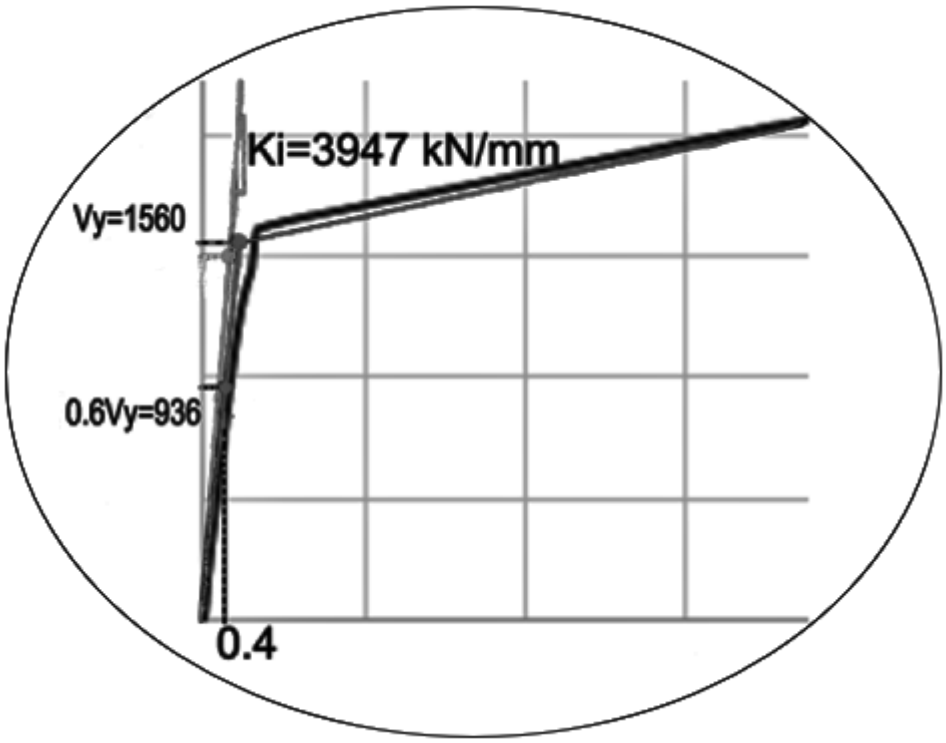

Figure 4.16. Details of Bilinearized Pushover Curve in Y-Direction

After obtaining the bilinear curve from the pushover curves, target displacements for each direction are calculated by employing Eq.4.14.

$$\delta_t = C_0\, C_1\, C_2\, C_3\, S_a \frac{T_e^2}{4\pi^2}\, g \qquad \text{Eq.4.14}$$

$$T_e = T_i \sqrt{\frac{K_i}{K_e}} \qquad \text{Eq.4.15}$$

$$R = \frac{S_{ae}}{Vy/W}\, C_m \qquad \text{Eq.4.16}$$

where,

C_0 = Modification factor with related spectral displacement of an equivalent single degree of freedom system to the roof displacement of the building multi degree of freedom system and it is taken as 1.2.

C_1 = Modification factor to relate expected maximum inelastic displacements to displacements calculated for linear elastic response.

1.0 for $T_e \geq T_B$

$[1.0 + (R-1)\, T_B / T_e] / R$

T_e = Effective fundamental period of the building [s]

T_i = Elastic fundamental period of the building [s]

T_B = Horizontal elastic design acceleration spectrum corner period [s]

R = Yield strength coefficient

C_2 = Modification factor to represent the effect of pinched hysteretic shape, stiffness degradation and strength deterioration on maximum displacement response. Shall be taken as 1.0 for nonlinear procedures.

C_3 = Modification factor to show increased displacements due to dynamic P- Δ effect. C_3 is taken as 1.0 for buildings with positive post-yield stiffness.

S_{ae} = Horizontal elastic design spectral acceleration [g]

V_y = Yield strength of building that is breaking point of bilinearized pushover curve [kN]

W = Effective seismic weight

C_m = Effective mass factor and taken as 1.0 for other type one-two stories building

The roof displacement demands according to FEMA356 are calculated as 9.0 mm (%0.13) and 9.0 mm (%0.13) along Y and X-directions respectively.

4.5. Discussion of Analysis Results

The definition of the structure performance level necessities the evaluation of the individual element performances for the calculated target displacement demand of the structure. The performance points of the elements are determined based on FEMA-356. There is no displacement limitation on shear hinge for spandrels. Therefore, performance analysis of elements is performed only for pier hinges. Performance points are defined according to drift ratio and rotation of piers. Selected performance levels according to FEMA-356 definitions, are given in Table 4.2. Performance levels, according to Pasticier et. al. (2007), is also given in Table 4.3.

Table 4.2. Performance Levels according to FEMA-356

	IO	LS	CP
Drift ratio	0.1%	0.3%	0.4%
Rotation	0.1%	$0.3h_{eff}$ /L %	$0.4h_{eff}$ /L %

*IO: Immediate Occupancy *LS: Life Safety *CP: Collapse Prevention

*h_{eff}: Effective height of pier *L: Length of Pier

Table 4.3. Performance Levels according to Pasticier et. al. (2007)

	IO	LS	CP
Drift ratio	0.007%	0.2%	0.3%
Rotation	0.007%	0.2%	0.3%

*IO: Immediate Occupancy *LS: Life Safety *CP: Collapse Prevention

The performance levels of the pier along each orthogonal direction are found and evaluated according to FEMA-356 definitions for comparison. Evaluated performance levels of piers according to TER-2018 target displacement points of 7.8mm and 7.2mm along Y and X-direction respectively and FEMA-356 target displacement points of 9.0mm for both directions are shown in Table 4.4. and Table 4.5.

Table 4.4. Number of Piers for Determined Performance Levels According to FEMA-356 at TER-2018 Target Displacement Points

		Performance Levels		
Loading Direction	**Floor**	**No of Piers**		
		IO	**LS**	**CP**
Y-Direction	**First Floor**	**0**	**13**	**0**
	Second Floor	**0**	**13**	**0**
X-Direction	**First Floor**	**0**	**15**	**0**
	Second Floor	**2**	**13**	**0**

Table 4.5. Number of Piers in Determined Performance Levels According to FEMA-356 at FEMA-356 Target Displacement Points

Loading Direction	Floor	Performance Levels		
		No of Piers		
		IO	LS	CP
Y-Direction	First Floor	0	13	0
	Second Floor	0	13	0
X-Direction	First Floor	0	15	0
	Second Floor	1	14	0

When the hinge conditions were compared at demands displacements according to the FEMA-356 performance definitions, it is seen that all hinges were below the limit of life safety conditions. As a result, all hinges provided life safety condition.

In order to determine the performance level of the building, pushover curves that were obtained in both directions were used. Three points on these curves were chosen for comparison. These three points are selected as the so-called yield point where initial slope of the curve has a major change, the target displacement points that are defined according to FEMA-356 and TER-2018 and the ultimate strength point corresponding to the maximum base shear force.

The first comparison is based on the hinge conditions at selected points. Accordingly, performance point definitions that are defined by FEMA-356 and Pasticier et. al. (2007) used for comparison at each selected point. According to the results given in Table 4.6., the first comparison is at the yield point. The hinges are in immediate occupancy (IO) performance level according to FEMA-356 and in life safety performance level according

to Pasticier et. al. (2007). The reason of this difference is the definition difference at the performance level of immediate occupancy as could be seen in Table 4.2. and Table 4.3.

Yield point could be commented as the point where linear elastic behavior of the piers transform to the plastic behavior. After this point, some of the piers are switched to from elastic to plastic behavior, respectively, and the capacity increase in the system slows down. The ratio of base shear force at the yield point to ultimate base shear force was found 74% and 67% in y and x directions, respectively in Table 4.7. These percentage values show the ratio of the linear elastic behavior strength of the building elements to their ultimate strength in plastic behavior.

The ratio of base shear force at target displacement point according to TER-2018 to ultimate base shear force is calculated as 95% and 92% respectively. These values show that the building is very close to its maximum capacity at demand level. According to the FEMA-356 hinge performance definitions, all pier elements of case study building are in the performance of life safety.

The ratios of base shear to calculated earthquake forces for both orthogonal directions at target displacement points was calculated and shown in Table 4.8 and 4.9. according to masonry building performance definitions in TER-2007 and TER-2018.

Table 4.6. Hinge Status at Selected Points on Pushover Curves

	HINGE STATUS			
Critical Points on Pushover Curves	FEMA-356		PASTICIER et.al. (2007)	
	PUSH-Y	PUSH-X	PUSH-Y	PUSH-X
Yield Point	IO	IO	LS	LS
Target Displacement Point	LS	LS	CP	LS
Ultimate Point	CP	CP	>CP	>CP

Table 4.7. Ratio of Base Shear Force at Selected Points to the Base Shear Force at Ultimate Point

Critical Points on Pushover Curves	% BASE SHEAR w.r.t. ULTIMATE POINT			
	FEMA-356		TER-2018	
	PUSH-Y	PUSH-X	PUSH-Y	PUSH-X
Yield Point	74%	67%	74%	67%
Target Displacement Point	98%	97%	95%	92%

Table 4.8. Ratio of Base Shear Force at Selected Points to the Calculated Earthquake Load According to TER-2007

Critical Points on Pushover Curves	% BASE SHEAR w.r.t.TER-2007 EQ. LOAD			
	FEMA-356		TER-2018	
	PUSH-Y	PUSH-X	PUSH-Y	PUSH-X
Yield Point	61%	59%	61%	59%
Target Displacement Point	82%	86%	80%	82%
Ultimate Point	83%	88%	83%	88%

Table 4.9. Ratio of Base Shear Force at Selected Points to the Calculated Earthquake Load According to TER-2018

Critical Points on Pushover Curves	% BASE SHEAR w.r.t.TER-2018 EQ. LOAD			
	FEMA-356		TER-2018	
	PUSH-Y	PUSH-X	PUSH-Y	PUSH-X
Yield Point	42%	40%	42%	40%
Target Displacement Point	55%	58%	54%	55%
Ultimate Point	56%	60%	83%	88%

According to linear elastic analysis performance level definitions in TER-2007 and TER-2018, limited damage performance level (immediate occupancy) is defined for the situation where earthquake forces could be resisted by all walls. Controlled damage (life safety) level is defined for cases where at least 80 and 60 percent of earthquake forces are

resisted by the walls in TER-2007 and TER-2018 respectively. The collapse situation is defined for percentage values of resisting force below percentage values defined according to both regulations.

According to the comparison of linear elastic analysis performance status in TER-2007 and TER-2018, that are determined in order to reveal the differences among each other, the case study building is at controlled damage level at the target displacement point according to TER-2007 elastic analysis performance criterion. The performance criterion that was found is the acceptable performance limit according to TER-2007. Conversely, the case study building performance level is found in collapse situation at target displacement point according to TER-2018 elastic analysis performance criterion. It was discussed in chapter 3 that the earthquake force calculated according to TER-2018 has 27% increase in proportion to the building mass according to the value calculated according to TER-2007. On the other hand, the definition of controlled damage performance level has been reduced from 80% to 60% ratio of resisting base shear force to total earthquake load. The decrease in these percentage values caused an 11% increase in earthquake forces corresponding to the controlled damage performance point in TER-2018.

According to FEMA-356 unreinforced masonry building general performance level definition at target displacements for nonlinear analysis, the structural performance levels are used. These levels are defined according to drift ratio. Drift ratios are defined as 0.1%, 0.3% and 0.6% respectively for immediate occupancy (IO), life safety (LS) and collapse prevention (CP) structural performance levels. In order to determine the general structure performance level, pushover curves are converted into base shear-drift ratio (%) format. In this conversion, the displacements at each step of the drift in both directions were noted at the control joints. The differences with the joint displacements on the ground floor were found. By dividing this difference by story height, the drift ratio vs base shear plots were drawn for both orthogonal directions in Figure 4.17. and 4.18.

Considering the drift ratios of 0.13% in each orthogonal direction corresponding to calculated target displacements according to FEMA-356, the structure is in life safety performance level in these target displacement points for both directions.

The case study building is in life safety performance level at the target displacement rate of TER-2018 because there is no hinge is in collapse prevention status as it obtained in Table 4.4. Considering the drift ratios of 0.11% in each orthogonal direction corresponding to calculated target displacements according to TER-2018, the case study building is also in life safety status according to performance criteria per FEMA-356.

In addition, these results showed that the results of the element-based performance level and the overall building performance results were consistent with respect to FEMA-356.

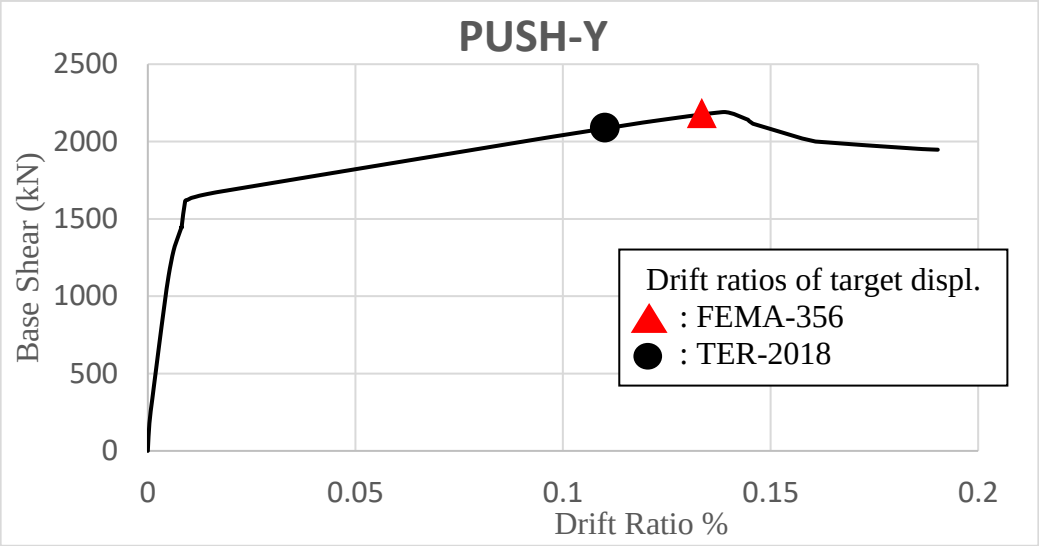

Figure 4.17. Base hear – Drift Ratio (%) Curve for Push-Y

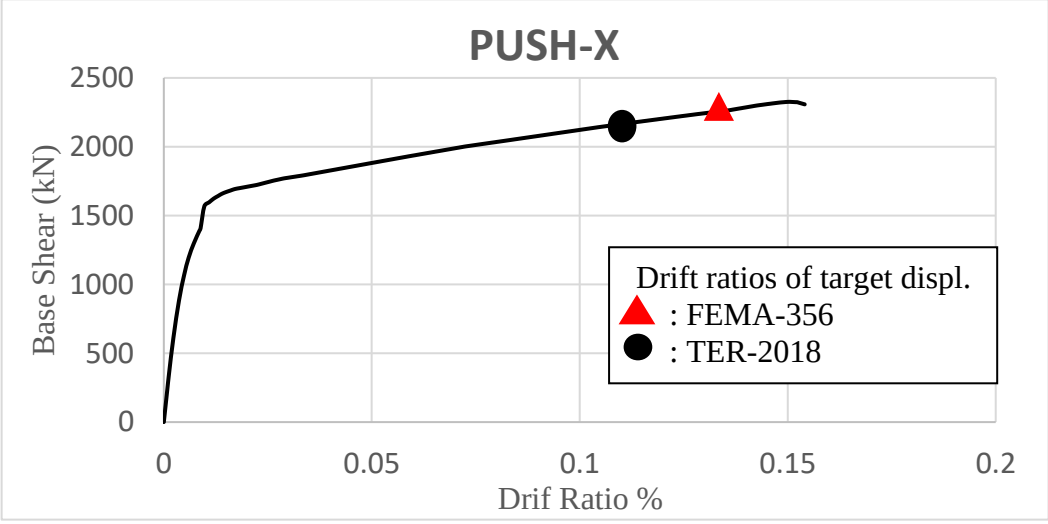

Figure 4.18. Base Shear – Drift Ratio (%) Curve for Push-X

CHAPTER 5

SUMMARY AND CONCLUSION

5.1. Summary and Conclusion

The study presented focuses on identifying the differences in the design of unreinforced masonry buildings per two versions of the Turkish earthquake regulations and examine its impact on the result. The goal is attempted to be achieved through a case study building. Upon observing that the results of the design procedures in the considered regulations are in a major conflict, also considering a performance analysis performed on the case study building. The performance analysis is based on modelling the wall panel's nonlinear flexural and shear responses and performing nonlinear static analysis.

A two-story unreinforced masonry case study building is designed with allowable stress method according to TER-2007 regulation and has a wall thicknesses of forty centimeters. As it defined for the selected region in TER-2007, the design is performed with 0.4g ground acceleration, and the seismic base shear force is calculated to be 50 percent of the weight of the building.

The case study building is then re-examined according to TER-2018 design requirements through modeling by equivalent frame and finite element models, as described in the regulation. The analysis is performed using the SAP2000 and ETABS structural analysis software. The ground acceleration is found to be 0.463g for the site's geographic coordinates, and the base shear force is calculated as 77 percent of weight per TER-2018. The analysis results show that the case study structure is found insufficient, with almost all the wall panels is beyond their acceptable limits. The shear strength of the walls that is based on flexural capacities are found to be the main cause of the insufficiency.

The case study structure is re-analyzed to obtain the seismic level, which the TER-2018 could accept as safe. It is found that a seismic level with a 0.075g peak acceleration satisfies the intended results. This spectral value belongs to one of the low seismic zones in Turkey.

Due to the major conflict in the results of the two regulations for the same building, a non-linear model is generated to obtain an analysis that is simulating the behavior with a better success. A nonlinear static analysis is performed for this purpose. The target displacement demands are found using procedures defined in FEMA-356 and TER-2018. The nonlinearities in the wall panels are defined by flexural and shear hinges. The definition of the structural framing and the properties of the nonlinear hinges are adopted from the literature. The individual wall and structure's overall performance is defined using the displacement demands defined per FEMA356 and TER-2018. According to the performance definition in FEMA356, which is based on the drift ratio, the case study building provides the life safety performance status according to displacement demands calculated per FEMA356 and TER-2018.

Based on the performed analyses, it is observed that;

- According to TER-2018, the seismic demands increase, and the base shear capacity of the unreinforced masonry structures decreases dramatically.
- Considering TER-2018 requirements, it is impossible to design an unreinforced masonry structure in high seismic zones.
- The same structure that the TER-2018 regulations indicate as deficient for seismic demands could be sufficient per TER-2007. It is acceptable to observe such a result due to the increase in the seismic demand, but the severe drop in the shear capacity needs further examination.
- The nonlinear static procedure, which could be accepted closer to real behavior, indicates that the same structure satisfies the life safety performance level for FEMA356 and TER-2018.

The performed study demonstrates that the capacity calculation of TER-2018 for the unreinforced masonry structures under seismic demands seem to be not realistic and needs further investigation. It is recommended to perform targeted analytical and experimental studies to provide the data to define realistic design procedures.

REFERENCES

Aldemir, Alper. A Simple Performance Assessment Technique for Unreinforced Brick Masonry Structures. MSc.Thesis, Ankara: Middle East Technical University, 2010, 76-107.

Anthoine, A., G. Magenes, and G. Magonette. "Shear Compression Testing and Analysis of Brick Masonry Walls." *Proc. 10th European Conference on Earthquake Engineering.* Vienna, 1994. 1657-1662.

Aydınoğlu, N., Z. Celep, H. Sucuoğlu, and E. Özer. *Turkish Earthquake Code Example Book.* Ankara: Ministry of Public Works and Settlement, 2007.

Computer and Structures. *ETABS Reference Manual.* California: University of Ave. Berkeley, 2019.

—. *SAP Reference Manual.* California: University of Ave. Berkeley, 2017.

Çöğürcü, T. M., and M. Kamanlı. "The Experimental Investigation of The Dynamic and Engineering Behavior of Masonry Structures Under Out-of-Plane Forces." *Journal of Selcuk-Technic vol.6 (2),* 2007: 83-108.

Dilsiz, A., and A Türer. "Creation of Seismic Hazard Map of Masonry Buildings in Turkey." *Charette on Increasing Earthquake Safety of Masonry Structure.* Ankara: Middle East Technical University, 2005.

Dolce, M. "Models for In-Plane Loading of Masonry Walls." Corso sul consolidamento degli edifici in muratura in zona sismica, Ordine degli Ingegneri, Potenza, 1989.

EN 1998-3:2005. *Eurocode 8: Design of Structures for Earthquake Resistance- Part 3 : Assessment and Retrofitting of Buildings.* 2005.

EN-1996-1-1:2005. *Eurocode 6: Design of Masonry Structures- Part 1-1: General Rules for Reinforced and Unreinforced Masonry Structures.* 2005.

Federal Emergency Management Agency. *FEMA-273, NEHRP Guidelines for the Seismic Rehabilitation of Buildings.* Washington, 1997.

—. *FEMA-306, Evaluation of Earthquake Damaged Concrete and Masonry Wall Buildings Basic Procedures Manual.* Washington, 1998.

—. *FEMA-307, Evaluation of Earthquake Damaged Concrete and Masonry Wall Buildings Technical Resources.* Washington, 1998.

—. *FEMA-356, Prestandard and Commentary for the Seismic Rehabilitation of Buildings.* Washington, 2000.

Kappos, J. A., G. G. Penelis, and G. C. Drakopoulos. "Evaluation of Simplified Models for Lateral Load Analysis of Unreinforced Masonry Buildings." *Journal of Structural Engineering vol.128*, 2002: 890-897.

Kuran F. et al. "An Evaluation on Turkey Building Earthquake Code-2018 Masonry Buildings' Section and a Comparative Analysis for Unreinforced Masonry Building Cases." *Turkish Journal of Earthquake Research vol.2 (1),* 2020: 47-60.

Lourenco, P. B. *Computational Strategies for Masonry Structures.* Ph.D. thesis, Delft: Delft University of Technology, 1996, 11.

Magenes, G., and M. G. Calvi. "In-Plane Seismic Response of Brick Masonry Walls." *Earthquake Engineering and Structural Dynamics Journal vol26.*, 1997: 1091-1112.

Ministry of Industry and Technology. *TS EN 771-1+A1, Specification for Masonry Units-Part 1: Clay Masonry Units.* Ankara: Turkish Standards Institution, 2015.

—. *TS EN-1015-11, Methods of Test for Masonry- Part 11: Detemination of Flexural and Compressive Strength of Hardened Mortar.* Ankara: Turkish Standards Institution, 2000.

—. *TS EN-1052-1, Methods of Tests for Masonry-Part 1: Determination of Compressive Strength.* Ankara: Turkish Standards Institution, 2000.

—. *TS EN-1052-3, Methods of Test for Masonry- Part 4: Determination of Initial Shear Strength.* Ankara: Turkish Standards Institution, 2004.

—. *TS EN-1052-4, Methods of Test for Masonry- Part 4: Determination of Shear Strength Including Damp Proof Course.* Ankara: Turkish Standards Institution, 2002.

—. *TS EN-772-1+A1, Methods of Test for Masonry Units- Part 1: Determination of Compressive Strength.* Ankara: Turkish Standards Institution, 2015.

—. *TS-2510, Design and Construction Methods for Masonry.* Ankara: Turkish Standards Institution, 1977.

—. *TS-498, Design Loads for Buildings.* Ankara: Turkish Standards Institution, 1997.

Ministry of Interior Disaster and Emergency Management Presidency, (AFAD). 06 16, 2020. https://tdth.afad.gov.tr/TDTH/main.xhtml.

Ministry of Interior, Disaster and Emergency Management Presidency. *TER-2018, Turkish Earthquake Regulation.* Ankara: Government of Republic of Turkey, 2018.

Ministry of Public Works and Settlement. *TER-2007, Turkish Earthquake Regulation.* Ankara: Government of Republic of Turkey, 2007.

Mısır, İ. S., F. Kuran, E. Tuna, Ö. Aldemir, and S. Fırat. "Design and Performance Evaluation of Unreinforced Masonry Buildings Considering Turkey Earthquake Building Code-2019." *5th International Conference on Earthquake Engineering and Seismology (5CIEES).* Ankara, 2019.

Pasticier, L., C. Amadio, and M. Fragiacomo. "Non-Lİnear Seismic Analysis and Vulnerability Evaluation of a Masonry Building by Means of the SAP2000 V.10 Code." *Earthquake Engng. Struct. Dyn. vol.37 (3)*, 2007: 467-485.

Penelis, G. G. "An Efficient Approach for Pushover Analysis of URM Structures." *Journal of Earthquake Engineering vol.10 (3)*, 2006: 359-379.

State Institute of Statistics. *DIE, Building Cencus.* Ankara: Prime Ministry of Republic of Turkey, 2000.

Tomazevic, M. "Shear Resistance of Masonry Walls and Eurocode 6: Shear Versus Tensile Strength of Masonry." *Materials and Structures vol.42 (7)*, 2009: 889-907.

Turnsek, V., and F. Cacovic. *Some Experimental Results on the Strength of Brick Masonry.* Ljubljana: Zavod za Raziskavo Materiala in Konstrukcij, 1971.

Turnsek, V., and P. Sheppard. "The Shear and Flexural Resistance of Masonry Walls." Skopje: Proceedings of the International Research Conference on Earthquake Engineering, 1980. 517-573.

Yi, T. *Experimental Investigation and Numerical Simulation of An Unreinforced Masonry Structure with Flexible Diaphragms.* PhD. Thesis, Atlanta: Georgia Institute of Technology, 2004, 16.

Yi, T., L. F. Moon, T. R. Leon, and F. L. Kahn. "Analyses of a Two-Story Unreinforced Masonry Building." *Journal of Structural Engineering vol.132*, 2006: 653-662.

Yi, T., L. F. Moon, T. R. Leon, and F. L. Kahn. "Lateral Load Tests on a Two-Story Unreinforced Masonry Building." *Journal of Structural Engineering vol.132*, 2006: 643-652.